Task 3. Catalyst Characterization

The objective of this task is to obtain characterization data of the prepared catalysts using routine and selected techniques.

A. Impact of Copper on an Alkali Promoted Iron Fischer-Tropsch Catalyst

Introduction

Copper has traditionally been added to precipitated iron Fischer-Tropsch (FT) catalysts to facilitate reduction of Fe_2O_3 to zero valent iron during activation (1) by lowering the reduction temperature when activating with hydrogen, carbon monoxide or syngas (2). This is particularly important when activating with hydrogen because metallic iron which is formed will sinter easily if the temperature is too high; however, it is not as critical when activating with carbon monoxide or syngas because iron carbides are formed and they are not as susceptible to sintering.

The effect of copper on activity and selectivity has not been studied as thoroughly as its effect on catalyst activation. Kölbel reported that copper loadings less than 0.1 % (weight % relative to iron) were sufficient to produce an active catalyst and that increased copper loading had no effect on FT activity (3). It has previously been shown that copper increases the activity of precipitated iron catalysts when operating at low temperature ($<250^{O}C$) (2). Bukur et al. have reported that copper increases FT activity and water gas shift activity (4). In addition, they reported that copper increased the average molecular weight of the product and increased hydrogenation of alkenes and isomerization of 1-alkenes. Soled et al. have reported that promotion with copper in conjunction with potassium increased FT activity but had little effect on alkene selectivity (5).

Water gas shift activity and FT selectivity have been shown to depend on syngas conversion (6). To determine the true impact of copper on FT selectivity and water gas shift

activity, comparisons should be done at similar conversion. No such study has been reported for the effects of copper. Herein are reported the effects of copper on FT activity and selectivity and water gas shift activity over a wide range of syngas conversions.

Experimental

A base catalyst with atomic composition 100Fe/4.6Si was prepared by precipitation as previously reported (7). The catalyst was impregnated with aqueous K_2CO_3 to give an atomic composition of 100Fe/4.6Si/1.4K. Copper was added by impregnation with aqueous $Cu(NO_3)_2 \cdot 3H_2O$. Catalyst compositions in atomic ratios were:

100Fe/4.6Si/1.4K
100Fe/4.6Si/0.10Cu/1.4K
100Fe/4.6Si/2.0Cu/1.4K

Approximately 5 g of catalyst were mixed with 300 g of Ethylflo 164 decene trimer in a one liter stirred tank reactor. Catalysts were activated with carbon monoxide at 270^{O}C and 1.3 MPa for 24 hours. Following activation, temperature and pressure were maintained and syngas (H_2/CO=0.67) was started at a space velocity of 10 l (STP) h^{-1} g-Fe^{-1}. The reactor stirring speed was maintained at 750 rpm. Within eight days syngas conversion had stabilized and the space velocity was varied between 5 and 65 l (STP) h^{-1} g-Fe^{-1}. Each space velocity was maintained for approximately 24 hours after which liquid samples were taken and a material balance was calculated. The space velocity was returned to 10 l (STP) h^{-1} g-Fe^{-1} after about two weeks on line to check for deactivation.

Results

FT Activity

Syngas conversion for each catalyst as a function of the reciprocal space velocity is shown in Figure 1. Copper increased syngas conversion over the entire range of space velocities studied. Copper also increased hydrocarbon productivity (Figure 2). At the lowest space

velocity the hydrocarbon productivity was about the same for all three catalysts (~1.1 g h^{-1} g-Fe^{-1}). As the space velocity was increased, hydrocarbon productivity increased with increasing copper loading. At the highest space velocity, the hydrocarbon productivity was 5.3, 3.9 and 3.0 g h^{-1} g-Fe^{-1} for the 100Fe/4.6Si/2.0Cu/1.4K, 100Fe/4.6Si/0.10Cu/1.4K and 100Fe/4.6Si/1.4K catalysts, respectively.

Water gas shift Activity

The rate of the water gas shift reaction is defined as the rate of carbon dioxide formation, mol h^{-1}g-Fe^{-1}, in this study. In general, the water gas shift rate increased initially with increasing space velocity. The water gas shift rate for the 100Fe/4.6Si/2.0Cu/1.4K catalyst increased over the entire range of space velocities studied; however, it leveled off for the 100Fe/4.6Si/0.10Cu/1.4K catalyst and reached a maximum for the 100Fe/4.6Si/1.4K catalyst (Figure 3). Copper slightly increased the water gas shift rate at the lowest space velocity. As the space velocity increased the impact of copper became more pronounced. At the highest space velocity, the water gas shift rates were 0.21, 0.14 and 0.1 for the 100Fe/4.6Si/2.0Cu/1.4K, 100Fe/4.6Si/0.10Cu/1.4K and 100Fe/4.6Si/1.4K catalysts, respectively. Similarly copper increased the water gas shift rate at all conversion levels studied, although the water gas shift rates were converging at the highest conversion (Figure 4). The approach to equilibrium for the water gas shift can be measured by the reaction quotient:

$$RQ_{WGS} = \frac{P_{CO_2} P_{H_2}}{P_{CO} P_{H_2O}} \quad \textbf{(1)}$$

The reaction quotient increased with increasing conversion; however, only at syngas conversion greater than 90% did the water gas shift reaction approach equilibrium (Figure 5). Copper had no effect on the water gas shift reaction quotient when compared at similar conversion.

FT Rate Versus Water Gas Shift Rate

The rate of the water gas shift and FT reactions can be defined by equations 2 and 3:

$$r_{wgs} = r_{CO_2} \tag{2}$$

$$r_{FT} = r_{CO} - r_{CO_2} \tag{3}$$

where r_{CO_2} is the rate of CO_2 formation and r_{CO} is the rate of CO conversion. The FT rate dominated the water gas shift rate at the highest space velocities (Figure 6). The FT and water gas shift rates decreased as the space velocity decreased and conversion increased. As the space velocity decreased the water gas shift rate approached the FT rate.

Selectivity

Carbon monoxide efficiency was not effected by copper promotion. In general, the selectivity to carbon dioxide decreased with decreasing syngas conversion (Figure 7). Copper had little effect on alkene selectivity (Figure 8) or isomerization of 1-butene (Figure 9) over the entire range of conversions studied. Methane selectivity was fairly constant up to 50-60 % conversion; however, at higher conversions, methane selectivity increased with increasing conversion. In general, the hydrocarbon selectivity shifted to heavier products with decreasing conversion (Figure 11). Copper lowered the methane selectivity at all conversions (Figure 10) and increased C_{12} and heavier products (Figure 11).

Kinetics

Satterfield et al. have proposed the following kinetic expression for the rate of consumption of syngas by the FT synthesis:

$$-r_{CO+H_2} = \frac{kP_{CO}P^2_{H_2}}{P_{CO}P_{H_2} + bP_{H_2O}} \tag{4}$$

where k is the intrinsic rate constant, b is the product of the adsorption equilibrium constant of CO and the desorption equilibrium constant of H_2O and the remaining variables are the partial pressures of CO, H_2 and H_2O (8). Equation 4 can be rearranged to give the following linear equation:

$$\frac{P_{H_2}}{-r_{CO+H_2}} = \frac{1}{k} + \frac{b}{k}\frac{P_{H_2O}}{P_{CO}P_{H_2}}. \quad (5)$$

A plot of $P_{H_2}/-r_{CO+H_2}$ versus $P_{H_2O}/(P_{CO}P_{H_2})$ will give a straight line with slope equal to b/k and y-intercept equal to 1/k if data fit the model. Data for the three runs are presented in this manner in Figure 12 and results are listed in Table 1. The rate constant, k increased with increasing copper and the adsorption parameter, b decreased with increasing copper.

Discussion

Activity and selectivity data for each catalyst are listed in Tables 2 through 4. Conversion and hydrocarbon productivity increased with increasing copper loading over the range of copper loadings studied and hydrocarbon productivity increased by a factor of 3 to 5 upon increasing the space velocity (decreasing conversion) from 5 to 65 l (STP) h^{-1} g-Fe^{-1}. The kinetic expression proposed by Satterfield et al. (8) adequately described the data acquired for all three catalysts. Copper increased the intrinsic FT rate constant and also decreased the adsorption parameter, b. Examination of equation 4 reveals that both of these effects result in an increase in the FT rate. The effect of copper on the FT rate is somewhat different than the effect of potassium. Potassium was previously found to decrease the intrinsic rate constant, k and the adsorption parameter, b (9). Since these trends have an opposite effect on FT rate (equation 4),

the effect of potassium depended on the conversion. At high conversion, increasing potassium slightly increased activity, at intermediate conversion (50%) there was an optimum potassium loading and at low conversion increasing potassium decreased FT activity.

Water gas shift

It is conventional wisdom that copper increases carbon dioxide selectivity and the water gas shift reaction quotient (4). In the present study it was found that copper increased the water gas shift rate; however, it did not effect the carbon dioxide selectivity or the water gas shift reaction quotient when comparisons were made at the same syngas conversion. The FT reaction rate was always higher than the water gas shift reaction. This can be seen in Figure 6 where the ratio of the water gas shift rate to the FT rate for all three catalysts increased from about 0.4 at the highest space velocity to greater than 0.8 at the lowest space velocity. The rate of the water gas shift reaction cannot be greater than the rate of the FT reaction because the water gas shift reaction is limited by the rate of water produced by the FT reaction.

FT reaction $CO + (1+(n/2))H_2 \rightarrow CH_n + H_2O$ (6)

water gas shift $CO + H_2O \rightarrow CO_2 + H_2$ (7)

It has been reported that copper effects hydrocarbon selectivity in much the same way as potassium, except secondary reactions are slightly enhanced (alkene hydrogenation and 1-alkene isomerization) (4); however, comparisons were not made at similar conversions. In the present study, methane selectivity was constant up to a conversion of approximately 50%, irrespective of copper loading. Above 50% conversion, methane selectivity increased with increasing conversion. Increasing copper did significantly lower methane selectivity and increase the selectivity to heavy products. Alkene selectivity and isomerization of 1-alkenes was not effected by copper when comparisons were made at similar conversion.

Conclusions

Copper is a promoter for the FT synthesis. The FT rate increased with increasing copper loading in the range reported here (0 to 2 atomic ratio per 100 Fe). The effect of copper on FT kinetics has been studied. According to a proposed kinetic expression, the FT reaction rate is dependent on a rate constant, k and an adsorption parameter, b. Copper has been found to increase the rate constant and decrease the adsorption parameter, both of which cause an increase in FT rate.

Copper also increased the water gas shift rate; however, it did not increase CO_2 selectivity when comparisons were made at similar conversion. The water gas shift reaction quotient only approaches the equilibrium constant at high conversion; furthermore, copper did not increase the reaction quotient.

The effect of copper on product selectivity has been determined over a wide range of conversions. Accurate comparisons of catalyst selectivity must be made at similar syngas conversion because selectivity can be greatly affected by the conversion. For example, methane selectivity increased and alkene selectivity decreased with increasing conversion. Copper had a similar effect on product selectivity as potassium. Methane selectivity decreased and products heavier than C_{11} increased with increasing copper loading. Copper did not effect alkene selectivity or the isomerization of 1-alkenes to 2-alkenes.

References

1. M. E. Dry, in J. R. Anderson and M. Boudart (Editors), Catalysis Science and Technology, Vol. 1, Springer-Verlag, New York, 1981, p. 179.
2. R. J. O'Brien, L. Xu, R. L. Spicer, S. Bao, D. R. Milburn, B. H. Davis, *Catal. Today*, 36 (1997) 325.
3. H. Kölbel, M. Ralek, *Catal. Rev. Sci. Eng.*, 21 (1980) 225.
4. D. B. Bukur, D. Mukesh, S. A. Patel, *Ind. Eng. Chem. Res.*, 29 (1990) 194.
5. S. L. Soled, E. Iglesia, S. Miseo, B. A. DeRites, R. A. Fiato, *Topics in Catal.*, 2 (1995) 193.
6. Raje, A. P., Davis, B. H., *Catal. Today* **36**, 335 (1997).
7. R. J. O'Brien, L. Xu, R. L. Spicer, B. H. Davis, *Energy & Fuels*, 10 (1996) 921.
8. G. A. Huff Jr., C. N. Satterfield, *Ind Eng. Chem. Process Des. Dev.*, 23 (1984) 696.
9. A. P. Raje, R. J. O'Brien, B. H. Davis, *J. Catalysis*, 180 (1998) 36.

Table 1 Effect of Copper on Kinetic Parameters		
	k (mol $h^{-1}g\text{-}Fe^{-1}kPa^{-1}$)	b
100Fe/4.6Si/1.4K	1.75×10^{-3}	3040
100Fe/4.6Si/0.1Cu/1.4K	2.04×10^{-3}	1940
100Fe/4.6Si/2.0Cu/1.4K	2.93×10^{-3}	1590

Table 2

Activity and Selectivity for 100Fe/4.6Si/1.4K Catalyst

	Space Velocity (sl h^{-1}g-Fe^{-1})								
	5.0	**6.67**	**10**	**15**	**22**	**30**	**40**	**50**	**65**
$CO + H_2$ Conversion %	80	76	71	57	44	36	29	25	20
Hydrocarbon Productivity (g h^{-1}g-Fe^{-1})	0.89	1.08	1.53	1.91	2.12	2.41	2.73	2.89	3.03
Water-Gas Shift $P_{H_2}P_{CO_2}/(P_{H_2O}P_{CO})$	20	15	9.7	4.0	2.4	1.6	1.2	1.0	0.92
H_2/CO usage ratio	0.57	0.58	0.60	0.65	0.72	0.78	0.81	0.90	0.96
Selectivity C basis									
CO_2	46	47	46	44	42	38	34	32	30
CH_4	7.1	7.1	4.8	5.3	5.2	5.0	4.8	4.7	4.9
Selectivity (wt.%)									
CH_4	7.9	7.9	6.5	5.9	5.8	5.6	5.4	5.2	5.5
C_2-C_4	27	27	24	23	24	23	22	22	22
C_5-C_{11}	35	36	34	35	34	32	32	30	30
C_{12}+	31	29	36	36	37	39	41	43	43
alkene									
C_2-C_4	60	63	71	77	80	82	83	85	85
C_5-C_{11}	69	73	75	78	82	83	84	85	75

Table 3

Activity and Selectivity for 100Fe/4.6Si/0.10Cu/1.4K Catalyst

	Space Velocity (sl h^{-1}g-Fe^{-1})								
	5.0	**6.67**	**10**	**15**	**22**	**30**	**40**	**50**	**65**
$CO + H_2$ Conversion %	86	83	76	64	54	44	37	31	25
Hydrocarbon Productivity (g h^{-1}g-Fe^{-1})	0.87	1.15	1.64	2.15	2.75	3.00	3.50	3.87	3.89
Water-Gas Shift $P_{H_2}P_{CO_2}/(P_{H_2O}P_{CO})$	48	32	12	6.3	3.6	2.4	1.8	1.5	1.3
H_2/CO usage ratio	0.57	0.58	0.60	0.60	0.64	0.68	0.72	0.71	0.78
Selectivity C basis									
CO_2	51	49	46	44	41	41	37	34	34
CH_4	8.7	7.9	6.0	5.2	4.7	5.1	4.8	4.9	5.3
Selectivity (wt.%)									
CH_4	9.7	8.9	6.7	5.9	5.3	5.7	5.4	5.4	6.0
C_2-C_4	29	28	23	22	20	22	21	20	22
C_5-C_{11}	42	39	35	34	31	33	33	31	32
C_{12}+	19	24	35	38	44	39	40	44	40
alkene									
C_2-C_4	57	58	69	75	79	81	83	83	85
C_5-C_{11}	66	67	73	77	80	82	82	84	84

Table 4

Activity and Selectivity for 100Fe/4.6Si/2.0Cu/1.4K Catalyst

	Space Velocity (sl h^{-1}g-Fe^{-1})								
	5.0	**6.67**	**10**	**15**	**22**	**30**	**40**	**50**	**65**
$CO + H_2$ Conversion %	89	88	86	77	66	56	48	42	35
Hydrocarbon Productivity (g h^{-1}g-Fe^{-1})	1.02	1.24	1.92	2.51	3.20	3.74	4.49	4.62	5.30
Water-Gas Shift $P_{H_2}P_{CO_2}/(P_{H_2O}P_{CO})$	42	56	30	14	6.5	4.3	2.6	2.0	1.6
H_2/CO usage ratio	0.58	0.60	0.58	0.60	0.63	0.66	0.66	0.75	0.74
Selectivity C basis									
CO_2	44	47	45	46	44	43	40	40	37
CH_4									
Selectivity (wt.%)									
CH_4	7.3	7.9	7.0	6.2	5.5	5.3	4.9	5.4	5.2
C_2-C_4	22	24	21	21	20	20	18	20	19
C_5-C_{11}	32	27	29	33	32	30	27	31	30
C_{12}+	39	41	42	40	42	45	49	44	46
alkene									
C_2-C_4	58	57	60	69	75	79	81	82	83
C_5-C_{11}	65	67	67	70	75	79	81	82	83

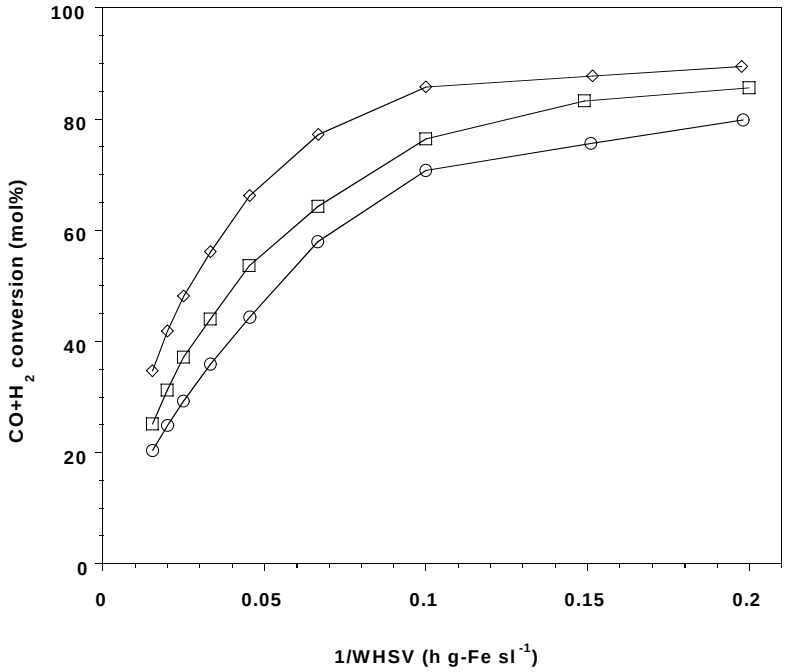

Figure 1. Syngas conversion as a function of reciprocal space velocity. F, 0 Cu, G, 0.1 Cu, ♢, 2.0 Cu.

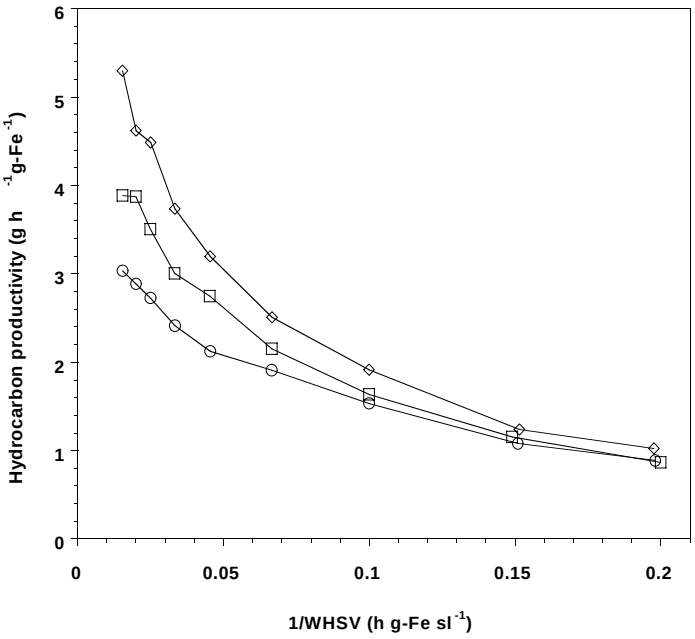

Figure 2. Hydrocarbon productivity as a function of reciprocal space velocity. F, 0 Cu, G, 0.1 Cu, ◊, 2.0 Cu.

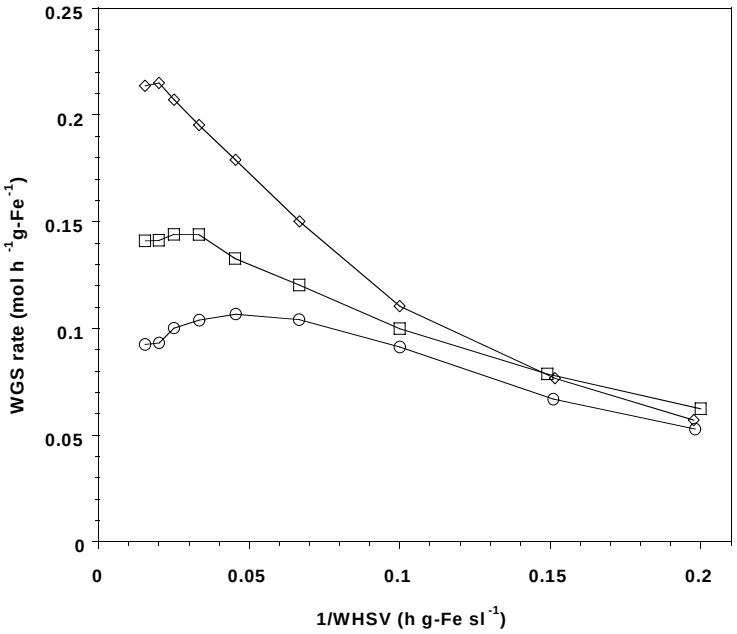

Figure 3. Water gas shift rate as a function of reciprocal space velocity. F, 0 Cu, G, 0.1 Cu, ♢, 2.0 Cu.

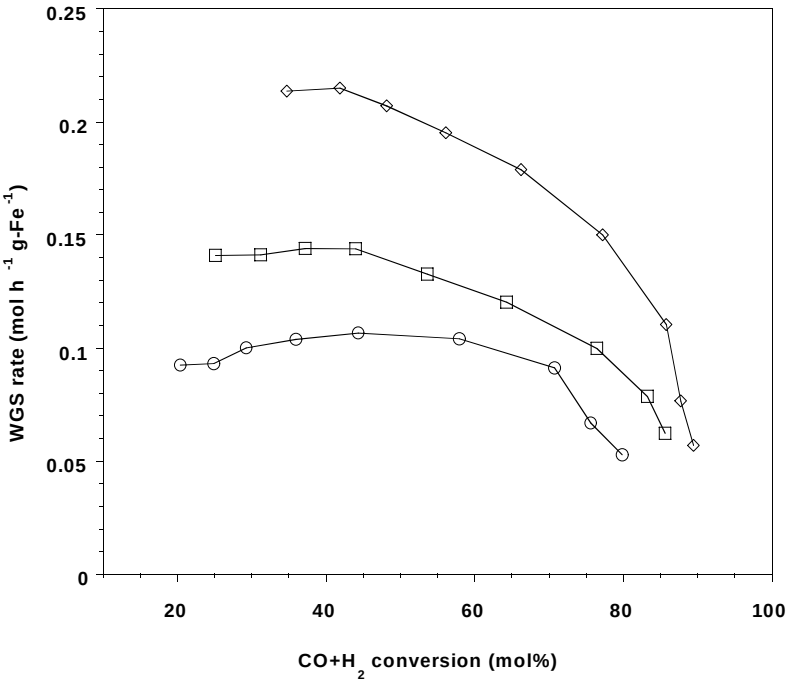

Figure 4. Water gas shift rate as a function of syngas conversion. F, 0 Cu, G, 0.1 Cu, ◊, 2.0 Cu.

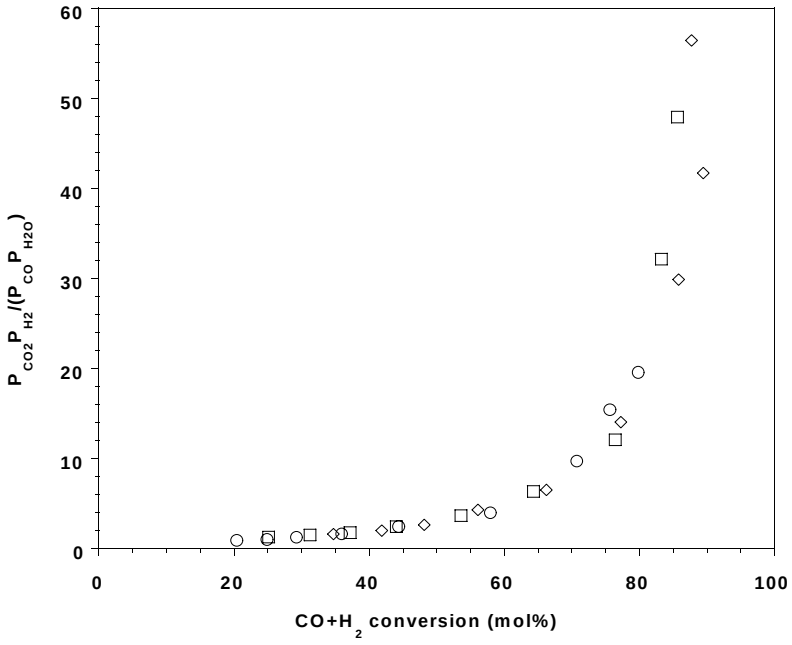

Figure 5. Water gas shift reaction quotient as a function of syngas conversion. F, 0 Cu, G, 0.1 Cu, ♢, 2.0 Cu.

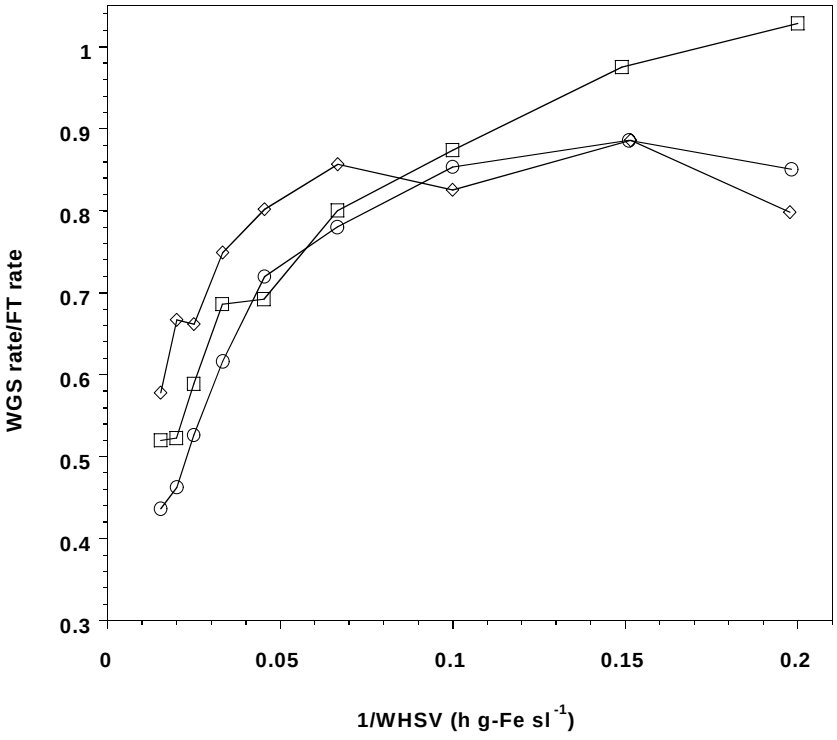

Figure 6. Ratio of water gas shift rate to FT rate as a function of syngas conversion. F, 0 Cu, G, 0.1 Cu, ♢, 2.0 Cu.

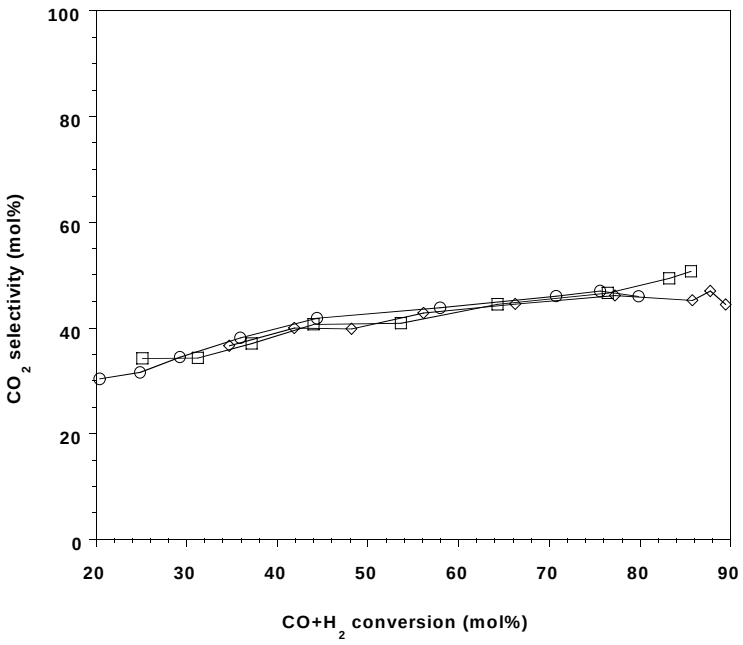

Figure 7. Carbon dioxide selectivity as a function of syngas conversion. F, 0 Cu, G, 0.1 Cu, ◊, 2.0 Cu.

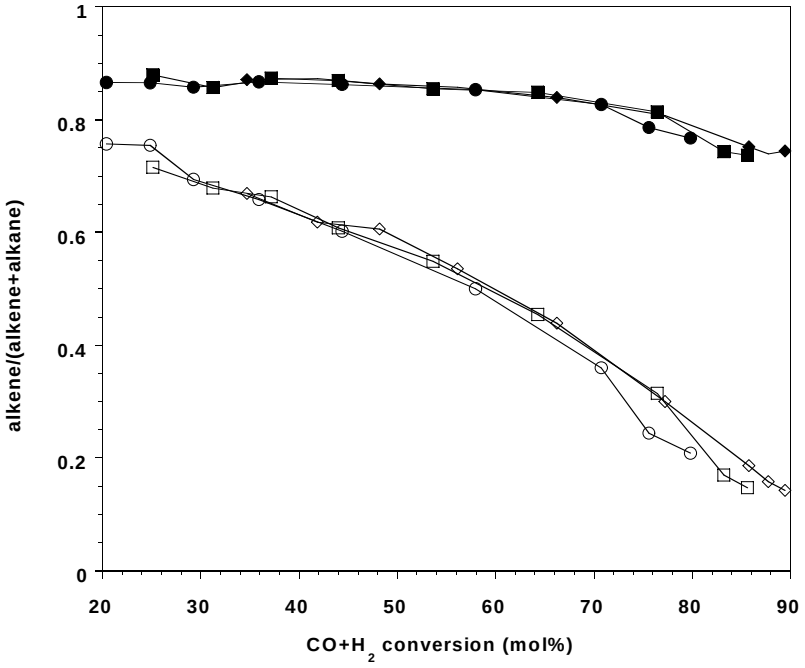

Figure 8. Alkene selectivity of C_2 (open symbols) and C_4 (closed symbols) as a function of syngas conversion. F and M, 0 Cu, G and O, 0.1 Cu, ◊ and ◆, 2.0 Cu.

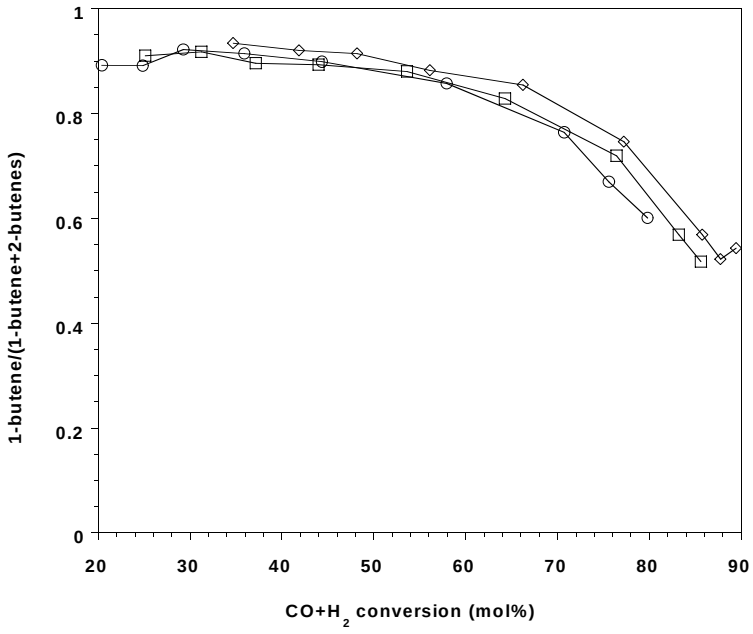

Figure 9. 1-butene selectivity as a function of syngas conversion. F, 0 Cu, G, 0.1 Cu, ◊, 2.0 Cu.

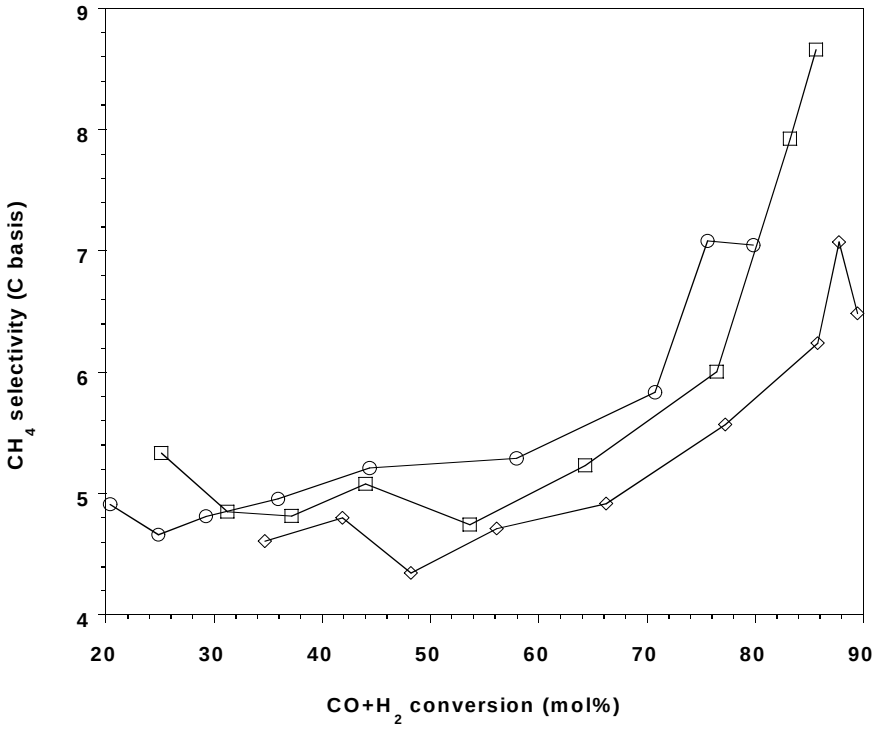

Figure 10. Methane selectivity as a function of syngas conversion. F, 0 Cu, G, 0.1 Cu, ♢, 2.0 Cu.

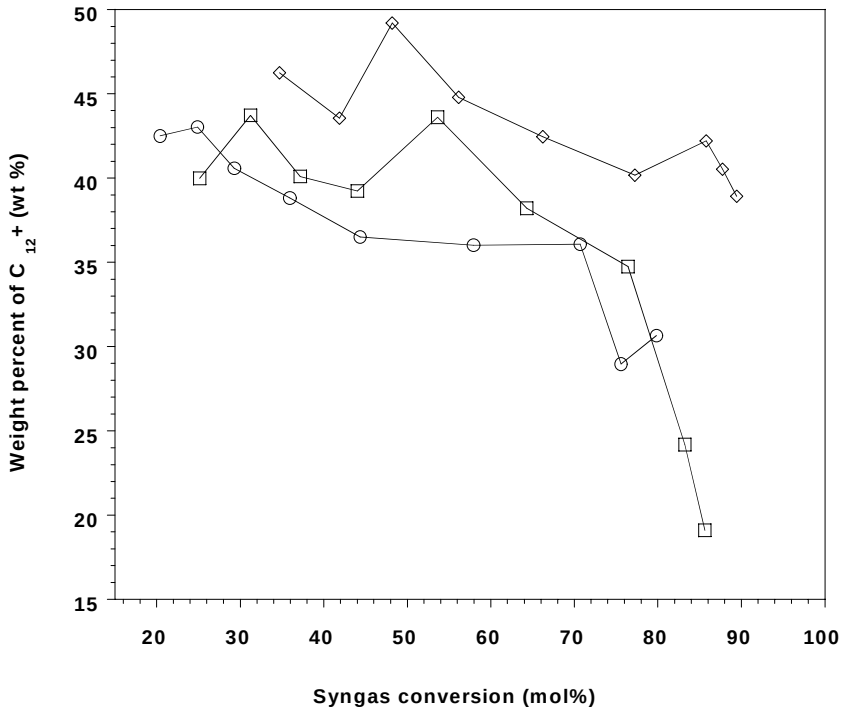

Figure 11. Selectivity of C_{12} and heavier products as a function of syngas conversion. F, 0 Cu, G, 0.1 Cu, ♢, 2.0 Cu.

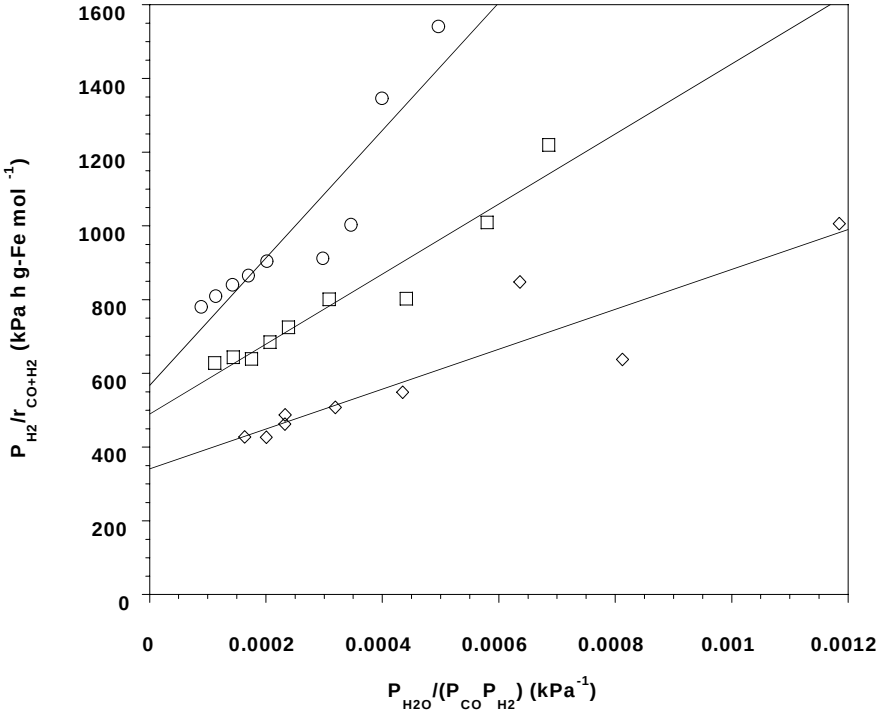

Figure 12. FT rate data fit according to equation 5. F, 0 Cu, G, 0.1 Cu, ♢, 2.0 Cu.

B. Mössbauer Spectroscopy of Iron-Based Fischer-Tropsch Catalysts: Impact of Activation Procedure

Abstract

The impact of activation procedure on the phase composition of precipitated iron Fischer-Tropsch (FT) catalysts has been studied. Catalyst samples taken during activation and FT synthesis have been characterized by Mössbauer spectroscopy. Formation of iron carbide is necessary for high FT activity. Hydrogen activation of precipitated iron catalysts results in reduction to predominantly metallic iron and Fe_3O_4. Metallic iron is not stable under FT conditions and is rapidly converted to ϵ'-$Fe_{2.2}C$. Activation with carbon monoxide or syngas with low hydrogen partial pressure reduces catalysts to χ-Fe_5C_2 and a small amount of superparamagnetic carbide. Exposure to FT conditions partially oxidizes iron carbide to Fe_3O_4; however, catalysts promoted with potassium or potassium and copper maintain a constant carbide content and activity after the initial oxidation. An unpromoted iron catalyst which was activated with carbon monoxide to produce 94% χ-Fe_5C_2, deactivated rapidly as the carbide was oxidized to Fe_3O_4. No difference in activity, stability or deactivation rate was found for χ-Fe_5C_2 and ϵ'-$Fe_{2.2}C$.

Introduction

Iron Fischer-Tropsch (FT) catalysts undergo numerous phase changes which may have profound effects on catalyst activity (1-3), selectivity (4), attrition (5) and deactivation (6). Precipitated and fused iron catalysts are typically oxides before use and need to be activated by reducing to the zero valent state. The activation procedure generally involves reducing with hydrogen to metallic iron or with carbon monoxide or syngas to various iron carbides. Metallic iron, produced by hydrogen activation, is rapidly converted to iron carbides when exposed to syngas under FT conditions (2,3). Additional phase transformations may occur during FT

synthesis. Water is a primary product of the FT synthesis and may reach concentrations high enough to oxidize iron carbides to Fe_3O_4 (7). In addition, carbon dioxide produced by the water-gas shift reaction can reach oxidizing concentrations at high conversion (7). A thermodynamic study of the iron carbide/oxide system under typical FT conditions has shown that both Fe_3O_4 and iron carbide are thermodynamically favored (8).

Several iron carbides have been identified in active iron FT catalysts. Among these are: χ-Fe_5C_2, ϵ'-$Fe_{2.2}C$, θ-Fe_3C and Fe_7C_3. The thermal stability of χ-Fe_5C_2, ϵ'-$Fe_{2.2}C$, and θ-Fe_3C carbides with increasing temperature has been reported to be: ϵ'-$Fe_{2.2}C \leq \chi$-$Fe_5C_2 < \theta$-Fe_3C (9, 10). Conducting FT synthesis at moderate to low temperatures ($<270^{O}C$) generally results in χ-Fe_5C_2 and/or ϵ'-$Fe_{2.2}C$ formation (2, 3). The θ-Fe_3C and Fe_7C_3 carbides have been reported at high temperature FT synthesis with fused iron catalysts (7). The role of iron carbides in FT synthesis has been debated since Fischer and Tropsch proposed hydrocarbons were formed by the hydrogenation of bulk iron carbide (11). Emmett demonstrated that hydrocarbons synthesized over a ^{14}C labeled iron carbide catalyst had lower radioactivity than the catalyst thereby demonstrating that bulk iron carbide does not directly participate in hydrocarbon production; however, Emmett did not rule out the possibility that a surface carbide was involved in hydrocarbon production (12). Subsequent studies with ^{13}C tracers have verified that carbon on the surface of carbided catalysts does become incorporated in FT products (13).

In addition to iron carbides, Fe_3O_4 (magnetite) is generally found in used iron FT catalysts. Magnetite has been reported to be both active (14) and inactive for FT synthesis (1). The discrepancy may be due to oxidation of iron carbides by improper passivation prior to analysis (15). Metallic iron has also been proposed to be active for FT synthesis (5). This is unlikely because thermodynamic data predict metallic iron will either be oxidized to Fe_3O_4 or converted to iron carbide(s) depending on the conversion level (8).

Herein, the impact of hydrogen, carbon monoxide and syngas activation on the phase composition of precipitated iron catalysts will be presented. Correlations between phase composition and FT activity and deactivation will be discussed.

Experimental

Catalysts with atomic composition 100Fe/4.6Si/1.0K, 100Fe/4.6Si/2.7Cu/1.0K, 100Fe/3.7Si/0.7K and an unpromoted catalyst were prepared by continuous precipitation and incipient wetness impregnation of promoters as previously described (1). A commercially prepared catalyst with mass composition 100Fe/8.9Cu/1.9K/67kaolin was obtained from United Catalysts Inc. Catalyst and Ethlyflo 164 (Ethyl) C_{30} oil were charged into a one liter autoclave operated as a continuous stirred tank reactor (cstr). Hydrogen activation was conducted by heating the reactor to 220^{O}C at 120^{O}C/h with hydrogen flow of 120 l h^{-1} (STP) at ambient pressure; conditions were maintained for 24 hours. Activation with carbon monoxide was conducted at 270^{O}C for 24 hours at 1.3 MPa pressure with a space velocity of 2 l h^{-1} g-Fe^{-1} (STP). Syngas activations were conducted at 270^{O}C for 24 hours with H_2/CO=0.7 and space velocity of 3.1 l h^{-1} g-Fe^{-1} (STP) at either ambient pressure or 1.3 MPa. Fischer-Tropsch synthesis was conducted at 270^{O}C, H_2/CO=0.7, space velocity=3.1 l h^{-1} g-Fe^{-1} (STP) and 1.3 MPa pressure.

Catalyst/slurry samples were removed from the reactor periodically during activation and throughout FT synthesis. Mössbauer spectra were obtained with a conventional constant acceleration spectrometer using 30 mCi ^{57}Co in rhodium matrix. Catalyst compositions are given as percent of total iron. For example, 80% Fe_5C_2 refers to 80% of the total iron in the catalyst being in Fe_5C_2.

Results

Hydrogen activation

Mössbauer spectroscopy data of 100Fe/4.6Si/2.7Cu/1.0K catalyst during hydrogen activation are shown in Figure 1. Exposure of the catalyst to hydrogen at 220^{O}C for 2 hours resulted in the catalyst being partially reduced to 20% Fe_3O_4 with the remaining 80% a superparamagnetic species. During the course of the activation, the Fe_3O_4 phase increased at the expense of the superparamagnetic species. Metallic iron (10%) was first detected after 10 hours of activation and after 24 hours of activation the catalyst composition was 65% Fe_3O_4, 24% metallic iron and 11% superparamagnetic species.

Exposure of the hydrogen activated catalyst to syngas at FT conditions caused rapid phase changes. Within 3 hours of starting FT synthesis, the superparamagnetic species had disappeared, the metallic iron decreased to 4% and ϵ'-$Fe_{2.2}C$ (34%) was formed. Following 20 hours of FT synthesis, the Fe_3O_4 had decreased slightly to 59% and the remainder of the catalyst was ϵ'-$Fe_{2.2}C$. Catalyst composition and syngas conversion as a function of time on stream are shown in Figure 3. The catalyst had high initial syngas conversion (85%) and deactivated slowly at the rate of 0.9% per week. The catalyst was run for over 3500 hours during which the catalyst composition remained constant at approximately 60% Fe_3O_4 and 40% ϵ'-$Fe_{2.2}C$.

Carbon monoxide activation

Phase changes for a typical iron-based catalyst during carbon monoxide activation are shown in Figure 4 (16). The 100Fe/8.9Cu/1.9K/67kaolin catalyst was initially α-Fe_2O_3 as determined by XRD and Mössbauer spectroscopy. The catalyst was reduced to 100% Fe_3O_4 during the heating from ambient temperature to 270^{O}C (2 hours) under carbon monoxide. Iron carbide phases began to appear after 4.5 hours of activation. The first carbide phase detected was a superparamagnetic carbide; this phase increased to approximately 10% of the iron and

remained constant throughout the activation. χ-Fe_5C_2 (26%) was first detected after 10 hours of activation and continued to increase at the expense of Fe_3O_4. The catalyst composition after 26 hours of activation was 90% χ-Fe_5C_2 and 10% superparamagnetic carbide. Carbon dioxide production as a function of time on stream is also plotted in Figure 4. Carbon dioxide can be produced by the reduction of α-Fe_2O_3 to Fe_3O_4 (equation 1), reduction of Fe_3O_4 to iron carbide (equation 2) and from the Boudouard reaction (equation 3).

$$3Fe_2O_3 + CO \rightarrow 2Fe_3O_4 + CO_2 \quad (1)$$

$$5Fe_3O_4 + 32CO \rightarrow 3Fe_5C_2 + 26CO_2 \quad (2)$$

$$2CO \rightarrow C + CO_2 \quad (3)$$

Figure 4 shows that enough carbon dioxide was produced after 8 hours to account for 100% carbiding of the catalyst; however, Mössbauer data reveal that the catalyst was approximately 10% iron carbide at this time. By the end of carbon monoxide activation, there was approximately 60% more carbon dioxide produced than was needed to completely carbide the catalyst. This indicates that a large amount of Boudouard carbon was produced.

Figure 5 shows that the iron carbide was partially oxidized to Fe_3O_4 (8%) after 20 hours of FT synthesis. Over the remainder of the run (140 h), the Fe_3O_4 content grew to 16% with the balance a mixture of χ-Fe_5C_2 and superparamagnetic carbide. Catalyst activity remained high during the run with carbon monoxide conversion greater than 65%.

An unpromoted iron catalyst was also activated with carbon monoxide under identical conditions to the catalyst described above. The catalyst was reduced to 94% χ-Fe_5C_2 and 6% Fe_3O_4 after 24 hours of activation; no superparamagnetic carbide was detected. This catalyst initially had high FT activity with syngas conversion of 84%; however, the catalyst was not stable and deactivated at the rate of 3.7% syngas conversion per day. The catalyst composition changed significantly during the deactivation; as the conversion decreased, the amount of χ-

Fe_5C_2 decreased and the amount of Fe_3O_4 increased. The catalyst was 100% Fe_3O_4 after 450 hours of FT synthesis and the syngas conversion had decreased to 18%.

Syngas activation

Catalyst composition and syngas conversion for the 100Fe/3.6Si/0.7K catalyst activated at FT synthesis conditions, syngas (H_2/CO=0.7) at 270^{O}C and 1.3 MPa, are shown in Figure 6 (16). Initial syngas conversion was 6% and it increased slowly to only 18% after 92 hours on stream; the catalyst was composed of 100% Fe_3O_4 during this time. Since the conversion was low, the catalyst was treated with carbon monoxide for 19 hours at 1.3 MPa and 270^{O}C. The catalyst was partially reduced to 42% χ-Fe_5C_2 and superparamagnetic carbide after the carbon monoxide treatment. Fischer-Tropsch synthesis was resumed and the syngas conversion increased rapidly to the same level obtained for another FT run when the catalyst was activated with carbon monoxide (Figure 6). This run was continued for 430 hours during which the syngas conversion remained close to 80% and the catalyst composition was approximately 40% χ-Fe_5C_2 and superparamagnetic carbide with the remainder Fe_3O_4.

Figure 7 shows the composition and syngas conversion for the 100Fe/3.6Si/0.7K catalyst after activation with syngas (H_2/CO=0.7) at ambient pressure and 270^{O}C for 24 hours (16). In contrast to activation with syngas at 1.3 MPa, activation at ambient pressure resulted in a catalyst with high syngas conversion (82%). The catalyst composition after activation was 68% χ-Fe_5C_2 and superparamagnetic carbide and 32% Fe_3O_4. The total iron carbide content decreased to 53% during the first 24 hours and then slowly decreased to 40% after 400 hours. The remainder of the catalyst was Fe_3O_4. Syngas conversion decreased slowly to 65% after 400 hours.

Discussion

Activation of the 100Fe/4.6Si/2.7Cu/1.0K catalyst with hydrogen at 220^{O}C for 24 hours partially reduced the catalyst to 24% metallic iron, 11% superparamagnetic species and 65%

Fe_3O_4. Exposing the activated catalyst to FT conditions caused the conversion of all of the metallic iron and superparamagnetic species and a small amount of Fe_3O_4 to ϵ'-$Fe_{2.2}C$. Throughout 3500 hours of FT synthesis, the catalyst composition remained constant at 40% ϵ'-$Fe_{2.2}C$ and 60% Fe_3O_4. The catalyst had high initial activity with syngas conversion greater than 80% and a deactivation rate of only 0.9% syngas conversion per week. In contrast, activation with carbon monoxide resulted in greater than 90% of an unpromoted iron catalyst and a 100Fe/8.9Cu/1.9K/67kaolin catalyst being reduced to χ-Fe_5C_2 and a small amount of superparamagnetic iron carbide. The superparamagnetic carbide was not identified because Mössbauer data were collected at room temperature; however, this may be small particle ϵ'-$Fe_{2.2}C$ (9). Activation with hydrogen lean syngas at ambient pressure was very similar to activation with carbon monoxide. The catalyst was composed of 68% χ-Fe_5C_2 and superparamagnetic carbide following activation.

Activation with hydrogen, carbon monoxide or syngas can result in high activity if the appropriate promoters and conditions are applied (Figure 8). Activation with hydrogen requires that the catalyst be promoted with copper to lower the reduction temperature and prevent sintering; catalysts activated with hydrogen that do not contain copper generally have lower activity and require a long induction period (17). In addition, a high space velocity of hydrogen is required to maintain a low water partial pressure in the reactor and thereby prevent sintering of metallic iron (7). In the case of syngas activation, a low hydrogen partial pressure is required to minimize the water concentration in the reactor which if too high prevents Fe_3O_4 from being reduced to χ-Fe_5C_2 (1). If the activation procedure is conducted properly, hydrogen, carbon monoxide or syngas activated catalysts will have similar activity. There does not seem to be a difference in the activity of hydrogen activated catalysts where the carbide phase of the active catalyst is ϵ'-$Fe_{2.2}C$ and the activity of carbon monoxide or syngas activated catalysts where the

predominant carbide phase is χ-Fe_5C_2. Likewise the deactivation characteristics of hydrogen, carbon monoxide and syngas activated catalysts are very similar over the span of at least 1000 hours (8). This is surprising because it has been reported that ϵ'-$Fe_{2.2}C$ is not as active as χ-Fe_5C_2 and the transformation of ϵ'-$Fe_{2.2}C$ into χ-Fe_5C_2 has been identified as a cause of deactivation of iron catalysts (6). Although it there is no difference in activity of ϵ'-$Fe_{2.2}C$ and χ-Fe_5C_2, a strong correlation between iron carbide content and FT activity has been observed. An unpromoted iron catalyst immediately following carbon monoxide activation was composed of 92% χ-Fe_5C_2 and 8% Fe_3O_4. The catalyst gradually oxidized to Fe_3O_4 during FT synthesis and after 450 hours was 100% Fe_3O_4. Catalyst activity, as measured by syngas conversion, decreased linearly from 84% to 19% as the catalyst was oxidized. Although the syngas conversion was 19% after the catalyst had been oxidized to Fe_3O_4, it is possible that the low activity was due to a small amount of iron carbide not detectable by Mössbauer spectroscopy (<5%) and not Fe_3O_4.

Catalysts which had stable activity were composed of 40% to 85% iron carbide and 60% to 15% Fe_3O_4 throughout FT synthesis. The question of how a catalyst can be partially and not completely oxidize during FT synthesis can be answered by thermodynamic analysis of the C/H/O/Fe system (8). A phase diagram of the C/H/O system is shown in Figure 9. The diagram is a ternary plot on the basis of mole % of C, H and O of the gases in the reactor atmosphere (CO, CO_2, H_2, H_2O and CH_x) at 300^{O}C and 1.5 MPa. Iron carbide and carbon are the stable phases in Region A, iron carbide, Fe_3O_4 and carbon are the stable phases in Region B, Fe_3O_4 and carbon are the stable phases in Region C and Fe_3O_4 is the stable phase in region D. Composition of the reactor atmosphere at syngas conversion ranging from 29% to 84% are shown on the phase diagram for a typical FT catalyst. The gas composition of the reactor atmosphere over this range of conversions lies close to the boundary of iron carbide/carbon and iron carbide/Fe_3O_4/carbon

regions. Another possible explanation for the presence of both iron carbide(s) and Fe_3O_4 is inhomogeneity within catalyst particles. The ultimate particle size of a precipitated iron catalyst is on the order of 200 Å and these particles form agglomerates which can be smaller than 1 μm or as large as 250 μm. Conversion of carbon monoxide and hydrogen to carbon dioxide, water and hydrocarbons in the interior of these agglomerates can cause the water and carbon dioxide concentrations within the particles to be higher than at the surface of the agglomerate which is exposed to the bulk gas phase. This could lead to the formation of particles with a Fe_3O_4 core and an iron carbide surface.

Conclusions

Formation of an iron carbide is necessary for high activity with precipitated iron catalysts. A precipitated iron catalyst (100Fe/4.6Si/2.7Cu/1.0K) which was activated with hydrogen at 220^{O}C and ambient pressure was partially reduced to metallic iron and Fe_3O_4. Metallic iron was not stable under FT conditions and exposure to syngas (H_2/CO=0.7) at 270^{o}C and 1.3 MPa converted all of the metallic iron to ϵ'-$Fe_{2.2}C$. Catalysts activated with carbon monoxide (unpromoted iron and 100Fe/8.9Cu/1.9K/67kaolin) or syngas with low hydrogen partial pressure (100Fe/3.6Si/0.7K) at 270^{O}C produced predominantly χ-Fe_5C_2 and had high initial syngas conversion. Activation with syngas at 270^{O}C and 1.3 MPa partially reduced the 100Fe/3.6Si/0.7K catalyst to 100% Fe_3O_4 which resulted in low FT activity. Iron carbides produced by carbon monoxide and syngas activation of promoted catalysts were partially oxidized to Fe_3O_4 during the first 24 hours of FT synthesis; however, these catalysts deactivated slowly. There was no difference in the activity, stability or deactivation characteristics of ϵ'-$Fe_{2.2}C$ and χ-Fe_5C_2 under the FT conditions employed in this study. Catalysts with stable activity maintained a constant iron carbide level. An unpromoted iron catalyst deactivated more rapidly than iron catalysts promoted with potassium, copper and a nonreducible metal oxide. The

deactivation of the unpromoted iron catalyst was caused by oxidation of active iron carbide to inactive/less active Fe_3O_4.

The presence of iron carbides and Fe_3O_4 together can be explained by inhomogeneity of gases within individual catalyst particles. Water and carbon dioxide produced by conversion of syngas within catalyst particles can cause the environment inside a particle to be oxidizing while the surface is exposed to reducing conditions of the reactor atmosphere. This would result in the formation of a Fe_3O_4 core and an iron carbide outer layer. Another possibility is that under typical FT conditions the redox potential of the reactor atmosphere lies within the narrow region of the C/H/O/Fe phase diagram where Fe_3O_4 and iron carbides can coexist.

Acknowledgment

This work was supported by the U.S. Department of Energy, Contract DE-FC26-98FT40308, and the Commonwealth of Kentucky.

References

1. R. J. O'Brien, L. Xu, R. L. Spicer, and B. H. Davis, *Energy & Fuels*, 10 (1996) 921.
2. R. J. O'Brien, L. Xu, D. R. Milburn, Y.-X. Li, K. J. Klabunde and B. H. Davis, *Topics in Catalysis*, 2 (1995) 1.
3. D. B. Bukur, M. Koranne, X. Lang, K. R. P. M. Rao and G. P. Huffman, *Applied Catal.*, 126 (1995) 85.
4. S. Soled, E. Iglesia and R. A. Fiato, *Catal. Letters*, 7 (1990) 271.
5. N. B. Jackson, A. K. Datye, L. Mansker, R. J. O'Brien, and B. H. Davis, in C. H. Bartholomew and G. A. Fuentes (Editors), Catalyst Deactivation, Elsevier Science B. V. 1997, pp. 517-526.
6. S. A. Eliason and C. H. Bartholomew, in C. H. Bartholomew and G. A. Fuentes (Editors), Catalyst Deactivation, Elsevier Science B. V. 1997, pp. 501-516.
7. M. E. Dry, in J. R. Anderson and M. Boudart (Editors), Catalysis Science and Technology, Vol 1, Springer-Verlag, New York, 1981, p. 157-255.
8. B. H. Davis, Department of Energy Final Report, Contract No. DE-AC22-94PC94055, 1998, pp. 66-82.
9. J. A. Amelse, J. B. Butt, and L. H. Schwartz, *J. Phys. Chem.*, 82 (1978) 558.
10. J. W. Niemantsverdriet, A. M. van der Kraan, W. L. van Dijk, and H. S. van der Baan, J. *Phys. Chem.*, 84 (1980) 3363.
11. F. Fischer, and H. Tropsch, *Ges. Abhandl. Kenntnis Kohle*, 10 (1932) 313.
12. J. T. Kummer, T. W. DeWitt and P. H. Emmett, *J. Am. Chem. Soc.*, 70 (1948) 3632.
13. D. M. Stockwell, D. Bianchi, and C. O. Bennett, *J. Catal.*, 113 (1988) 13.
14. J. P. Reymond, P. Mériaudeau, and S. J. Teichner, *J. Catal.*, 75 (1982) 39.

15. M. D. Shroff, D. S. Kalakkad, K. E. Coulter, S. D. Köhler, M. S. Harrington, N. B. Jackson, A. G. Sault and A. K. Datye, *J. Catal.*, 156 (1995) 185.

16. K. R. P. M. Rao, F. E. Huggins, G. P. Huffman, R. J. Gormley, R. J. O'Brien, and B. H. Davis, *Energy & Fuels*, 10 (1996) 546.

17. R. J. O'Brien, L. Xu, R. L. Spicer, S. Bao, D. R. Milburn, and B. H. Davis, Catalysis Today, 36 (1997) 325.

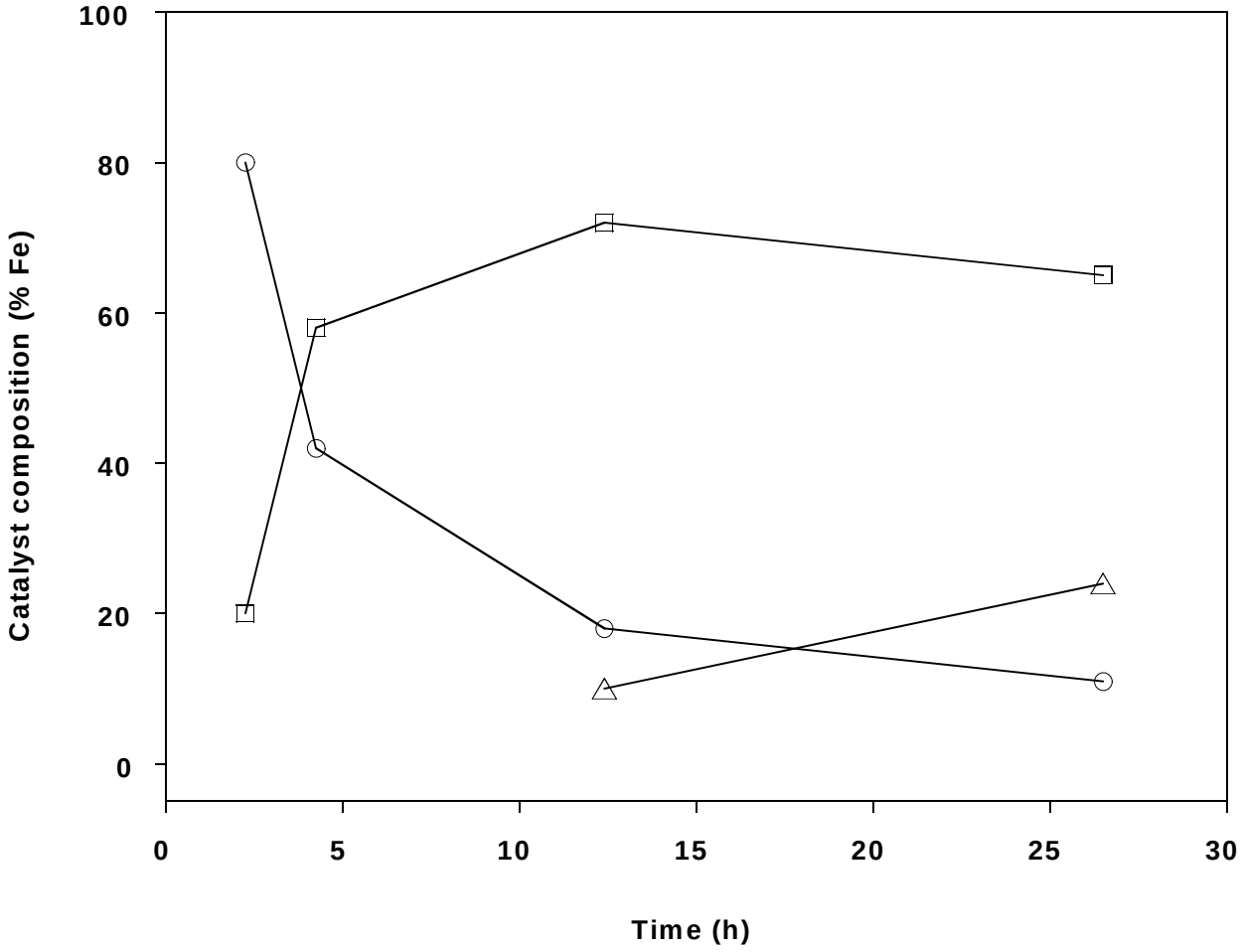

Figure 1. Phase composition changes of 100Fe/4.6Si/2.7Cu/1.0K catalyst during activation with H_2 at 220^{O}C, 0.1 MPa. (F), superparamagnetic oxide; (G), Fe_3O_4; (△), Fe^{O}.

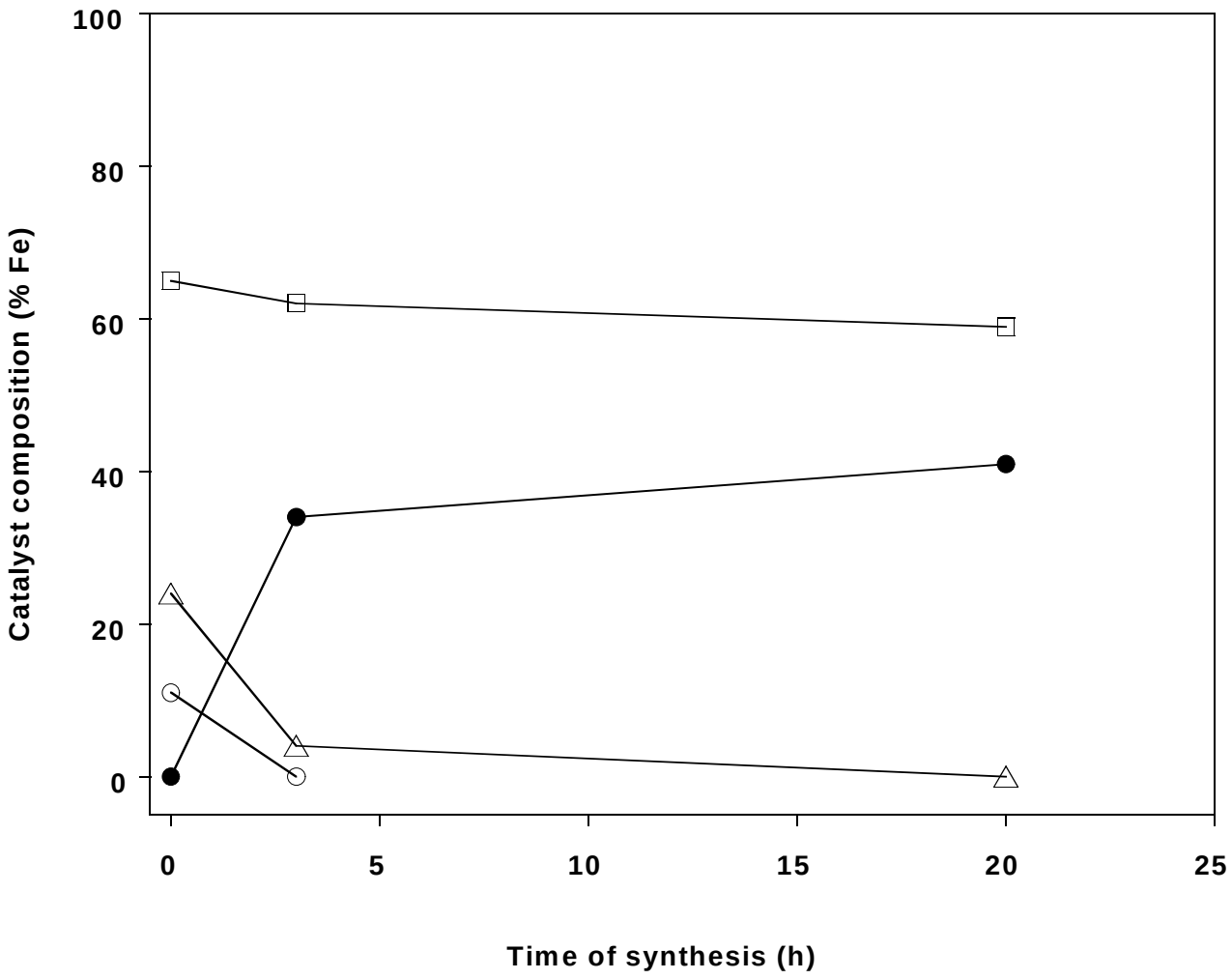

Figure 2. Phase composition changes of H_2 activated 100Fe/4.6Si/2.7Cu/1.0K catalyst during first 24 hours of FT synthesis (270^{O}C, 1.3 MPa, H_2/CO=0.7, whsv=3.1 sl h^{-1} g-Fe^{-1}). (F), superparamagnetic oxide; (G), Fe_3O_4; (△), Fe^{O}; (M), ϵ'-$Fe_{2.2}C$.

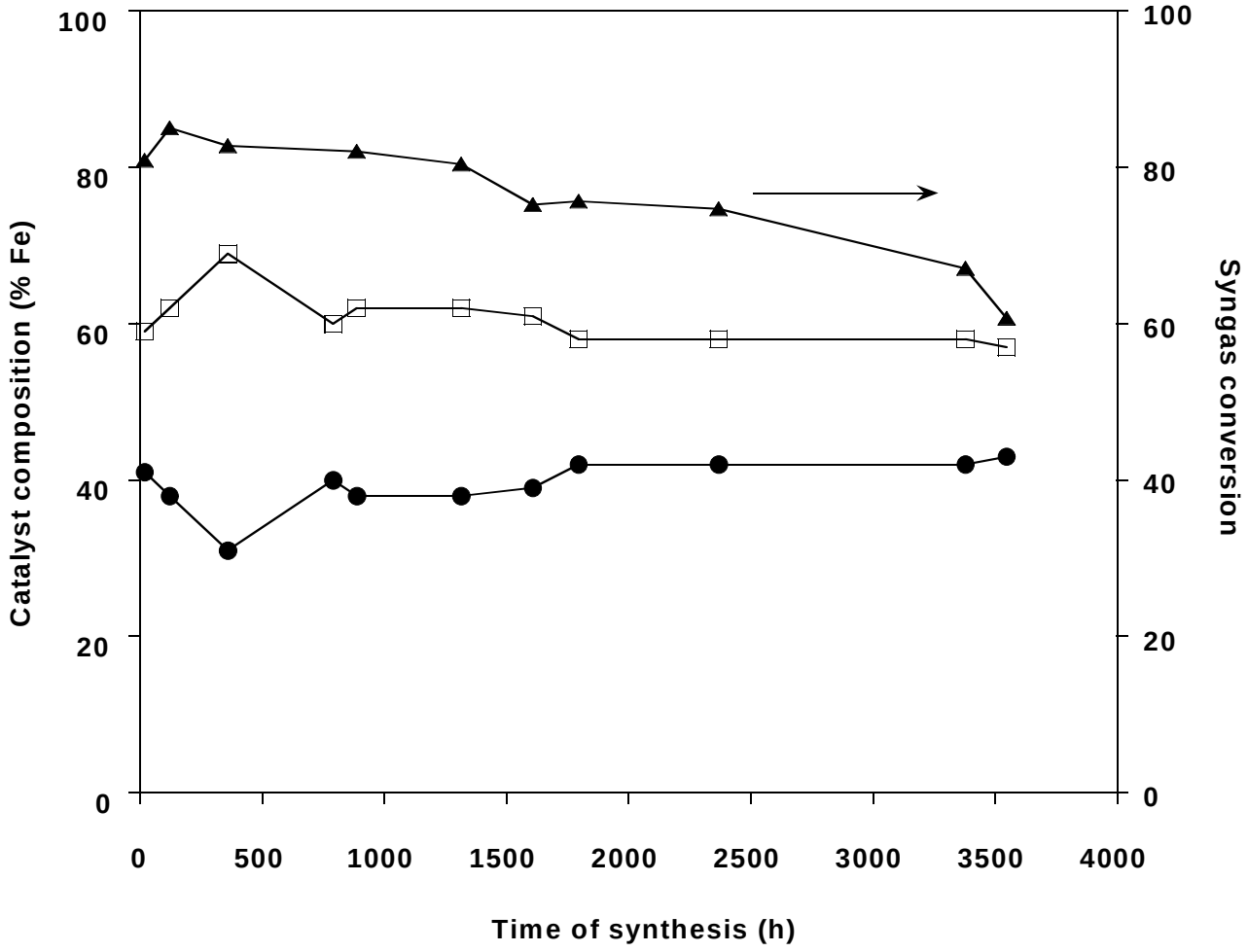

Figure 3. Long term phase composition of H_2 activated 100Fe/4.6Si/2.7Cu/1.0K catalyst during FT synthesis (270^{O}C, 1.3 MPa, H_2/CO=0.7, whsv=3.1 sl h^{-1} g-Fe^{-1}). (G), Fe_3O_4; (M), ϵ'-$Fe_{2.2}C$; (▲), syngas conversion.

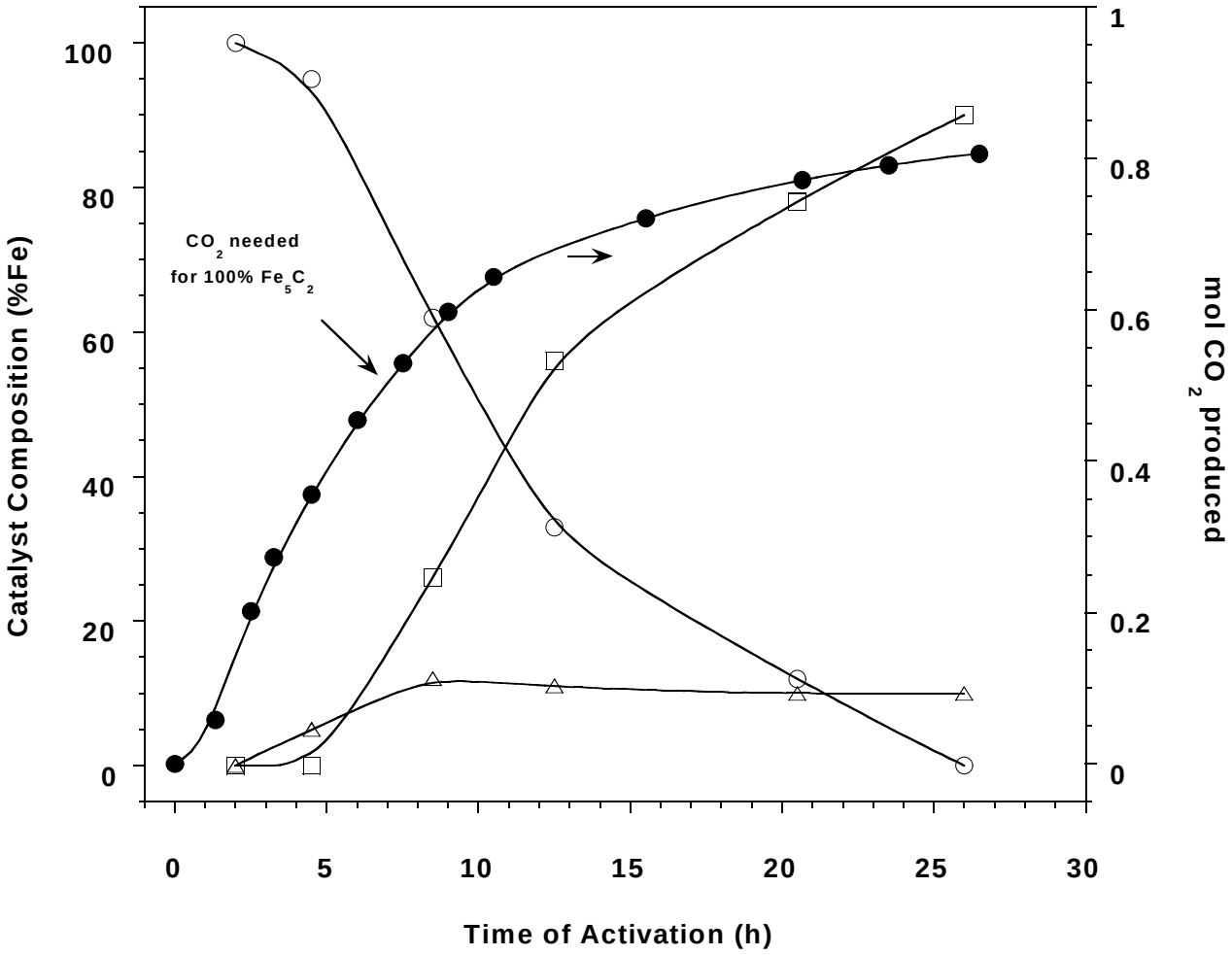

Figure 4. Phase composition changes of commercial 100Fe/8.9Cu/1.9K/67kaolin catalyst and moles of CO_2 generated during CO activation. (F), Fe_3O_4; (G), χ-Fe_5C_2; (△), superparamagnetic carbide; (M), moles of CO_2. Mössbauer data from reference 16.

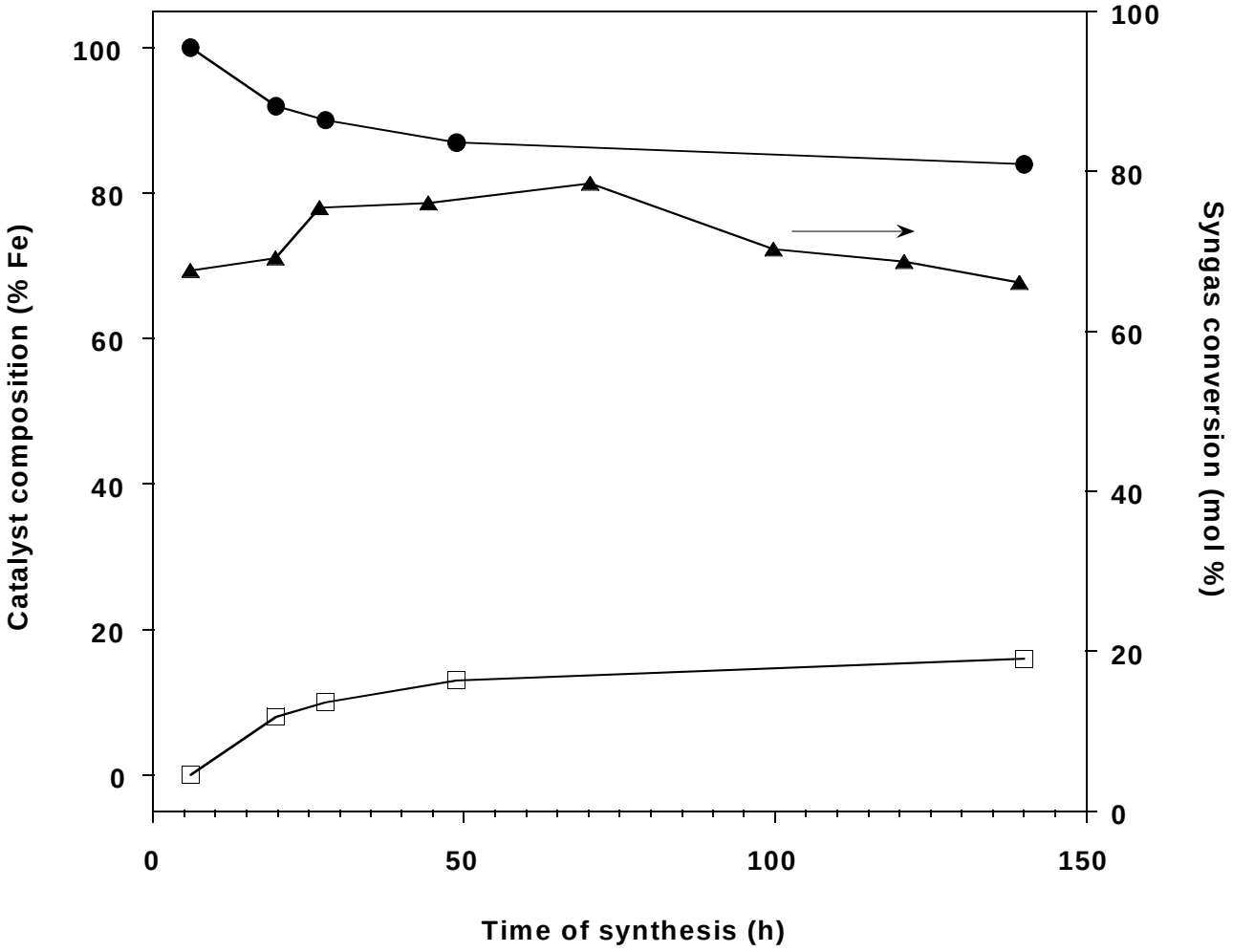

Figure 5. Phase composition of CO activated 100Fe/8.9Cu/1.9K/67kaolin catalyst during FT synthesis (270^{O}C, 1.3 MPa, H_2/CO=0.7, whsv=3.1 sl h^{-1} g-Fe^{-1}). (M), χ-Fe_5C_2 and superparamagnetic carbides; (G), Fe_3O_4; (▲), syngas conversion. Data from reference 16.

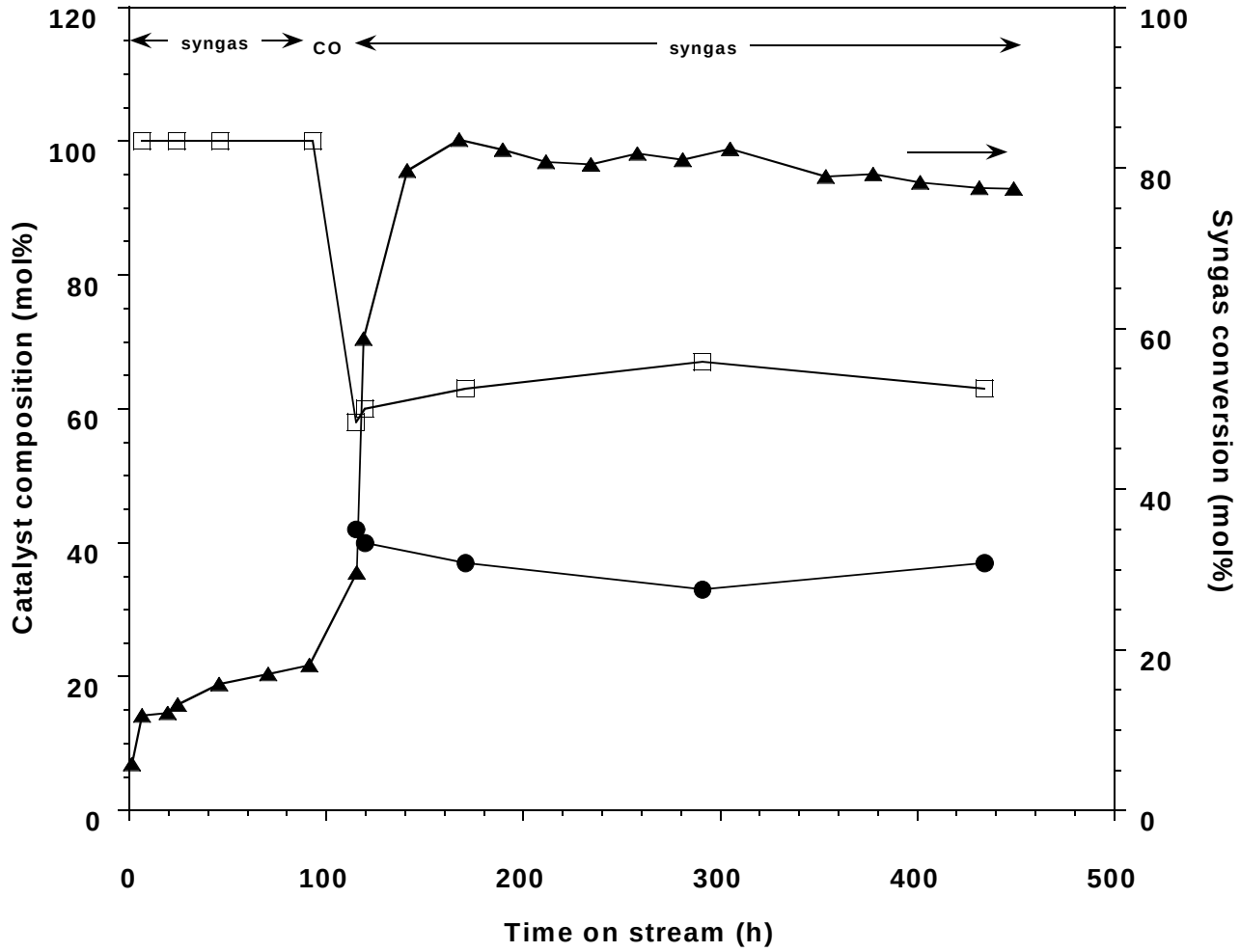

Figure 6. Phase composition of 100Fe/3.7Si/0.7K catalyst during syngas activation at 270^{O}C, 1.3 MPa followed by CO treatment at 270^{O}C, 1.3 MPa followed by FT synthesis (270^{O}C, 1.3 MPa, $H_2/CO=0.7$, whsv=3.1 sl h^{-1} g-Fe^{-1}). (G), Fe_3O_4 and superparamagnetic oxide; (M) χ-Fe_5C_2 and superparamagnetic carbides; (▲) syngas conversion. Data from reference 16.

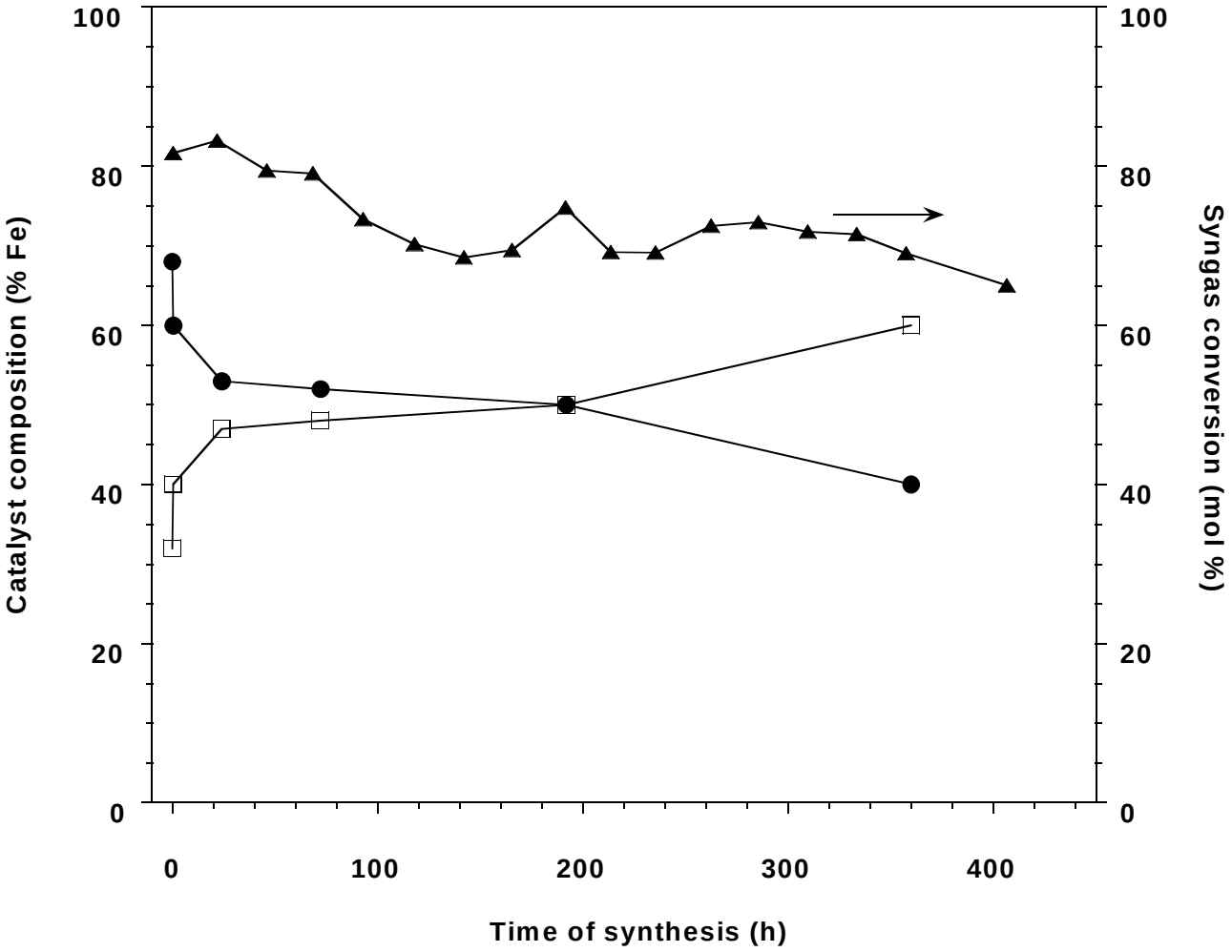

Figure 7. Phase composition of syngas activated (H_2/CO=0.7, 0.1 MPa, 270^{O}C) 100Fe/3.7Si/0.7K catalyst during FT synthesis (270^{O}C, 1.3 MPa, H_2/CO=0.7, whsv=3.1 sl h^{-1} g-Fe^{-1}). (M), χ-Fe_5C_2 and superparamagnetic carbides; (G), Fe_3O_4; (▲) syngas conversion. Data from reference 16.

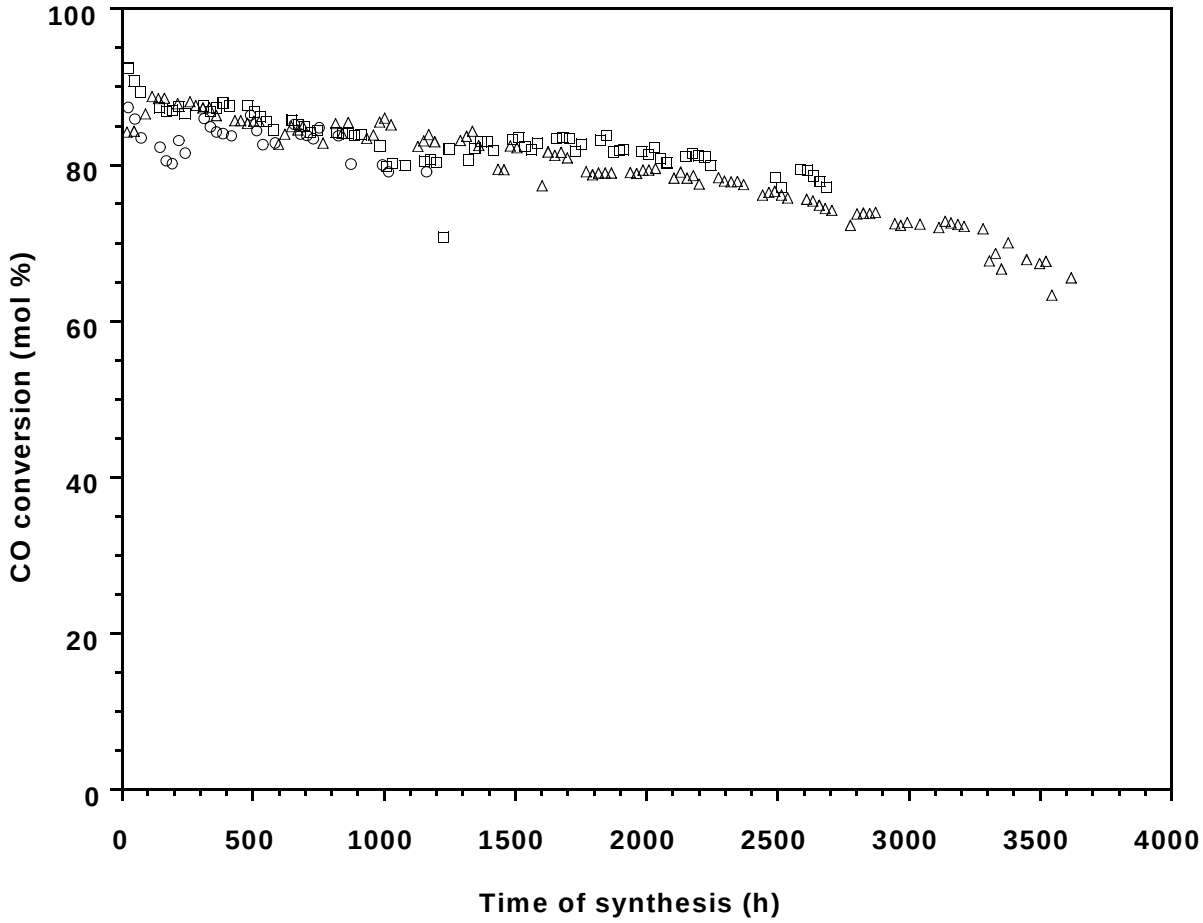

Figure 8. Comparison of CO conversion for (F), 100Fe/4.6Si/1.0K activated with CO at 270^{O}C, 0.1MPa; (G), 100Fe/4.6Si/1.0K, activated with syngas (H_2/CO=0.7) at 270^{O}C, 0.1 MPa; and (△) 100Fe/4.6Si/2.0Cu/1.0K activated with H_2 at 220^{O}C, 0.1 MPa. FT conditions: 270^{O}C, 1.3 MPa, H_2/CO=0.7, whsv=3.1 sl h^{-1} g-Fe^{-1}).

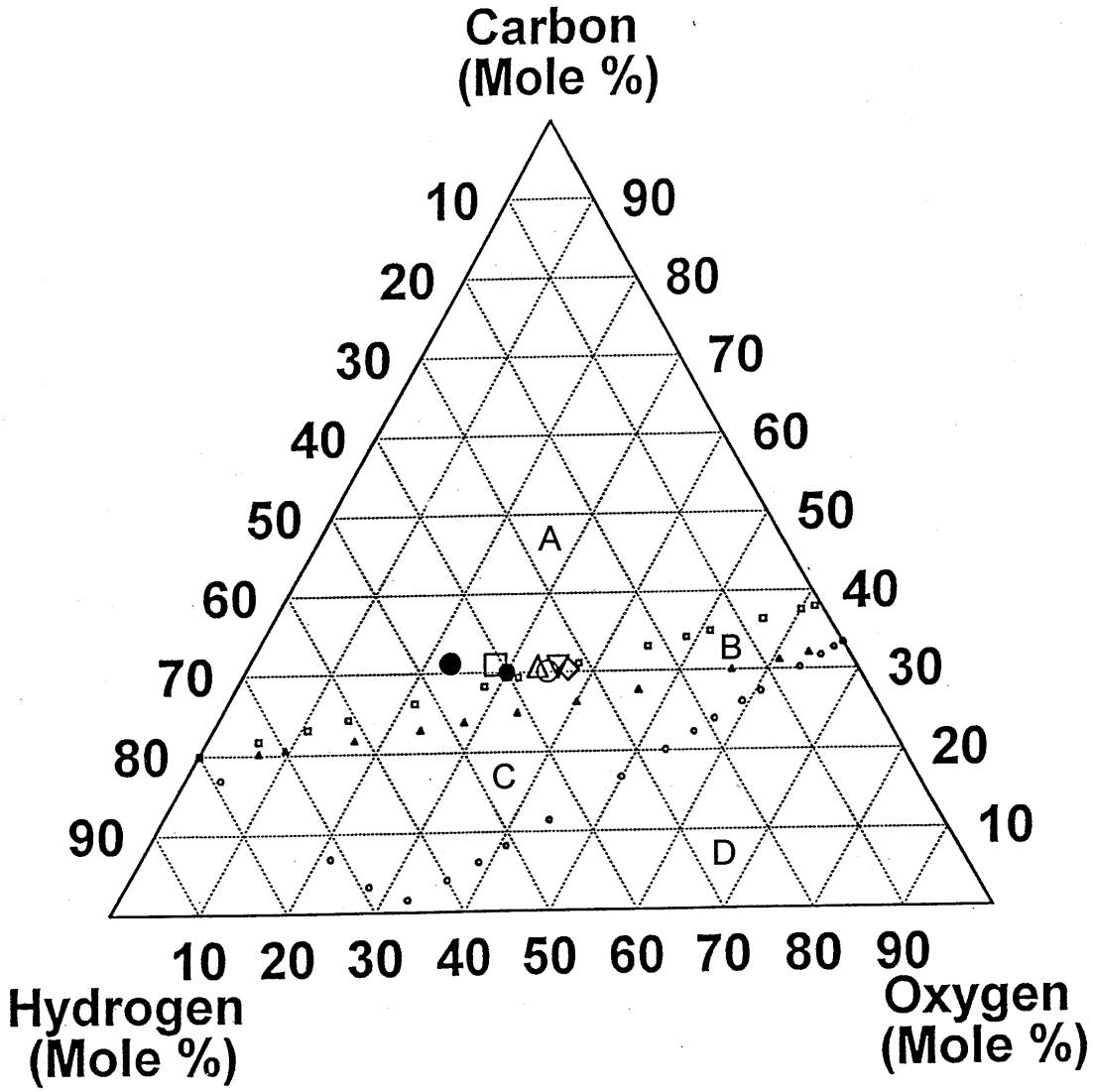

Figure 9. Ternary phase diagram for solid phase(s) present for graphite/gases (F), Fe/Fe_3O_4/gases (G) and Fe/Fe_3C/gases (△) at equilibrium at 300^{O}C ant 1.5 MPa. Region A: Fe_3C and C; Region B: Fe_3O_4, Fe_3C and C; Region C: Fe_3O_4 and C; Region D: Fe_3O_4. Gases = H_2O, CO, CO_2, H_2 and CH_4. Gas phase composition during FT synthesis (270^{O}C, 1.3 MPa) at various conversions: CO=86%, H_2=80% (M); CO=78%, H_2=76% (G); CO=68%, H_2=69% (△); CO=46%, H_2=54% (◇); CO=32%, H_2=45% (▽); CO=23%, H_2=37% (F) and syngas composition of H_2/CO=0.67 (M).

C. Mössbauer Study of Precipitated Unpromoted and Potassium Promoted Iron Fischer-Tropsch Synthesis Catalyst

Introduction

As the alternative route to synthesize hydrocarbons other than petroleum industry, Fischer-Tropsch synthesis has been one of the most extensively studied subject in catalysis for several decades. Although most of the recent effort in industry concentrated on cobalt catalyst, iron is still a promising catalyst due to its several advantages, especially for slurry phase reactor. The complexity of phase transformation of iron catalyst during activation and synthesis cause difficulty to accurately elucidate the active phase. Studies to correlate the structure of catalysts with FTS activity were conducted by different authors to define the active phase of iron catalyst. At present the question remains whether magnetite is active for FTS. Early work by Reymond et al (1) and recent work by Kuivila et al. (2) suggest that magnetite is the active phase. Reymond's experiments were performed on both unreduced and reduced iron catalyst. Similar hydrocarbon product distributions were found on these two catalysts, with a maximum activity occurring over a material consisting of approximately equal amounts of magnetite and Hägg carbide. Further carbide formation in the unreduced catalyst coincided with a diminished rate of FT synthesis; therefore, it was concluded that magnetite is an active catalyst. Kuivila studied the reduced and unreduced iron catalyst using the combination of XPS and FTS performance. Their conclusion was based on the fact that they observed only magnetite on the surface of the catalyst after reaction. A similar study was carried out by Dictor and Bell (3) in a slurry-phase reactor using reduced and unreduced Fe_2O_3 powder. However, they concluded that the active phase is Hägg carbide and magnetite is not active.

The work described in this report shows that with appropriate methods to withdraw catalyst samples for characterization, the catalyst situation in the continuous stirred tank reactor

can be revealed during activation and synthesis. Correlation between catalyst composition and FTS activity is made to define the nature of active phase. Comparison with results previously obtained on ultrafine iron catalyst and unpromoted precipitated iron catalyst is made in this report.

Experimental

Catalyst activation and FTS reaction

The catalyst used was prepared by continuous precipitation at a pH of about 9 from aqueous solution of $Fe(NO_3)_3 9H_2O$ and concentrated NH_4OH. The precipitate was throughly washed with distilled-deionized water and dried at 120^0C. A mixture of 64.44g iron catalyst which contains 50.00% Fe, 0.457g of $(CH_3)_3COK$ and 290g C_{30} startup oil (Shell decene trimer) was charged into a 1L autoclave operated as a continuous stirred tank reactor (CSTR). The catalyst slurry was heated to 270^0C at 2^0C/min under a flow rate of 2.0[NL/hg-(Fe)] CO. CO activation continued at 270^0C and 1.20MPa for 24h. Flowing activation, hydrogen flow was started to give a H_2/CO ratio of 0.68 with a flow rate of 3.1NL/hg-(Fe). Catalyst slurry samples (5-10g) were removed from the reactor under the protection of Ar following activation and during different stages of synthesis. Mössbauer samples were prepared in sample holders in a glove bag filled with Ar. Wax products on the catalyst was extracted using THF as the solvent.

Mössbauer analysis

Mössbauer samples were loaded into plexiglass compression holders after extract of wax with THF in a glove bag filled with Ar.

Results

CO conversion versus time on stream was plotted in Fig. 1 for unpromoted iron catalyst and Fig 2 for potassium promoted iron. After 24 hours of activation in CO, both catalysts exhibited high activity (over 80%), and the induction time to attain maximum conversion is very

short. The activity of the catalyst slowly, but continuously, declined with increasing time-on-stream. The deactivation rate for the unpromoted iron is slower than for potassium promoted iron, as observed previously.

Mössbauer analysis results of samples (unpromoted iron) withdrawn from reactor are listed in Table 1. Immediately after CO activation, the catalyst composition was predominantly Hägg carbide (Fe_5C_2), and the Mössbauer spectrum of this sample contains very small magnetite peaks. Fitting results revealed that 93.6% of iron phase is Hägg carbide. No metallic iron was detected. The spectrum of the sample removed after 23h of FT synthesis is more complicated; peaks of magnetite grows larger and overlap with the peaks of iron carbide. As indicated in Table 1, about 83.3% of spectra area was associated with Hägg carbide, and the area ratio of A to B patterns obtained for this phase was 0.76:2; still no metallic iron was found in the spectrum. After exposed to syngas for 168h, peaks of Hägg carbide became relatively lower and the area of magnetite contribute the largest part to the overall spectrum. The data show 58.5% of the iron exists in the form of magnetite and 41.5% Hägg carbide. The A to B site ratio is 0.71:2. The Mössbauer spectrum of sample removed after 453h of Fischer-Tropsch synthesis is simple since the amount of iron carbide is so low that it cannot be observed in the Mössbauer spectrum. The A to B site ratio is 0.95:2.

Discussion

The excellent agreement of catalytic activity with the percentage of iron carbide clearly shows that iron carbide is the active phase while the Fischer-Tropsch synthesis activity of magnetite is negligible.

Mössbauer studies of ultrafine iron catalyst by Huang et al., (4) suggested that after 24h of CO pretreatment, the catalyst was the carbide (ca. 4% iron oxide). With the increase of time on stream, reoxidation of iron carbide took place during the synthesis. After 100h of FT

synthesis, no iron carbide can be observed in Mössbauer spectrum. Consistency of results on precipitated and ultrafine catalyst proved that our results are reliable and repeatable. The work described in this note also supports Huang et als. conclusion that CO pretreatment for 24h almost completely transform Fe_2O_3 to Hägg carbide even without the presence of potassium promoter.

Shroff et al (5) emphasized the importance of passivation of iron Fischer-Tropsch catalysts. They claimed that active phase of iron could get oxidized without sufficient attention to passivation. Mössbauer spectroscopy is an ex situ characterization technique. However, our results show that with appropriate methods to withdraw the sample from the reactor, remove wax and load into the sample holder, the iron active phase could be protected without oxidation. The fact that the initial sample withdrawn from the reactor is always found to be nearly all iron carbide eliminates sample contamination after withdrawal determining the sample compositin. Furthermore, sample contamination by oxidation by exposure to air should be random, and not to always show a gradual decline. The problem of only observing magnetite as the only detectable phase in the catalyst is most likely due to the sample handling method.

From our results, iron carbide is reoxidized to magnetite with increasing time-on-stream. Water and/or CO_2 are believed to be responsible for such oxidations (6). Rao et al. (7) studied the correlation of catalytic activity of iron catalyst promoted by potassium. They concluded that when a catalyst activation produces both an active catalyst and a high fraction of iron carbide, during the synthesis there will be a conversion of the carbide to the oxide with the attainment of a “pseudo-steady-state” composition. However, our result on precipitated unpromoted iron catalyst shows that oxidation of iron carbide takes place throughout the synthesis procedure. According to Amelse et al (8) and Bianchi et al (9), even at the low conversion rate, there is a strong interaction of water with iron surfaces. Actually, besides accelerating carburization, the

alkali promoter is also believed to stabilize the carbidic phase (3,10). Therefore, the pseudo-steady-state is likely to happen only under the presence of alkali and other promoters which stabilize iron carbide from oxidation.

Magnetite has a unit cell composed of 32 close-packed oxygen atom in which cations occupy 8 tetrahedral (A) and 16 octahedral (B) sites (11). The theoretical value of the A to B ratio for the ideal spinel structure is 1:2. Generally, cation vacancies selectivity form on the B-sites; thereby producing a ratio greater than 1:2. A to B site ratios of our sample are 0.77:2 (after activation), 0.76:2 (after 23h FTS), 0.71:2 (after 168h FTS), and 0.95:2 (after 453h FTS). This means that A sites are not occupied by Fe ions. This appears to require that cation vacancies exist or carbon occupies the B-sites. If carbon occupies these sites, the fraction of carbon per "molecule" would be 0.23, 0.24, 0.29 and 0.05, respectively. Therefore, we concluded that magnetite phase contains carbon atoms on the A-sites, especially in the samples with the multiple phases.

The potassium promoted catalyst samples withdrawn from the reactor will be analyzed by Mossbauer spectroscopy and the data will be included in the next report.

References

1. J. P. Reymond, P. Meriaudeau and S. J. Teichner, *J. Catal*., **75** (1982) 39.
2. C. S. Kuivila, P. C. Stair, and J. B. Butt, *J. Catal*., **118** (1989) 299.
3. R. A. Dictor and A. T. Bell, *J. Catal*., **97** (1986) 121.
4. C. S. Huang, B. Ganguly, G. P. Huffman, F. E. Huggins and B. H. Davis, *Fuel Sci. Technol. Int*., **11** (1993) 1289.
5. M. D. Shroff and A. K. Datye, *Catal. Lett*., **37** (1996) 101.
6. J. F. Schulz, W. K. Hall, B. Seligman and R. B. Anderson, *J. Am. Chem. Soc*., **77** (1955) 213.
7. K. R. P. M. Rao, F. E. Huggins, G. P. Huffman, R. J. Gormley, R. J. O'Brien, B. H. Davis, *Energy & Fuel*, **10** (1996) 547.
8. J. A. Amelse, L. H. Schwartz, and J. B. Butt, *J. Catal*., **72** (1981) 95.
9. D. Bianchi, S. Borcar, F. Toule-Gay, and C. O. Benett, *J. Catal*, **82** (1983) 442.
10. G. L. Vogler, X. Z. Jiang, J. A. Dumesic, and R. J. Madon, *J. Catal*., **89** (1984) 116.
11. E. Murad, and J. H. Johnson, in "Mossbauer spectroscopy applied to inorganic chemistry", Plenum Press, New York, NY, 1987, Vol. 2, pp 512.

Table 1

Mössbauer parameters for precipitated iron catalyst after activation and during synthesis

Sample	Site	HMF(KG)	IS(mm/s)	QS(mm/s)	FW(mm/s)	Fraction
After activation	Fe_3O_4 A	483	0.28	0.04	0.26	1.7
	Fe_3O_4 B	455	0.64	-0.08	0.41	4.4
	Fe_5C_2 I	220	0.26	0.04	0.40	33.6
	Fe_5C_2 II	182	0.20	-0.01	0.42	29.3
	Fe_5C_2 III	101	0.22	0.08	0.50	30.7
FTS run 23h	Fe_3O_4 A	485	0.32	-0.07	0.26	4.6
	Fe_3O_4 B	455	0.67	0.01	0.46	12.1
	Fe_5C_2 I	220	0.26	0.04	0.38	31.1
	Fe_5C_2 II	182	0.24	-0.01	0.36	26.2
	Fe_5C_2 III	100	0.16	-0.1	0.44	26.0
FTS run 168 h	Fe_3O_4 A	487	0.27	0.0	0.28	15.3
	Fe_3O_4 B	458	0.65	-0.01	0.50	43.2
	Fe_5C_2 I	218	0.27	0.04	0.90	23.9
	Fe_5C_2 II	180	0.19	0.09	0.28	5.1
	Fe_5C_2 III	100	0.18	0.11	0.68	12.5
FTS run 453 h	Fe_3O_4 A	488	0.28	0.01	0.25	32.2
	Fe_3O_4 B	459	0.65	0.0	0.32	67.8
	Fe_5C_2 I	----	----	----	----	----
	Fe_5C_2 II	----	----	----	----	----
	Fe_5C_2 III	----	----	----	----	----

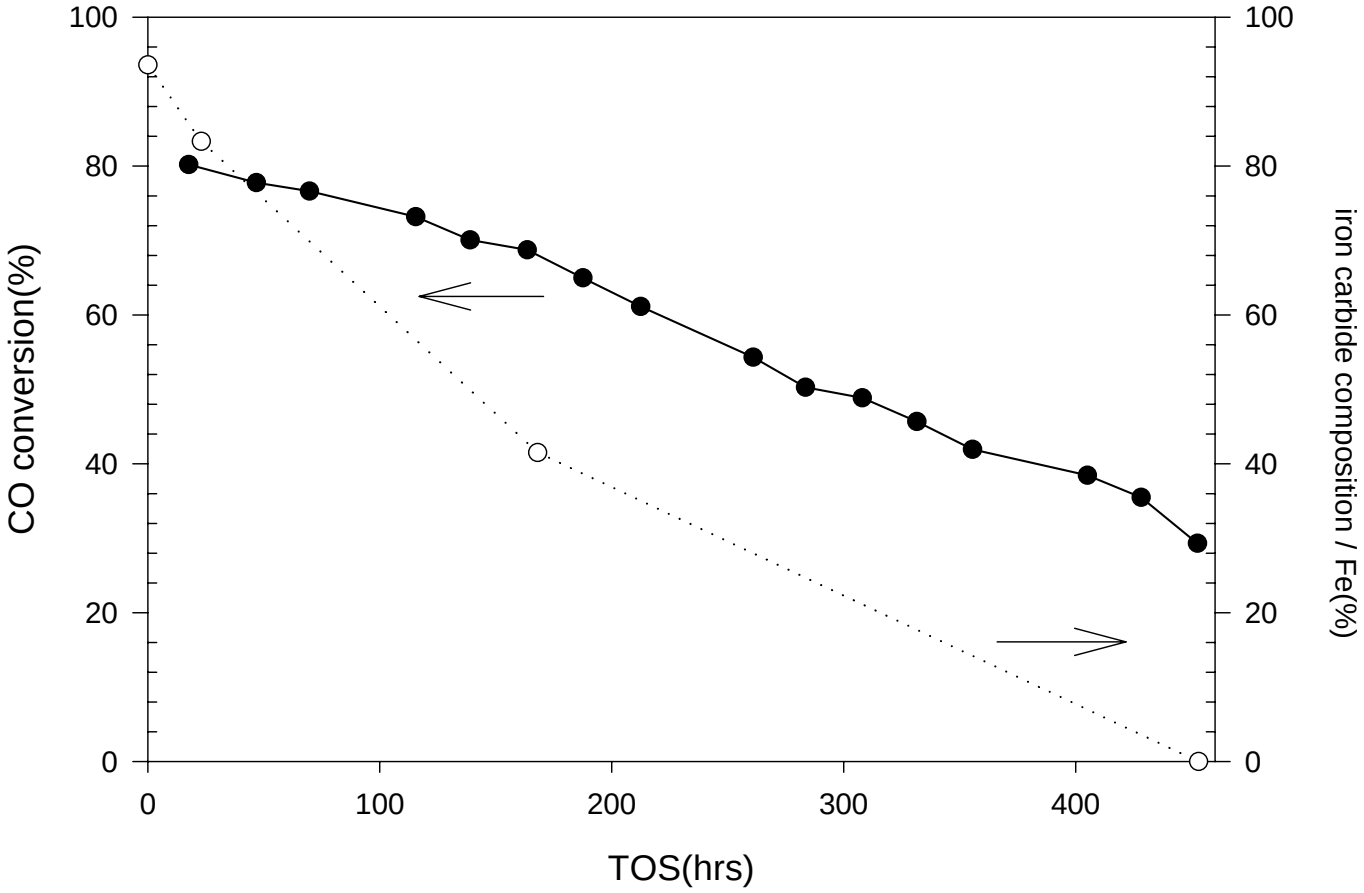

Fig. 1 Catalytic activity and iron carbide percentage versus reaction time

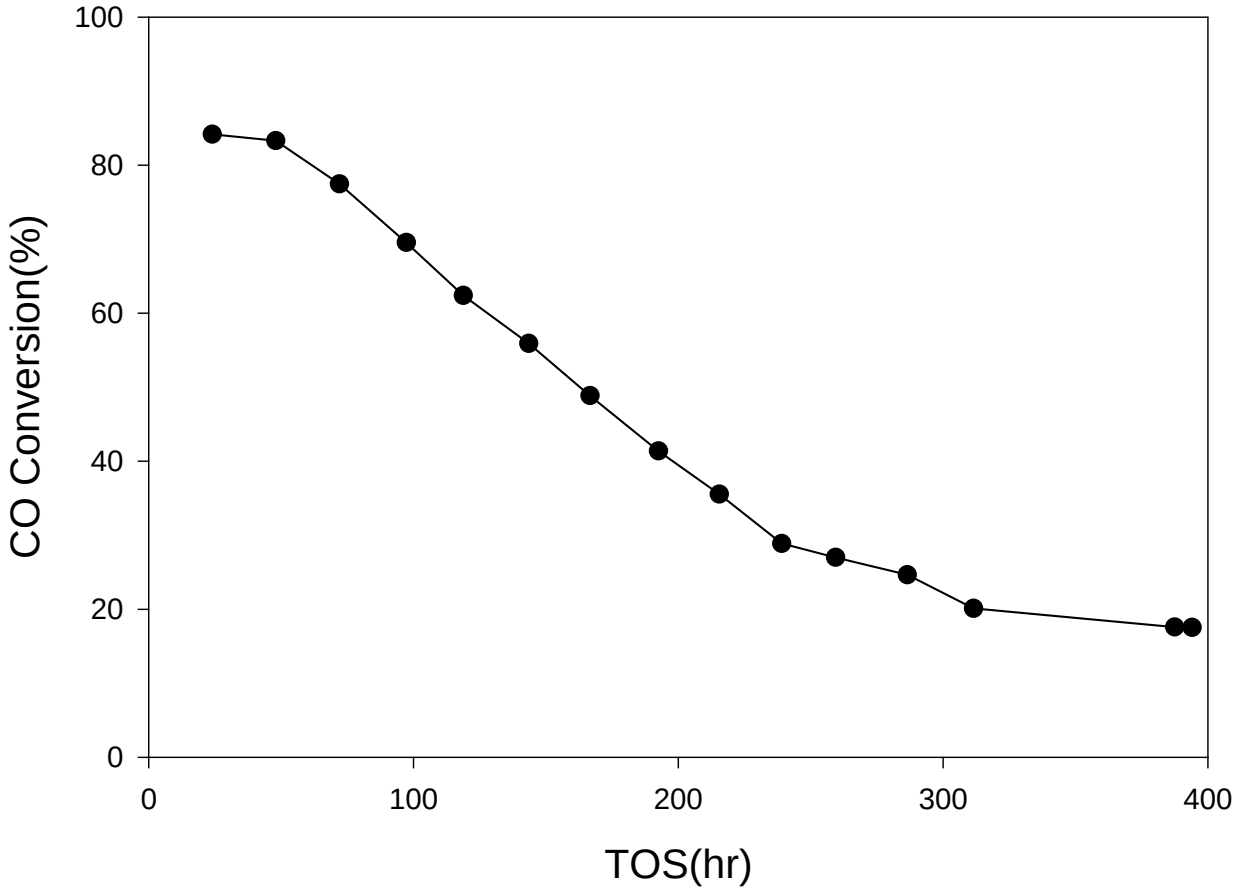

Fig 2. CO Conversion as a function of time on stream

D. Characterization of Iron Phase Change During Fischer-Tropsch Synthesis Reaction

Introduction

Iron-based Fischer-Tropsch (FT) catalysts undergo a series of phase transformations during activation and use (1). Activation with carbon monoxide or syngas typically results in the conversion of Fe_2O_3 to Fe_3O_4 and ultimately to one or more carbides (2). During FT synthesis, iron carbides can be oxidized to Fe_3O_4 if the H_2O/H_2 or CO_2/CO ratios are high enough (1). There has been considerable debate about the active phase of the FT synthesis. Some studies have indicated an active oxide species (3) while most have supported a carbide species (2,4). Mössbauer spectroscopy has proven to be an effective technique for the analysis of iron-based FT catalysts. *In situ* Mössbauer studies have been reported (5,6); however, these studies have been performed at low pressure and low conversions. Studies performed at industrially relevant conditions have generally involved removing the catalyst from the reactor followed by passivation (7) which, if not performed properly, will oxidize the catalyst (4). Herein are reported the Mössbauer results obtained on an unpromoted precipitated iron catalyst that was activated and reacted in a slurry phase, continuous stirred tank reactor at high conversion and under industrially relevant conditions. Strict measures were observed to prevent oxidation of the catalyst samples. The Fe-Si, Fe-K, Fe-Si-K catalysts were all studied using the same methods.

Experimental

Catalysts were prepared by a previously described procedure (2). A slurry of 64.4 g of catalyst (32.2 g Fe) and 290 g of Ethylflo 164 decene trimer was charged into a one liter autoclave operated as a continuous stirred tank reactor. The catalyst was activated with carbon monoxide (2 L h^{-1} g·Fe^{-1}, STP) at 270^{O}C and 1.3 MPa for 24 hours. Following activation, syngas flow was initiated (3.1 L h^{-1} g·Fe^{-1}, STP) and the temperature and pressure were maintained. Catalyst slurry samples (5-10 g) were removed from the reactor under an argon atmosphere via a

dipleg immediately after activation and at various times during FT synthesis. Light wax was extracted from the cooled slurry samples under an argon atmosphere with deoxygenated tetrahydrofuran. Catalyst samples were loaded into sealed plexiglass holders for analysis by Mössbauer spectroscopy. The spectra were collected by a conventional constant acceleration spectrometer using a 30 mCi ^{57}Co in rhodium matrix.

Results

Syngas conversion versus time on stream for unpromoted iron catalyst is shown in Figure 1. Syngas conversion after 24 hours of FT synthesis was above 84%. Catalyst activity declined steadily throughout the run with an average rate of deactivation of 0.16 % h^{-1} (absolute syngas conversion).

Catalyst samples for Mössbauer spectroscopy were withdrawn immediately after activation and at 23 h, 168 h and 453 h of FT synthesis. The distribution of iron in the catalyst after activation with carbon monoxide was 94 % χ-Fe_5C_2 and 6 % Fe_3O_4. Exposure to syngas initiated oxidation of the χ-Fe_5C_2 to Fe_3O_4. After 23 hours of FT synthesis, 83 % of the iron was present as χ-Fe_5C_2 and the balance was Fe_3O_4. The amount of iron present as χ-Fe_5C_2 had decreased to 18 % after 168 hours of FT synthesis. The only detectable phase after 453 hours of FT synthesis was Fe_3O_4.

The deactivation rates of Fe-Si, Fe-K, and Fe-K-Si have been determined and the catalyst samples have been withdrawn from the reactor right after activation and at different conversion levels. The Mössbauer spectra of the catalysts are going to be recorded to identify the phase changes.

The Fischer-Tropsch synthesis activity of unpromoted, potassium promoted (100Fe/0.71K), silica promoted (100Fe/4.6Si) and double promoted (100Fe/4.6Si/0.71K)

catalysts were plotted in Figure 2. It can been seen from Figure 2 that Fe and Fe-K catalysts have essentially the same activity during the initial induction period (within 50hrs time on stream) which is higher than Fe-Si and Fe-Si-K catalysts. But the activity of both Fe and Fe-K catalyst decrease steadily with time on stream. For Fe-Si and Fe-Si-K catalysts, they both undergoes an induction period, the activity first goes up until it reaches the maximum and then decrease slowly. After 94 hours of synthesis, the CO conversion of Fe-Si catalyst was 76.1% while the Fe-Si-K catalyst reaches its maximum conversion of 84.04% at 163 hrs time on stream. The average deactivation rate for the catalysts are Fe-K(48%/week), Fe(41%/week), Fe-Si(39%/week) and Fe-Si-K(33%).

Discussion

Based on data generated from several catalysts, a model of the working FT catalyst was developed. In this model, the initial catalyst was essentially comprised of a mixture of iron carbides. As the reaction progressed, the carbide fraction decreased to attain a value of about 30-40%. During this phase change, the conversion did not decrease appreciably. To account for the nearly constant activity while the phase changed a model was proposed. This model had the assumption that the core of each particle was oxidized to form Fe_3O_4 and an out layer remained a carbide form; thus, the surface of the catalyst remained essentially the carbide form while the ratio of oxide/carbide increased as the core consisting of Fe_3O_4 expanded to approach a "steady state at carbide/oxide ratio.

The results with the unpromoted catalyst do not agree with this model. Instead, it appears that the catalyst particle converts from the carbide to the oxide form in parallel with the decline in conversion. Thus, it appears that a steady-state surface carbide phase/core Fe_3O_4 phase is not formed for the unpromoted iron catalyst. One explanation to account for this is that the rate of carbide oxidation is dependent upon the particle size for the unpromoted catalyst.

Work underway with single and doubly promoted catalysts should allow us to define the role of each promoter in determining the composition of the working catalysts.

References

1. Dry, M. E. In Catalysis-Science and Technology; Anderson, J. R., Boudart, M. Eds.; Springer-Verlag: New York, 1981; Vol. 1, pp 196-198.
2. O'Brien, R. J., Xu, L., Spicer, R. L., Davis, B. H., Energy & Fuels, 10, 921 (1996).
3. Reymond, J. P., Mériaudeau, P., Teichner, S. J., J. Catal., 75, 39 (1982).
4. Shroff, M. D., Kalakkad, D. S., Coulter, K. E., Köhler, S. D., Harrington, M. S., Jackson, N. B., Sault, A. G., Datye, A., J. Catal., 156, 185 (1995).
5. Berry, F. J., Smith, M. R., J. Chem. Soc. Faraday Trans., 85, 467 (1989).
6. Raupp, G. B., Delgass, W. N., J. Catal., 58, 361, (1979).
7. Huang, C. S., Ganguly, B., Huffman, G. P., Huggins, F. E., Davis, B. H., Fuel Sci. Technol. Int., 11, 1289 (1993).

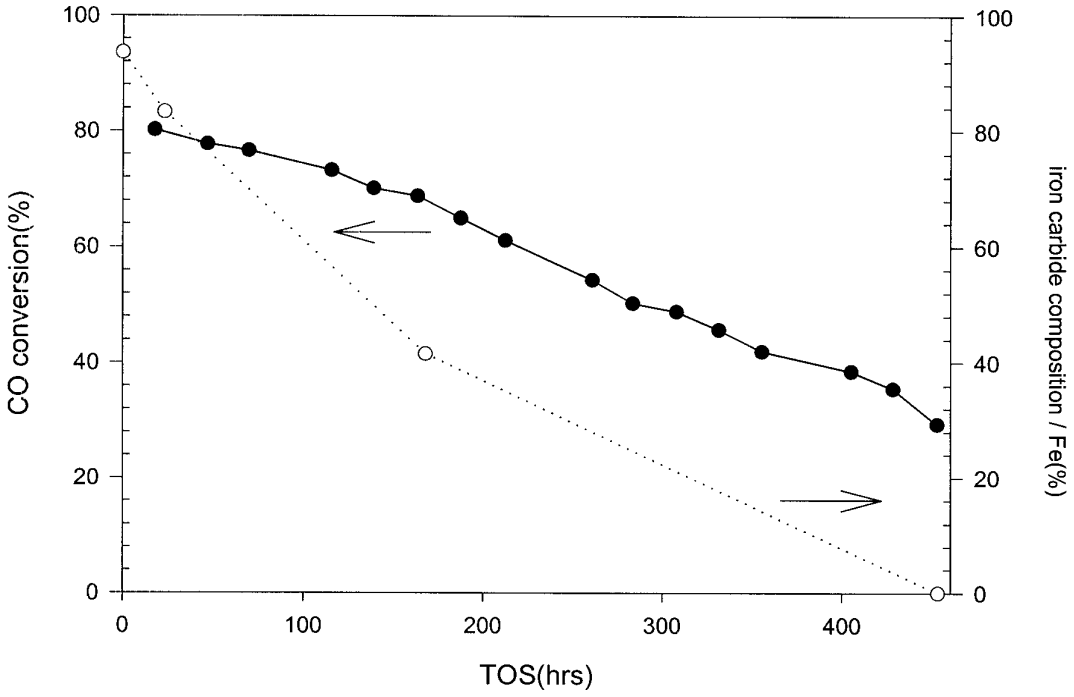

Figure 1. Catalytic activity and iron carbide percentage versus reaction time.

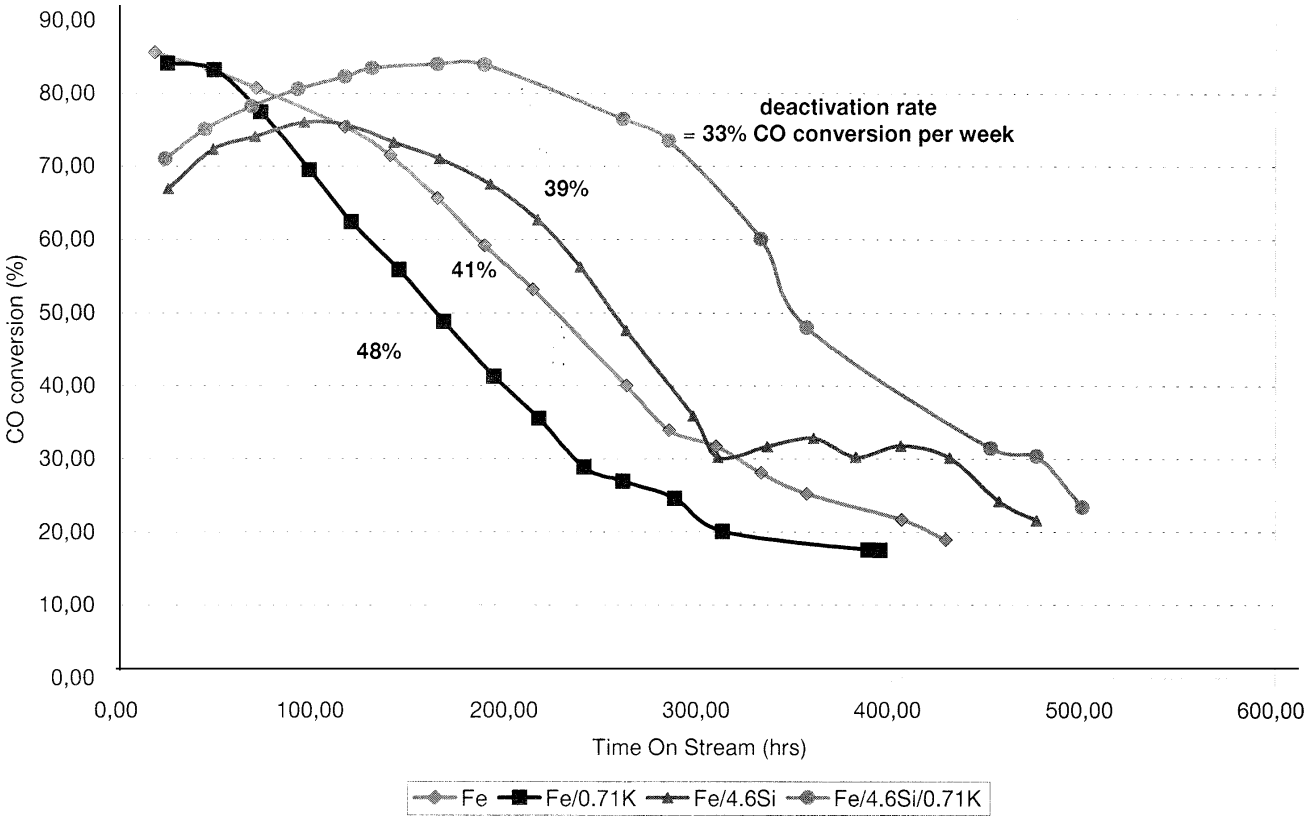

Figure 2. CO conversion as a function of time-on-stream.

E. Characterization of promoted Cobalt FTS Catalysts

Introduction

We have studied and are continuing to study the impact on reducibility of cobalt by the use of different supports and by the incorporation of different promoters and additives to supported cobalt catalysts. Although the use of different supports and promoters is well documented, what is less well understood are the reasons for the differences in deactivation rates of these catalysts. Only by rigorous characterization can the properties of the catalysts brought about by differences in preparation, support, and degree and type of promoter be linked to the resulting catalytic properties under reaction. We therefore have spent considerable attention on the characterization of not only the fresh catalysts, but also the spent catalysts sampled after many days on stream in the continuously stirred tank reactor. With this approach, it is our goal to understand what properties are required for high initial activity and, just as importantly, for the maintaining of high stability, and how to achieve them in the catalyst preparation and activation steps. Interestingly, while addition of promoters can markedly improve the reducibility of cobalt FTS catalysts, leading to more available catalytic sites for reaction, these catalysts often display significantly high rates of deactivation. This raises many questions, which should be able to be addressed through careful characterization. For example, is the reducibility of the metal sites changing under reaction conditions and if so, what are the reasons? Is the cobalt and/or promoter cluster size changing under reaction or is there loss in the degree of interaction between the two? Are we forming mobile metal carbonyl species by the addition of CO that leads to loss of metallic sites and changes in the morphology of the clusters with time onstream? To address these questions, we are employing several characterization techniques, including temperature programmed reduction (TPR), hydrogen chemisorption, X-ray diffraction (XRD), transmission electron microscopy (TEM), and in the near future, diffuse

reflectance infrared Fourier transform spectroscopy (DRIFTS) and X-ray absorption spectroscopy methods (XAS) such as extended X-ray absorption fine structure (EXAFS) and X-ray absorption near edge structure (XANES).

Experimental

BET Surface Area Measurements

BET measurements for all catalysts were conducted to determine the loss of BET surface area with loading. These experiments were conducted using a Micromeritics Tri-Star system. Prior to testing, samples were slowly ramped to 160°C and evacuated for 4hrs to approximately 50mTorr.

Hydrogen Chemisorption by the Temperature Programmed Desorption (TPD) Method

Hydrogen chemisorption was measured using a Zeton Altamira AMI-200 unit which incorporates a thermal conductivity detector (TCD). Catalysts were activated using pure hydrogen at the desired reduction temperature (usually 300 or 350°C) for 10hrs and cooled under flowing hydrogen to 100°C. The sample was held at that temperature under flowing argon to remove physisorbed and weakly bound species, prior to increasing the temperature slowly to the activation temperature. At that temperature, the catalyst was held under flowing argon to desorb remaining chemisorbed hydrogen until the TCD signal returned to the baseline. The TPD spectra was integrated and the amount of desorbed hydrogen determined by comparing to the areas of calibrated hydrogen pulses. Table 2 shows the resulting dispersion based on total weight of metal in the sample for a number of cobalt FTS catalysts.

X-ray Diffraction

Diffraction patterns were recorded using a Rigaku X-ray diffractometer utilizing CuK_{Alpha} radiation. Because quantitative information was desired on particle size, we scanned the oxidized samples for the peak corresponding to the (311) planes of Co_3O_4, which appears at a 2θ

value of approximately 37. Scans were taken using a step size of 0.010°. Because of the level of noise for small cobalt clusters, each point was scanned for 10 seconds to improve resolution. Two different software packages were used to fit the results, Jade and Winfit. Peak position and size values for both software packages are included in Table 2.

Transmission Electron Microscopy

Transmission electron microscopy (TEM) imaging was conducted using a JEOL2000FX, which incorporates a 200keV LaB_6 gun. Samples were first reduced in hydrogen at 350°C for 10hrs in a 2:1 Ar:H_2 mixture (as performed prior to catalytic activity testing) and passivated using 1%O_2 in helium passivation gas. Next, they were passed through a 75 micron sieve, and suspended in isopropyl alchohol, prior to loading onto the Lacey carbon on Cu grid, and subsequent drying. Imaging was conducted at various magnifications including 50, 100, 250 and 400K. Negatives and prints were developed, and clusters counted with size to obtain a distribution, where possible. Figures 1 a and b show a TEM micrograph and resulting particle size distribution for a fresh 0.5% Re promoted 15%Co/Al_2O_3 catalyst, while Figures 2 a and b display results for a spent 0.2% Re promoted 15%Co/Al_2O_3 catalyst sampled after reaching a steady state conversion in the CSTR.

Temperature Programmed Reduction

Temperature programmed reduction (TPR) profiles of fresh and spent catalysts were also recorded using the Zeton Altamira AMI-200 unit. Calcined fresh samples were first purged in flowing inert gas to remove traces of water. Spent catalysts were either removed from the reactor via a dip tube during the run, or sampled after completion of a run. In each case, the catalyst sampled reflected the steady state condition of the run. The wax was first extracted using xylenes in a Soxhlet apparatus and the catalyst collected in a 33mm×80mm extraction thimble. The catalyst was dried in an oven at 110°C and then reoxidized under flowing dry air

after ramping to 250°C before TPR was conducted. TPR was performed using a 10%H_2/Ar mixture and referenced to Ar. Resulting profiles were normalized to the height of the main peak so that shifts in the peak positions could be ascertained.

Results and Discussion

BET Surface Area Measurements

Table 1 displays the BET surface area results. The 15%Co catalysts loaded onto Condea Vista B Al_2O_3 had an average BET surface area of 157 m^2/g. The Davisil SiO_2 supported catalysts had higher BET surface areas, with the 15% loaded catalysts on Davisil 644 SiO_2 support averaging 208 m^2/g and the 15% loaded catalysts on Davisil 952 SiO2 support averaging 229 m^2/g. The 20% loaded catalysts on Davisil 952 SiO_2 support modified by ZrO_2 had a lower average BET area of 197 m^2/g. Not surprisingly, the series of catalysts supported on Davisil 952 (ZYQ028 through ZYQ032) exhibited decreasing surface areas with increasing Co loading. Each 5% increase in loading yielded drops in BET surface area in the order 260, 234, 226, 190, and 170 m^2/g, respectively. The 15% Co catalysts prepared on Shell 980F had an average BET surface area of 103 m^2/g, while the one prepared on Shell 980G was much lower at 52.3 m^2/g. The 15% cobalt catalyst on Dagussa P25 TiO_2 had the lowest BET surface area of 41.8 m^2/g.

H_2 Chemisorption, XRD and TEM

Dispersion calculations were based on the assumption that the H:Co stoichiometric ratio was 1:1. In general, particle size estimates from H_2 chemisorption measurements are based on the assumption that the metal clusters are completely reduced. One determines the total number of atoms from knowledge of the weight % of loading of the metal and the surface atoms from the desorption of hydrogen. By assuming a particular geometry (e.g., a spherical or cubic structure), one is able to deduce the average cluster size. However, in our case, the assumption of complete reduction may or may not be valid, depending on the support used and type and degree of

promotion. TPR results provide a general indicator for the extent of reduction. In the case where metal oxide clusters remain on the surface during chemisorption (incomplete reduction), the cluster size determination will overestimate the cluster size. This may be particularly important for unpromoted catalysts supported on TiO_2 and Al_2O_3, where significant metal-support effects occur. For these samples, a considerable fraction of clusters is reduced at very high temperatures in the TPR profiles. For example, assuming complete reduction for 15%Co/Al_2O_3 leads to a value of 64 nm for the average cluster size. XRD clearly reveals, however, that the cluster is no different in size from the promoted catalysts, however, which are accurately predicted by H_2 chemisorption measurements. Despite the problem with cluster size approximation, the calculated dispersion based on hydrogen uptake should provide an accurate indicator of the number of surface atoms available for reaction, and these can be used appropriately for determining turnover numbers in catalytic testing.

Reaction testing in CSTRs has been conducted primarily on promoted 15%Co/Al_2O_3 catalysts (ZYQ036, 039, 040, and 041). These catalysts displayed the highest uptakes of H_2, significantly higher than that of the unpromoted catalyst (ZYQ000). Assuming complete reduction of the Co in the case of the promoted catalysts, the clusters for fresh catalysts were determined to be approximately 12 nm, 14 nm, 12 nm, and 11 nm for 0.5%Pt-15%Co/Al_2O_3, 0.2%Re-15%Co/Al_2O_3, 0.5%Re-15%Co/Al_2O_3, and 1%Re-15%Co/Al_2O_3 catalysts, respectively. These values are in reasonably good agreement with the values determined by XRD and TEM. For the 0.5%Re-15%Co/Al_2O_3 catalyst, the metal clusters were found to be primarily approximately 10 nm. For the case of XRD, to convert to the metallic particle size, the multiplier 0.75 should be used. Therefore, it appears that the XRD fitting software Jade fits the results more closely to the actual value, while Winfit apparently underestimates the cluster size.

Characterization of the spent samples was also attempted, and values are reported in parentheses. Further testing is currently being conducted to verify the validity of the results. For example, in hydrogen chemisorption, clusters must be cleaned sufficiently of wax before accurate TPD measurements are obtained. Due to time constraints, in XRD, we only scanned the range where the Co_3O_4 (311) peak occurred at a 2θ of 37. However, further tests are necessary to determine if any other species are present. For example, cobalt rhenium oxide may form after reoxidation for the case of the Re promoted catalysts. Interestingly, a new peak formed at 2θ = 38.5 for spent catalysts, and often dominated in intensity over the peak positioned at $2\theta = 37$. We are currently investigating the nature of this new peak, which did not appear in the case of the fresh catalysts.

Temperature Programmed Reduction

Figure 3 shows the TPR profiles for the unpromoted cobalt catalysts. For the two SiO_2 supported catalysts, two peaks emerged, attributed to the reduction of Co_3O_4 to CoO, which decomposes at higher reduction temperatures to metallic Co. As shown in the figure, the addition of surface ZrO_2 to silica did not significantly change the reducibility. In addition to the two peaks observed for the Co/SiO_2 catalysts, the TiO_2 and Al_2O_3 supported cobalt catalysts displayed broad peaks at higher temperatures, due to the metal support interaction, which increases with decreasing cluster size. For the Co/Al_2O_3 catalyst, an additional low temperature peak is observed, which we assign to the reduction of cobalt nitrate species. Calcining the catalyst at higher temperatures removed this low temperature (200°C) peak.. Therefore, the decomposition of Co precursors was concluded to be more difficult on Al_2O_3 support.

Figure 4 shows a TPR comparison of noble metal promoted catalysts prepared using a variety of supports. The addition of Pt or Ru to the support had a similar effect on each of the

supported catalysts. All the peaks shifted markedly to lower temperatures, presumably due to spillover of H_2 from the reduced promoter to reduce Co oxide species. Of particular importance, peaks attributed to the metal support interaction for Co species on TiO_2 and Al_2O_3 are reduced at much lower temperatures, freeing up the availability of metal atoms for reaction. For the case of Re, the reduction of Re occurs at higher temperatures than Pt or Ru. This is clearly shown in Figure 4. Although the low temperature peaks are not significantly affected, Re still plays a valuable role in reducing the reduction temperature of species for which there is a significant metal-support interaction.

Figures 5 through 12 show the effect of increasing promoter or additive loadings on the reduction temperature for different supported cobalt catalysts. Figure 5 reports the addition of Ru to the 15%Co/SiO_2 catalysts. With the addition of 0.2% Ru, the greatest shift was found to be that of the low temperature peak which we ascribed to the reduction of Co_3O_4 to CoO. The position of the higher temperature peak assigned to further reduction of CoO to metallic increased slightly. However, further increases in promoter shifted both peaks to lower temperatures. Interestingly, further addition of Ru beyond 1% loading led to only marginal further decrease in temperature.

For the Pt series, the same atomic ratios were used as with Ru, so higher weight percentages of Pt were used. Increasing the Pt loading, in general, led to expected decreases in the reduction temperature, and lower temperatures were achieved on a molar basis with Pt relative to Ru. One exception to the trend was the 0.97% loaded catalyst. Catalysts will be tested in the future by ICP to verify weight percentages.

Figure 7 demonstrates the impact of modifying the surface of SiO_2 with ZrO_2 and incorporating noble metal promoters. As with the SiO_2 catalysts, a large shift was observed for the low temperature peak when Ru or Pt was added, while only a modest shift to lower reduction

temperatures was observed for the higher temperature peak. Interestingly, the Re promoted catalyst behaved much differently, where both peaks shifted slightly to higher temperatures. This suggests that reduction of Re occurs at much higher temperatures than the Pt or Ru catalysts.

Examination of Figure 8 reveals an interesting result when the K concentration is increased for the 15%Co/SiO_2 support. Addition of a small amount (0.5%K) to the catalyst resulted in a remarkable shift to lower temperatures for both peaks (160°C for the low temperature peak and 60°C for the high temperature peak). However, further increases in the K content shifted both peaks back up to higher temperatures, beyond the peak positions of the unpromoted reference catalyst.

Figures 9 through 12 focus on promoting Al_2O_3 support. Unlike the SiO_2 supported cobalt catalysts, there is a strong interaction of the cobalt with the support for a large fraction of the cobalt clusters. Again, evidence for this effect is demonstrated by the broad peak at high temperatures in the TPR profile for the unpromoted catalyst. Therefore, the potential for achieving gains in activity by promoting the support are high.

Figures 9 and 10 show profiles for Re promoted 15%Co/Al_2O_3 catalysts. The difference between the two series of catalysts is in the preparation. The series in Figure 9 references catalysts ZYQ039, 040 and 041, which were prepared by loading the Co three times by successive incipient wetness impregnation steps, where the catalyst was dried between each step. Only one calcination was used after the last step. Figure 10 references catalysts ZYQ051, 052, and 052. These catalysts were prepared in a similar manner, except that the each of the catalysts was calcined after each sequential impregnation and drying step, for a total of three times. Comparing Figure 10 to Figure 9 reveals that no benefit to reducibility was achieved by calcining the catalyst sequentially.

Figure 9 shows that with each increase in loading of Re promoter, the low temperature peak did not change. Again, we ascribe this to the higher reduction temperature of Re in comparison with the Ru and Pt promoters. Interestingly, however, the high temperature peak shifts markedly with each increase in the Re loading. Therefore, we conclude that after reduction

temperature of Re is reached, then spillover of H_2 occurs to lower the reduction temperature of Co oxide species for which there is a significant interaction with the support.

As described earlier, both Pt and Ru promoters behave in a similar manner and shift both reduction peaks to lower temperatures for 15%Co/Al_2O_3. Figure 11 demonstrates that by increasing the loading of Ru, both reduction peaks shift to lower temperatures, with the effect being more pronounced for the low temperature peak. Remarkably, when a loading of 0.5% Ru is achieved, the broad high temperature peak ascribed to the interaction of the support with the metal has shifted by approximately 100°C. Unfortunately, further increases in loading, and in fact doubling the loading, shows only a marginal improvement in reducibility. Two additional catalysts were prepared incorporating La and Zr to the catalysts. However, no change in the low temperature peak was observed.

Metal-support effects were also seen for the 10%Co/TiO_2 catalysts. Therefore, the potential benefits for increasing available metal atoms for reaction by promoting the catalyst were high. A number of different promoted catalysts were tested by TPR, and results are depicted in Figure 13. While addition of B to the catalyst had adverse effects on reducibility, the noble metals had an enhancing effect. In a similar manner with Al_2O_3, both Pt and Ru shifted all peaks in the TPR profiles to lower temperatures, while Re only benefitted the high temperature peaks.

Although promoted catalysts displayed a higher initial activity as expected, due to increased availability of metal atoms for reaction, the deactivation rates differed greatly. In an effort to further understand the differences in deactivation patterns of promoted supported Co catalysts, we have begun to characterize the spent samples, either removed during the run by a dip tube or after the run. In each case, the catalyst was removed after a steady state conversion was achieved. Again, catalysts was sampled, the wax was removed first by extraction with xylenes in a Soxhlet apparatus, and the catalyst was oxidized in flowing dry air at 250°C.

We wished to determine if significant differences in reducibility occurred by comparing TPR profiles for the spent catalysts in reference to the fresh catalyst. We hypothesized that one route to deactivation might be if the promoter-cobalt interaction was decreased due to segregation, agglomeration, or removal by the leaching out of one or both metals as a mobile species (e.g., a metal-carbonyl). If the reducibility changed, then the TPR for the spent would become more like the TPR profile of the unpromoted catalyst. Therefore, in Figures 15 through 18, we have displayed TPR spectra of the fresh, spent, and unpromoted catalysts such that qualitative comparisons could be ascertained.

Before examining the TPR profiles of the promoted catalysts, it is instructive to first review the TPR profiles of the fresh and spent unpromoted catalysts (see Figure 14). Interestingly, both peaks shift to higher reduction temperatures, and the high temperature peak for the spent catalyst is significantly sharpened. This raises questions as to the reducibility of the Co with changes in the cluster size. XRD results indicate a decrease in cluster size for the unpromoted catalyst. One might conclude that a smaller cluster would lead to an increase in the interaction between the support and the cobalt and a shift to higher reduction temperatures in the TPR spectra.

Although Pt promotion gave the largest shifts in reduction temperature for the fresh catalysts, in comparison with other promoted catalysts such as Re and Ru, a 0.53% promoted 14.3%Co catalyst displayed a very high rate of deactivation under FTS reaction. Comparison of the TPR for the spent catalyst in reference to the fresh catalyst showed a strong shift to higher reduction temperatures. There is a strong possibility, therefore, that the metal-promoter surface interface decreases under reaction conditions. Future EXAFS investigations may reveal these changes, as EXAFS is one of the most powerful techniques available for determining local structure surrounding the atom of interest. The TPR spectra for the spent catalyst looks much more like the spectra of the unpromoted catalyst than that of the fresh.

Interesting the comparisons for Re and Ru display a much different result. For these catalysts, the reduction peaks appear near or below the peaks observed for the fresh catalysts, indicating that the metal-promoter interaction remains intact under reaction. Interestingly, these catalysts displayed lower rates of deactivation in comparison with the Pt. The peaks of the Re catalysts also were found to be sharper for the case of the spent catalysts. Again, future EXAFS, XRD, and H_2 chemisorption experiments may reveal the reason for the sharpening.

Conclusions

The activity of cobalt catalysts is generally ascribed to the active sites located on the surface of cobalt metal clusters formed after reduction of the oxidic species formed after calcination. However, the reducibility of cobalt catalysts is strongly influenced by the nature of the support and the degree of promotion by additives, which is the focus of this work. In general, a tradeoff exists as one increases the reduction temperature to activate the cobalt catalyst. Although more sites are reduced, cobalt clusters sinter at higher reduction temperatures. Therefore, TPR and hydrogen chemisorption studies should be conducted prior to catalytic testing, in order to determine the appropriate temperature for catalyst activation. In

general, the number of active sites available after reduction varies with support, promoter type, and degree of promotion. The reason for deactivation of promoted FTS catalysts is a subject requiring further study. TPR studies suggest that there is a difference in the degree of interaction of the promoter with the cobalt after reaction testing for each promoter. However, further experiments, using such techniques as EXAFS, are necessary to determine the extent of these morphological changes. Not only will EXAFS allow the determination of cluster size, but the local structure surrounding Co, including the promoter interaction, may be quantified for the fresh and spent catalysts.

The addition of Pt or Ru to the support had a similar effect on each of the fresh supported catalysts. All the reduction peak positions shifted markedly to lower temperatures, due to spillover of H_2 from the reduced promoter to reduce Co oxide species. Of particular importance, peaks attributed to the metal support interaction for Co species on TiO_2 and Al_2O_3 are reduced at much lower temperatures, freeing up the availability of metal sites for reaction. For the case of Re, the reduction of Re occurs at higher temperatures than Pt or Ru. Although the low temperature peaks are not significantly affected, Re still plays a valuable role in reducing the reduction temperature of species for which there is a significant metal-support interaction.

TPR analysis of spent promoted 15%Co/Al_2O_3 catalysts revealed that while observed peaks for Ru and Re promoted catalysts remained shifted to low temperatures, the peaks had shifted substantially to higher temperatures in the case of the Pt catalyst. This suggests that the Co and Pt interaction is rapidly lost under reaction, and may be the reason for the higher observed deactivation rate.

Table 1

Catalyst Characteristics

Sample ID	Sample Composition	Calcination	BET SA (m_2/g)	+/-	Avg. Pore (nm)	Additional Comments
ZYQ000	15%Co/Al_2O_3	400°C, flow, 1X	157.7	0.2	4.2	IWI (3X); Condea Vista B, 100-200 mesh
ZYQ001	15%Co/SiO_2	400°C, no flow, 1X	217.1	0.7	7.7	IWI (3X); Davisil 644 SiO_2
ZYQ002	0.2%Ru-15%Co/SiO_2	400°C, no flow, 1X	222.0	0.6	7.7	IWI (3X); Davisil 644 SiO_2
ZYQ003	0.5%Ru-15%Co/SiO_2	400°C, no flow, 1X	233.6	0.5	7.4	IWI (3X); Davisil 644 SiO_2
ZYQ004	1.0%Ru-15%Co/SiO_2	400°C, no flow, 1X	205.6	0.6	7.6	IWI (3X); Davisil 644 SiO_2
ZYQ005	2.0%Ru-15%Co/SiO_2	400°C, no flow, 1X	208.9	0.5	7.6	IWI (3X); Davisil 644 SiO_2
ZYQ006	0.39%Pt-15%Co/SiO_2	400°C, no flow, 1X	200.7	0.6	7.7	IWI (3X); Davisil 644 SiO_2
ZYQ007	0.97%Pt-15%Co/SiO_2	400°C, no flow, 1X	224.2	0.7	7.6	IWI (3X); Davisil 644 SiO_2
ZYQ008	1.93%Pt-15%Co/SiO_2	400°C, no flow, 1X	169.6	0.5	4.4	IWI (3X); Davisil 644 SiO_2
ZYQ009	3.86%Pt-15%Co/SiO_2	400°C, no flow, 1X	217.0	0.6	7.3	IWI (3X); Davisil 644 SiO_2
ZYQ010	0.5%K-15%Co/SiO_2	400°C, no flow, 1X	210.9	0.5	7.9	IWI (3X); Davisil 644 SiO_2
ZYQ011	1.5%K-15%Co/SiO_2	400°C, no flow, 1X	200.8	0.5	8.1	IWI (3X); Davisil 644 SiO_2
ZYQ012	3.0%K-15%Co/SiO_2	400°C, no flow, 1X	168.6	0.4	8.9	IWI (3X); Davisil 644 SiO_2
ZYQ013	5.0%K-15%Co/SiO_2	400°C, no flow, 1X	214.0	0.6	7.5	IWI (3X); Davisil 644 SiO_2
ZYQ014	15%Co/SiO_2	400°C, flow, 1X	223.9	0.6	7.5	IWI (3X); Davisil 644 SiO_2
ZYQ015	15%Co/SiO_2	400°C, flow, 1X	100.0	0.4	15.0	Excess H_2O Impreg (2X); Shell SiO_2 980F, 500 μm
ZYQ016	15%Co/SiO_2	400°C, flow, 1X	103.4	0.4	15.2	Excess H_2O Impreg (1X); Shell SiO_2 980F, 500 μm

Sample ID	Sample Composition	Calcination	BET SA (m_2/g)	+/-	Avg. Pore (nm)	Additional Comments
ZYQ017	15%Co/SiO_2	400°C, no flow, 1X	84.7	0.3	17.3	Excess H_2O Impreg (2X); Shell SiO_2 980F, 500 μm
ZYQ018	15%Co/SiO_2	400°C, flow, 1X	112.3	0.3	14.8	Excess H_2O Impreg (2X); Shell SiO_2 980F, 250 μm
ZYQ019	15%Co/SiO_2	400°C, flow, 1X	114.2	0.4	15.3	Excess H_2O Impreg (2X); Shell SiO_2 980F, 150 μm
ZYQ020	15%Co/SiO_2	400°C, flow, 1X	105.5	0.4	15.8	Excess H_2O Impreg (2X); Shell SiO_2 980F, 50 μm
ZYQ021	15%Co/SiO_2	400°C, flow, 1X	52.3	0.2	10.9	IWI (3X); S 980G 2.3, 60-200 mesh
ZYQ022	15%Co/Al_2O_3	400°C, flow, 1X	171.3	0.7	2.0	IWI (3X); Condea Vista B, 100-200 mesh
ZYQ023	15%Co/SiO_2	400°C, flow, 1X	231.9	0.8	7.2	IWI (3X); Davisil 952 SiO_2
ZYQ024	15%Co/TiO_2	400°C, flow, 1X	41.8	0.2	12.3	IWI (3X); Degussa TiO_2 (P25), 100-200 mesh
ZYQ025	15%Co/SiO_2	400°C, flow, interval 3X	226.0	0.7	9.1	IWI (3X); Davisil 952 SiO_2
ZYQ026	15%Co/SiO_2	400°C, flow, 1X	229.3	0.5	7.3	IWI (3X); Davisil 644 SiO_2
ZYQ027	15%Co/SiO_2	400°C, flow, 1X	240.1	0.7	9.3	Excess H_2O Impreg (2X); Davisil 952 SiO_2
ZYQ028	5%Co/SiO_2	400°C, no flow, 1X	259.7	1.0	10.0	IWI (1X); Davisil 952 SiO_2, 60-80 mesh
ZYQ029	10%Co/SiO_2	400°C, no flow, 1X	234.1	0.9	9.8	IWI (2X); Davisil 952 SiO_2, 60-80 mesh
ZYQ030	15%Co/SiO_2	400°C, no flow, 1X	226.3	0.7	9.6	IWI (3X); Davisil 952 SiO_2, 60-80 mesh
ZYQ031	20%Co/SiO_2	400°C, no flow, 1X	190.0	0.5	9.0	IWI (4X); Davisil 952 SiO_2, 60-80 mesh
ZYQ032	25%Co/SiO_2	400°C, no flow, 1X	170.0	0.6	7.8	IWI (5X); Davisil 952 SiO_2, 60-80 mesh
ZYQ036	0.53%Pt-14.3%Co/Al_2O_3	400°C, flow, 1X	161.6	0.2	4.1	IWI (3X); Condea Vista B, 100-200 mesh
ZYQ037	5%La-15%Co/Al_2O_3	400°C, flow, 1X	155.1	0.2	3.9	IWI (3X); Condea Vista B, 100-200 mesh
ZYQ038	15%Zr-15%Co/Al_2O_3	400°C, flow, 1X	160.9	0.1	4.1	IWI (3X); Condea Vista B, 100-200 mesh
ZYQ039	0.2%Re-15%Co/Al_2O_3	400°C, flow, 1X	156.5	0.2	4.2	IWI (3X); Condea Vista B, 100-200 mesh

Sample ID	Sample Composition	Calcination	BET SA (m_2/g)	+/-	Avg. Pore (nm)	Additional Comments
ZYQ040	0.5%Re-15%Co/Al_2O_3	400ºC, flow, 1X	136.7	0.2	3.8	IWI (3X); Condea Vista B, 100-200 mesh
ZYQ041	1.0%Re-15%Co/Al_2O_3	400ºC, flow, 1X	187.7	0.2	4.0	IWI (3X); Condea Vista B, 100-200 mesh
ZYQ042	20%Co/ZrO_2-SiO_2	400ºC, flow, 1X	200.0	0.6	8.8	IWI (3X); Davisil 952 SiO_2, 60-80 mesh
ZYQ043	0.5%Ru-20%Co/ZrO_2-SiO_2	400ºC, flow, 1X	197.0	0.6	8.4	IWI (3X); Davisil 952 SiO_2, 60-80 mesh
ZYQ044	0.5%Pt-20%Co/ZrO_2-SiO_2	400ºC, flow, 1X	205.5	0.6	9.2	IWI (3X); Davisil 952 SiO_2, 60-80 mesh
ZYQ045	0.5%Re-20%Co/ZrO_2-SiO_2	400ºC, flow, 1X	191.9	0.6	8.9	IWI (3X); Davisil 952 SiO_2, 60-80 mesh
ZYQ050	0.5%Ru-15%Co/Al_2O_3	400ºC, flow, interval 3X	161.0	0.2	3.2	IWI (3X); Davisil 952 SiO_2, 60-80 mesh
ZYQ051	0.2%Re-15%Co/Al_2O_3	400ºC, flow, interval 3X	148.2	0.1	4.0	IWI (3X); Davisil 952 SiO_2, 60-80 mesh
ZYQ052	0.5%Re-15%Co/Al_2O_3	400ºC, flow, interval 3X	151.8	0.1	4.1	IWI (3X); Davisil 952 SiO_2, 60-80 mesh
ZYQ053	2%Re-15%Co/Al_2O_3	400ºC, flow, interval 3X	153.3	0.1	3.9	IWI (3X); Davisil 952 SiO_2, 60-80 mesh
ZYQ054	0.2%Ru-15%Co/Al_2O_3	400ºC, flow, interval 3X	153.8	0.1	4.0	IWI (3X); Davisil 952 SiO_2, 60-80 mesh
ZYQ055	1%Ru-15%Co/Al_2O_3	400ºC, flow, interval 3X	159.1	0.2	3.1	IWI (3X); Davisil 952 SiO_2, 60-80 mesh
LIJ001	10%Co/TiO_2	300ºC, no flow, 1X	---	---	---	IWI: Degussa TiO_2 P25
LIJ002	10%Co-0.1%B/TiO_2	300ºC, no flow, 1X	---	---	---	IWI: Degussa TiO_2 P25
LIJ003	10%Co-0.2%Ru/TiO_2	300ºC, no flow, 1X	---	---	---	IWI: Degussa TiO_2 P25
LIJ004	0.2%Ru-10%Co-0.1%B/TiO_2	300ºC, no flow, 1X	---	---	---	IWI: Degussa TiO_2 P25
LIJ005	10%Co-0.37%Re/TiO_2	300ºC, no flow, 1X	---	---	---	IWI: Degussa TiO_2 P25
LIJ006	10%Co-0.39%Pt/TiO_2	300ºC, no flow, 1X	---	---	---	IWI: Degussa TiO_2 P25

Table 2
Hydrogen Chemisorption and XRD Results

Sample ID	Sample Composition	H_2 Chemisorption % Dispersion	2θ	XRD Co_3O_4 (311) Jade (nm)	XRD Co_3O_4 (311) Winfit (nm)
ZYQ000	15%Co/Al_2O_3	2.40	37.0 (36.9)	18.3 (9.7)	10.3 (6.3)
ZYQ001	15%CoSiO_2	0.85	---	---	---
ZYQ007	0.97%Pt-15%Co/SiO_2	1.24	---	---	---
ZYQ022	15%Co/Al_2O_3	3.03	---	---	---
ZYQ036	0.53%Pt-14.3%Co/Al_2O_3	9.02	37.4 (17.3, 38.6)	13.7 (11.6, 24.5)	9.7 (6.2, 14.4)
ZYQ039	0.2%Re-15%Co/Al_2O_3	7.59 (spent 6.23)	37.0 (36.8, 38.4)	12.5 (6.1, ---)	10.2 (4.9, 20.1)
ZYQ040	0.5%Re-15%Co/Al_2O_3	9.07	---	---	---
ZYQ041	1.0%Re-15%Co/Al_2O_3	9.88 (spent 10.73)	37.1 (37.0, 38.5)	13.0 (8.4)	9.3 (3.3, 32.2)
ZYQ044	0.5%Pt-20%Co/ZrO_2-SiO_2	0.98	---	---	---
ZYQ050	0.5%Ru-15%Co/Al_2O_3	5.00	37.1 (37.1)	---	9.9 (3.0)
ZYQ052	0.5%Re-15%Co/Al_2O_3	5.59	---	---	---
ZYQ053	2%Re-15%Co/Al_2O_3	6.25	---	---	---
ZYQ054	0.2%Ru-15%Co/Al_2O_3	5.58	---	---	---
ZYQ055	1%Ru-15%Co/Al_2O_3	7.11	---	---	---
LIJ001	10%Co/TiO_2	3.64	---	---	---
LIJ002	10%Co-0.1%B/TiO_2	3.19	---	---	---
LIJ003	10%Co-0.2Ru/TiO_2	4.46	---	---	---
LIJ004	0.2%Ru-10%Co-0.1%B/TiO_2	5.12	---	---	---
LIJ005	10%Co-0.37%Re/TiO_2	4.78	---	---	---
LIJ006	10%Co-0.39%Pt/TiO_2	5.11	---	---	---

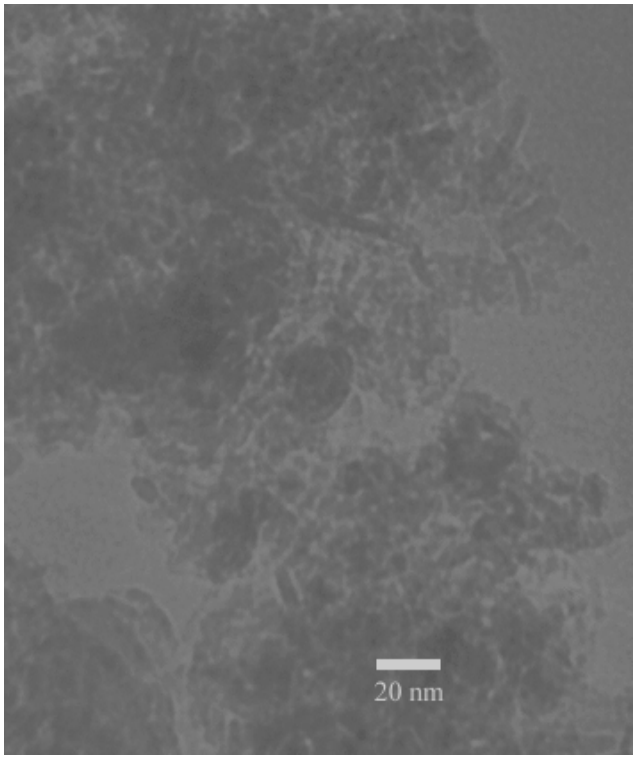

Figure 1a. TEM micrographs for a 0.5% Re promoted 15%Co/Al_2O_3 fresh catalyst.

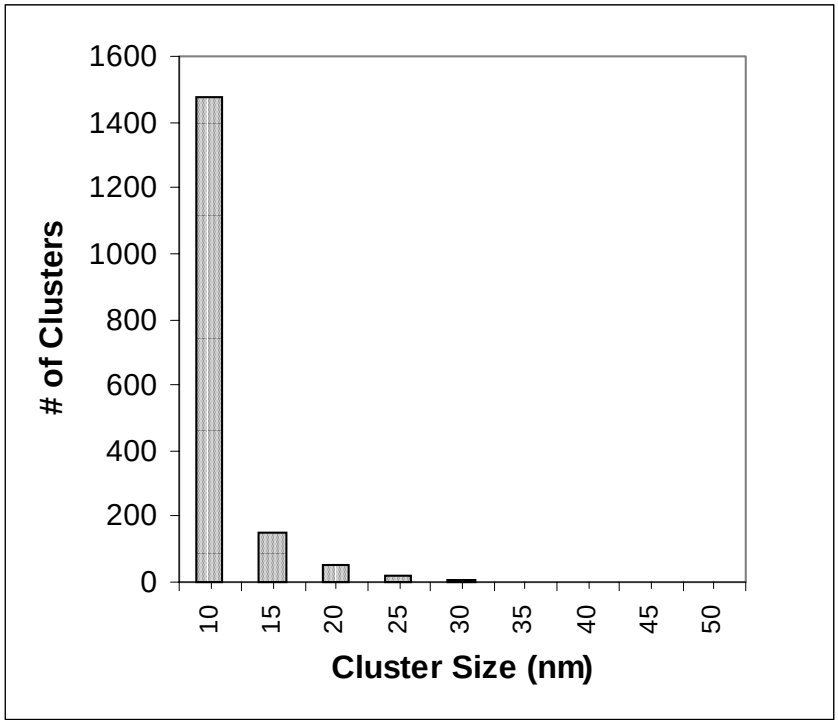

Figure 1b. Particle size distribution from analysis of TEM micrographs for a 0.5% Re promoted fresh 15%$CoAl_2O_3$ catalyst.

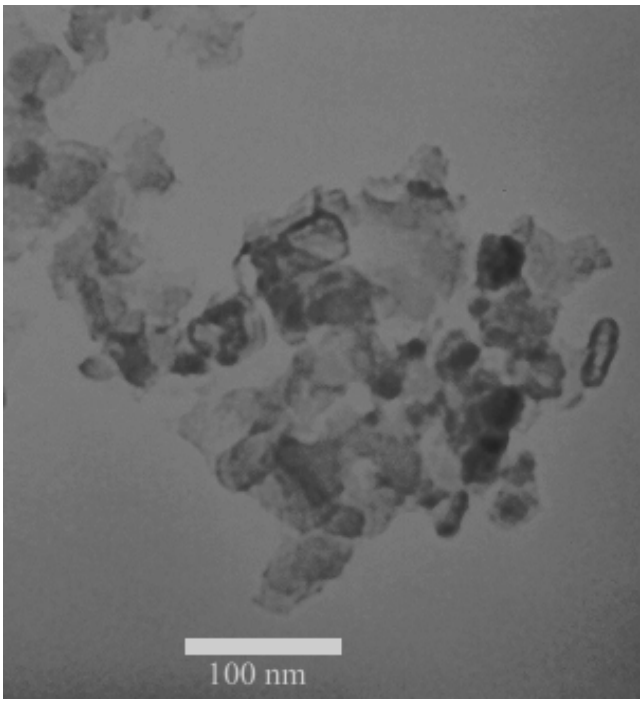

Figure 2a. TEM micrographs for a 0.2% Re promoted 15%Co/Al_2O_3 fresh catalyst.

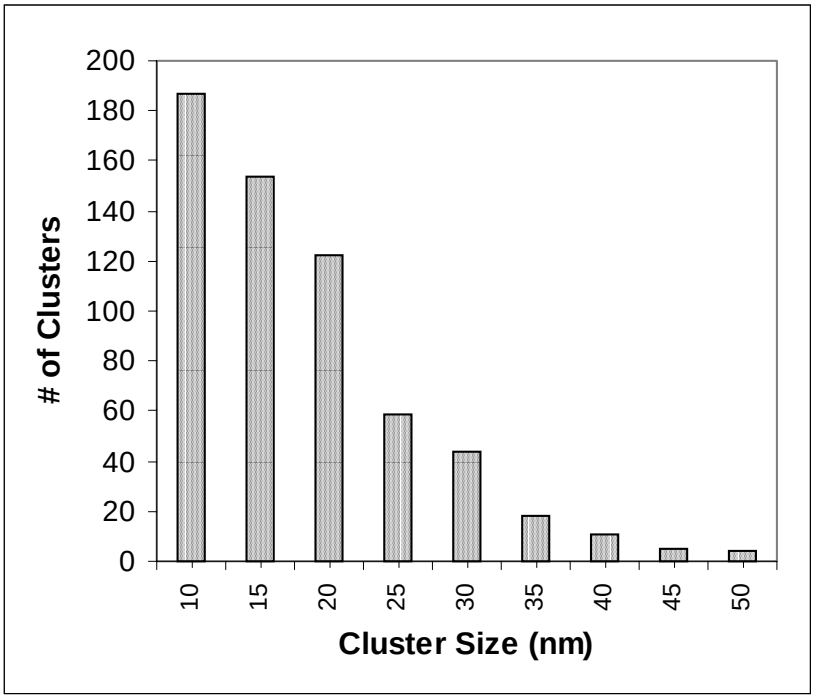

Figure 2b. Particle size distribution from analysis of TEM micrographs for a 0.2% Re promoted 15%Co/Al_2O_3 spent catalyst sampled after reaching a steady-state conversion in the CSTR.

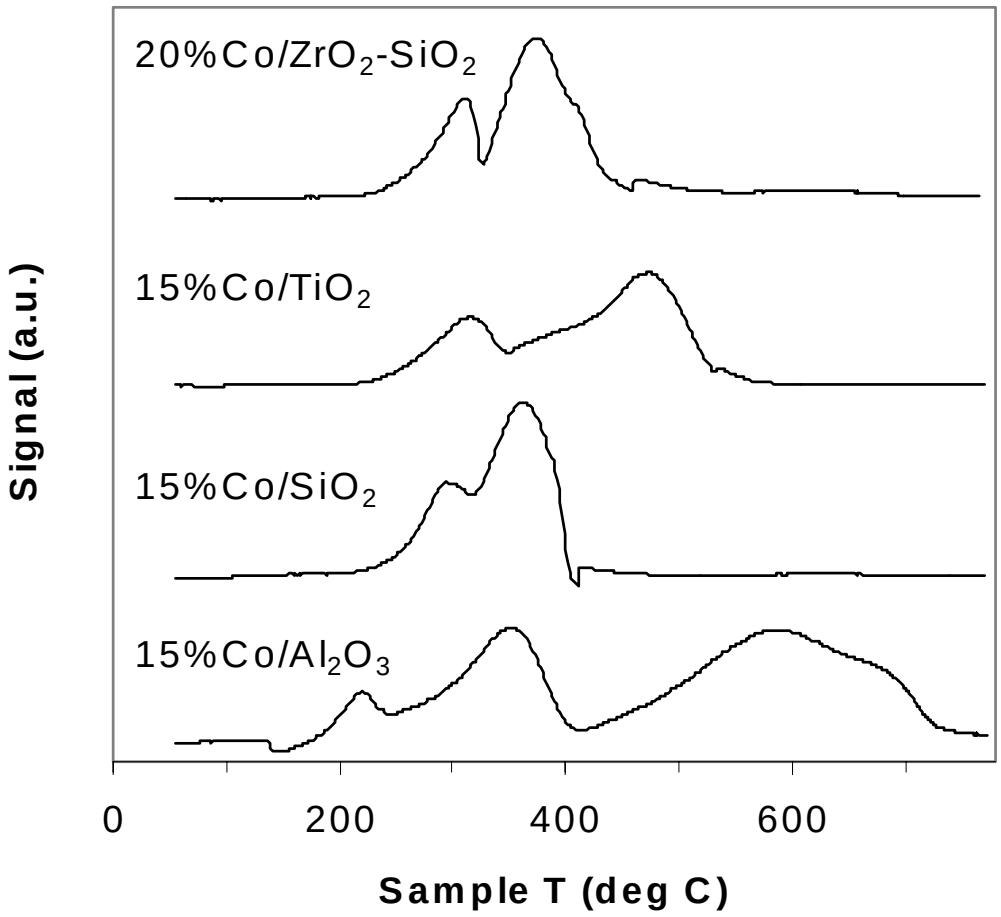

Figure 3. TPR of unpromoted Co catalysts.

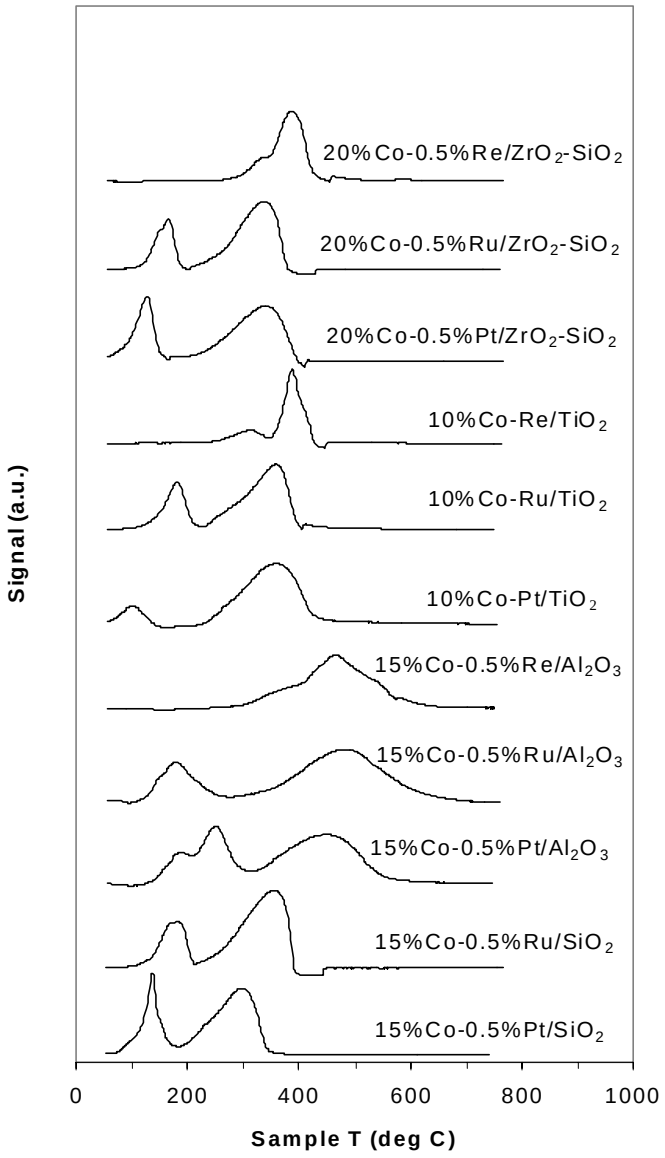

Figure 4. TPR of noble metal promoted Co catalysts.

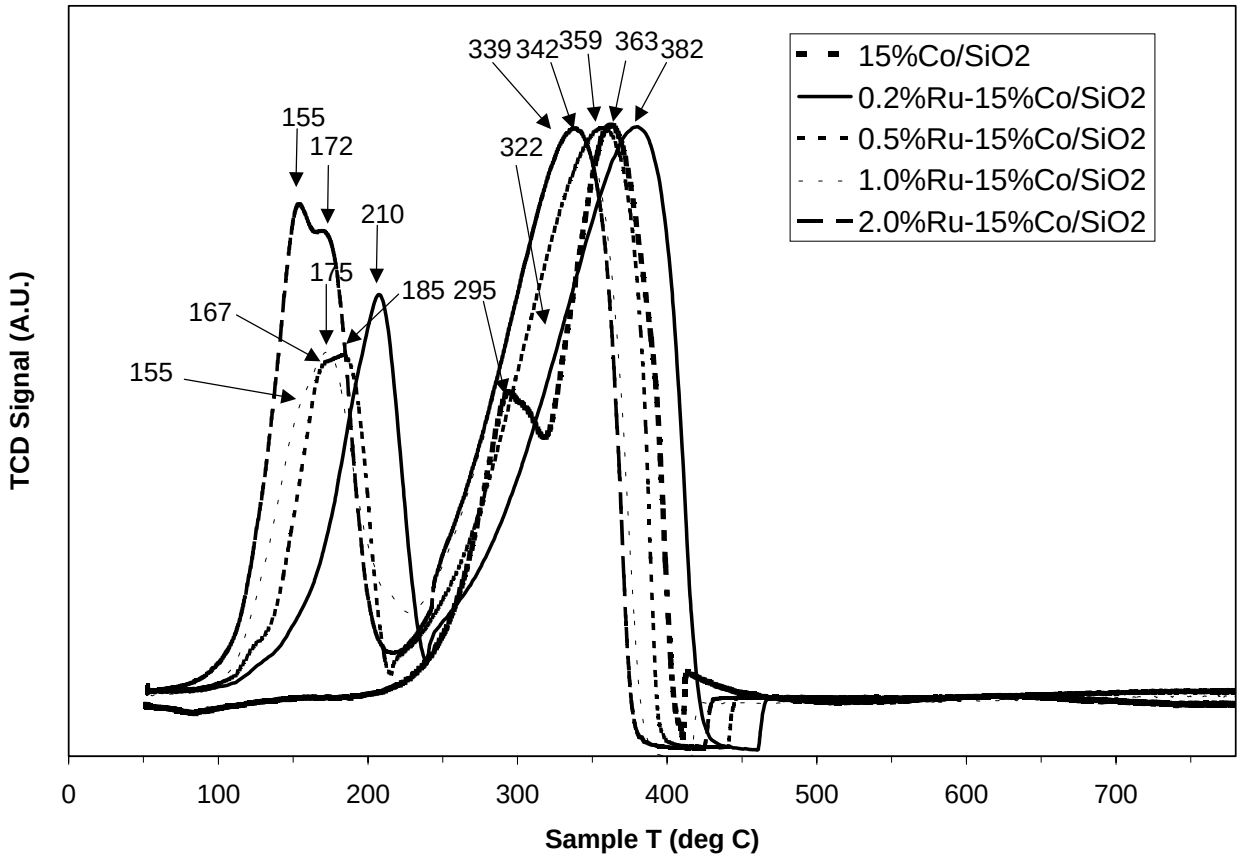

Figure 5. Effect of increasing Ru promoter loading on the reduction temperature of 15%Co/SiO_2.

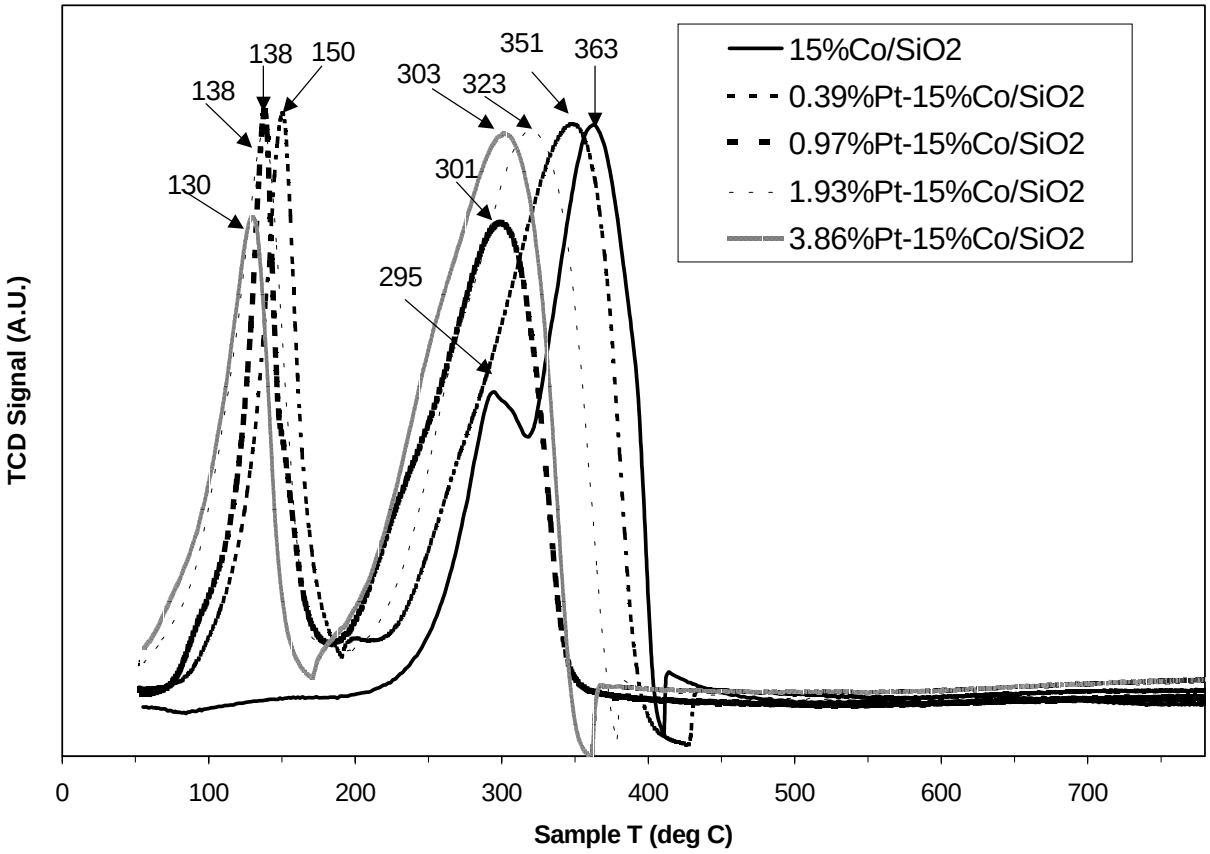

Figure 6. Effect of increasing Pt promoter loading on the reduction temperature of 15%Co/SiO_2.

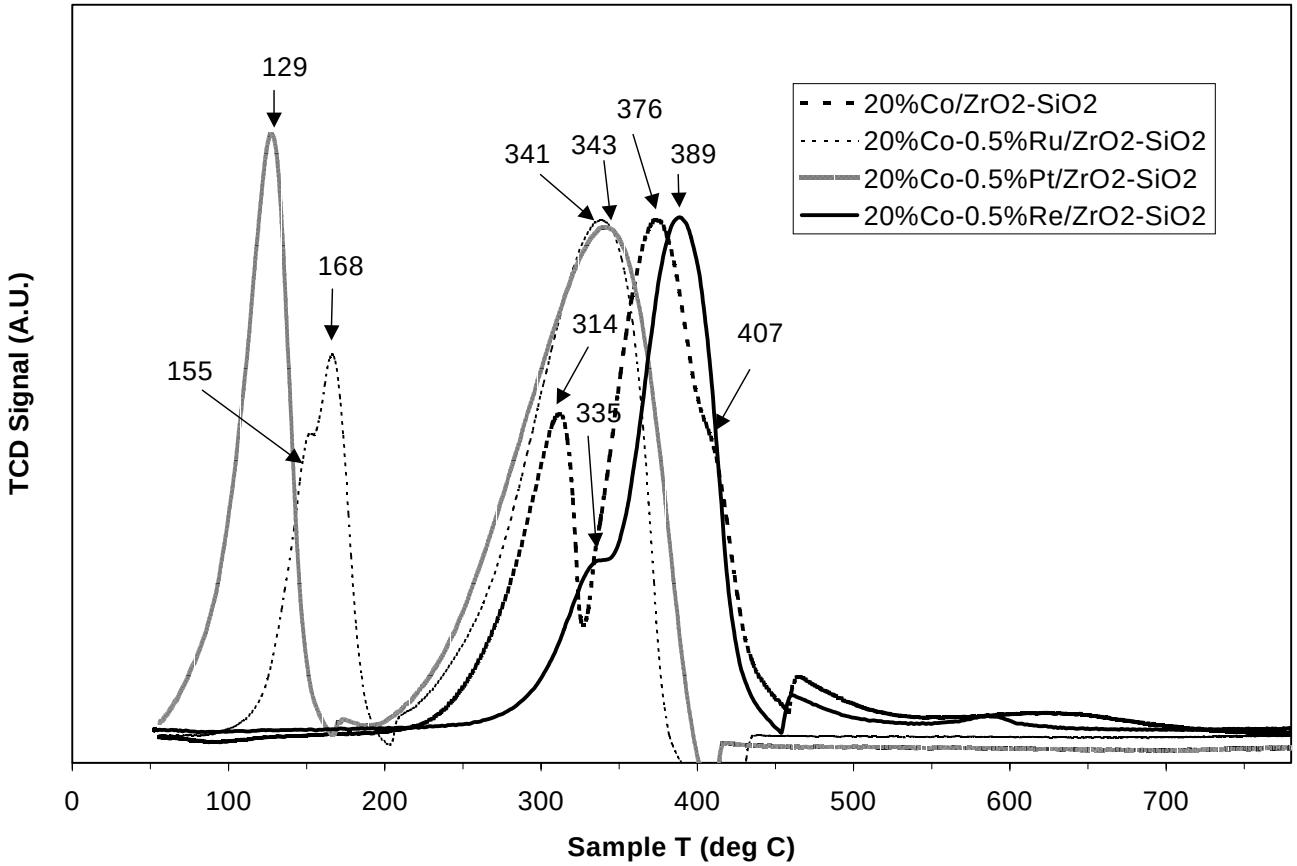

Figure 7. Effect of noble metal promoter type on the reduction temperature of 20%Co/ZrO_2-SiO_2.

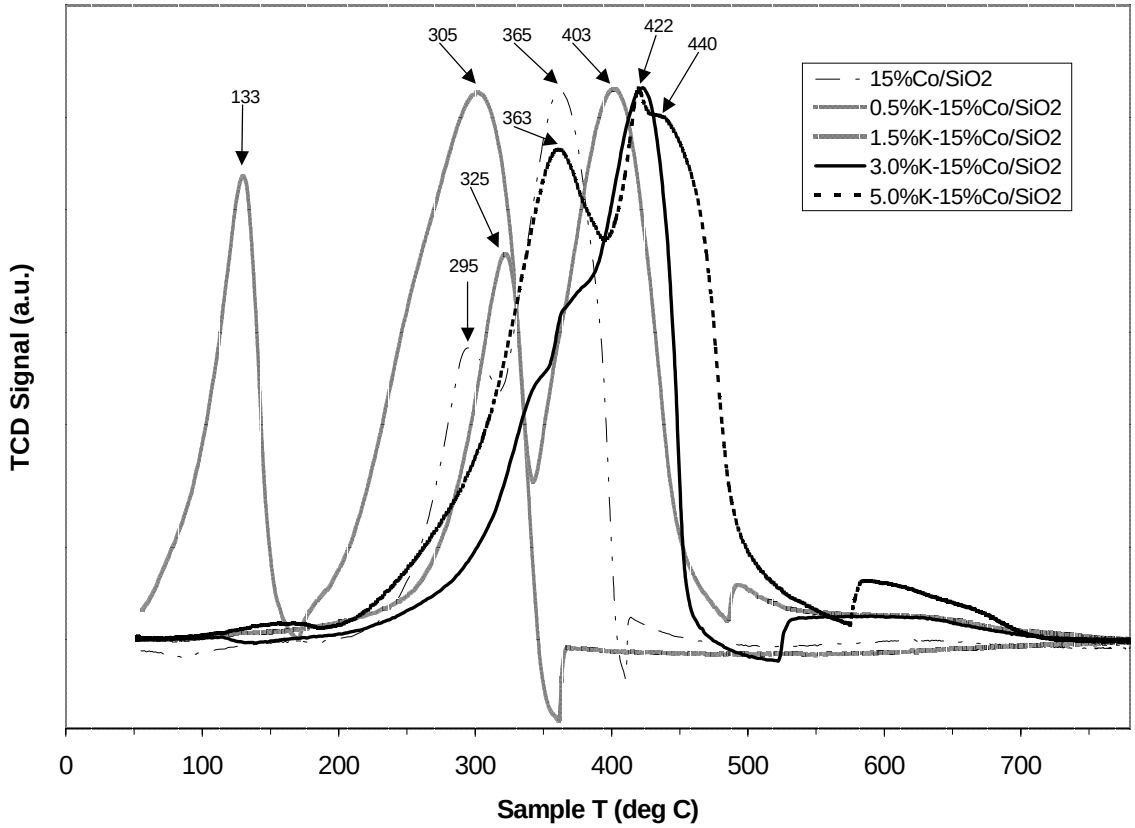

Figure 8. Effect of increasing K additive loading on the reduction temperature of 15%Co/SiO_2.

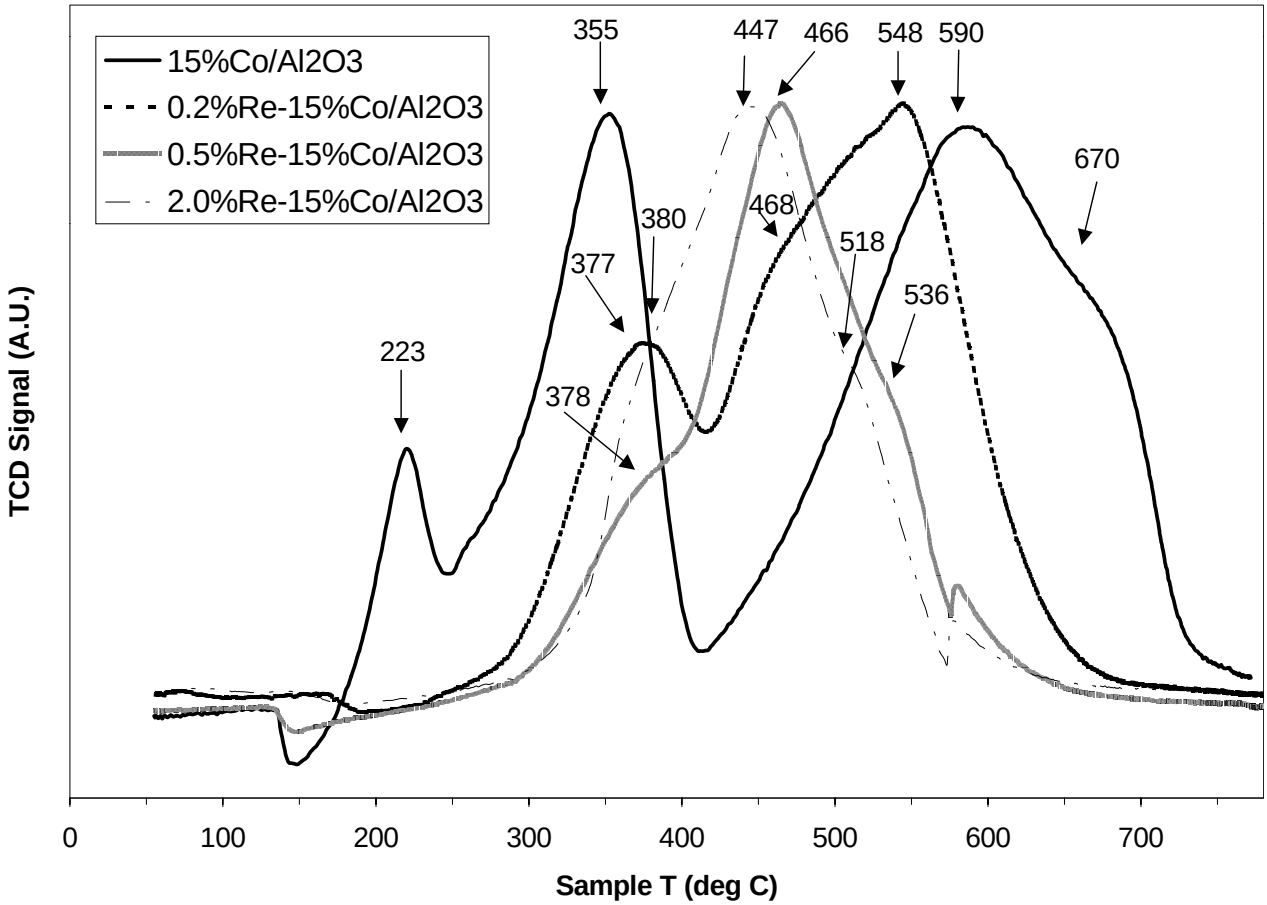

Figure 9. Effect of increasing Re promoter loading on the reduction temperature of 15%Co/Al_2O_3 (three interval drying steps and one final calcination step).

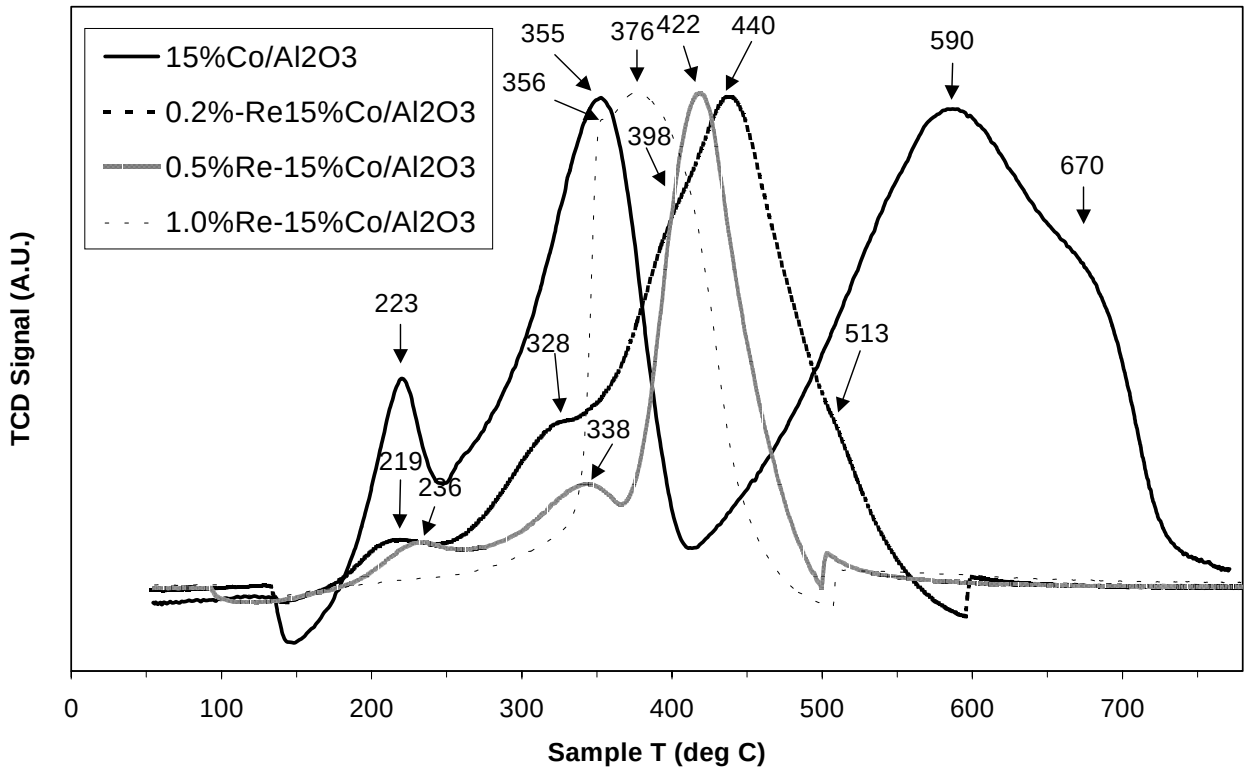

Figure 10. Effect of increasing Re promoter loading on the reduction temperature of 15%Co/Al_2O_3 (three interval drying steps and three interval calcination steps).

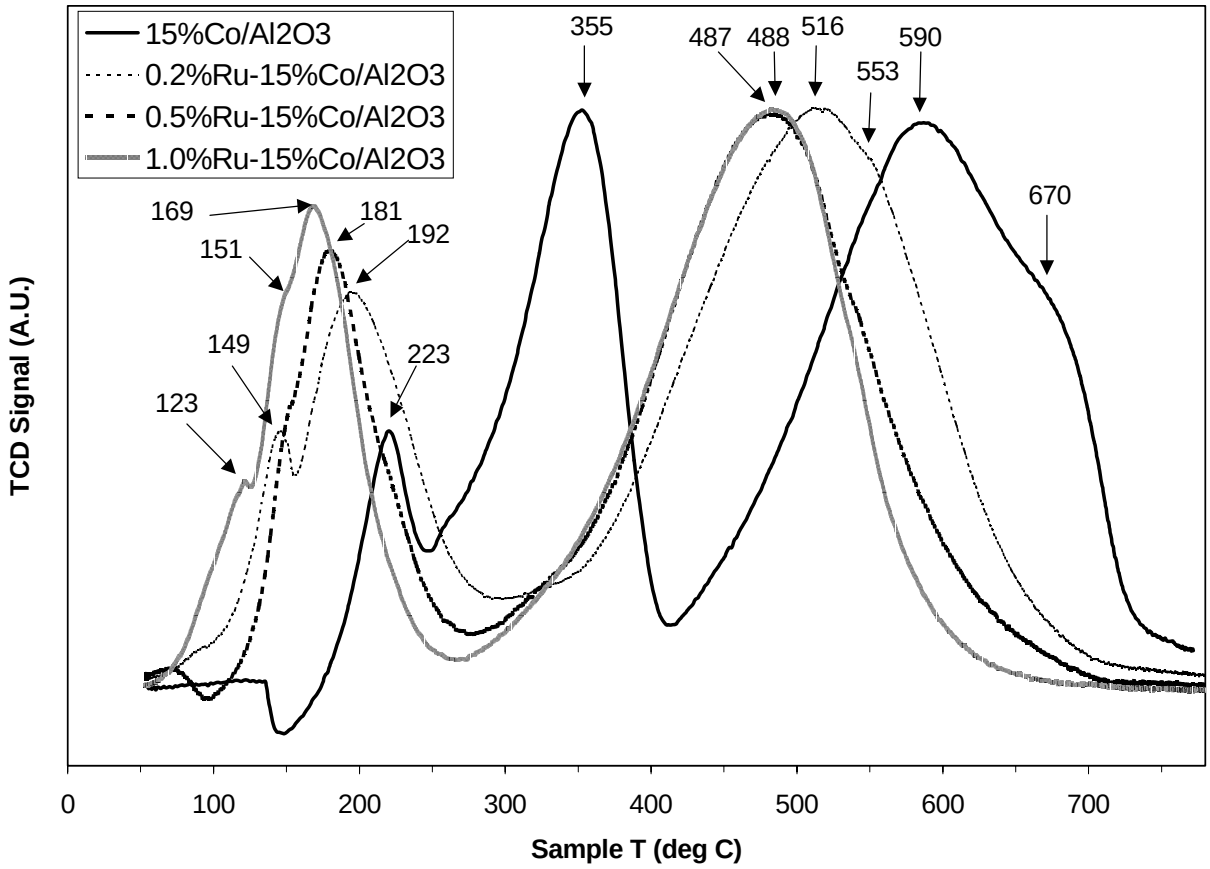

Figure 11. Effect of increasing Ru promoter loading on the reduction temperature of 15%Co/Al_2O_3.

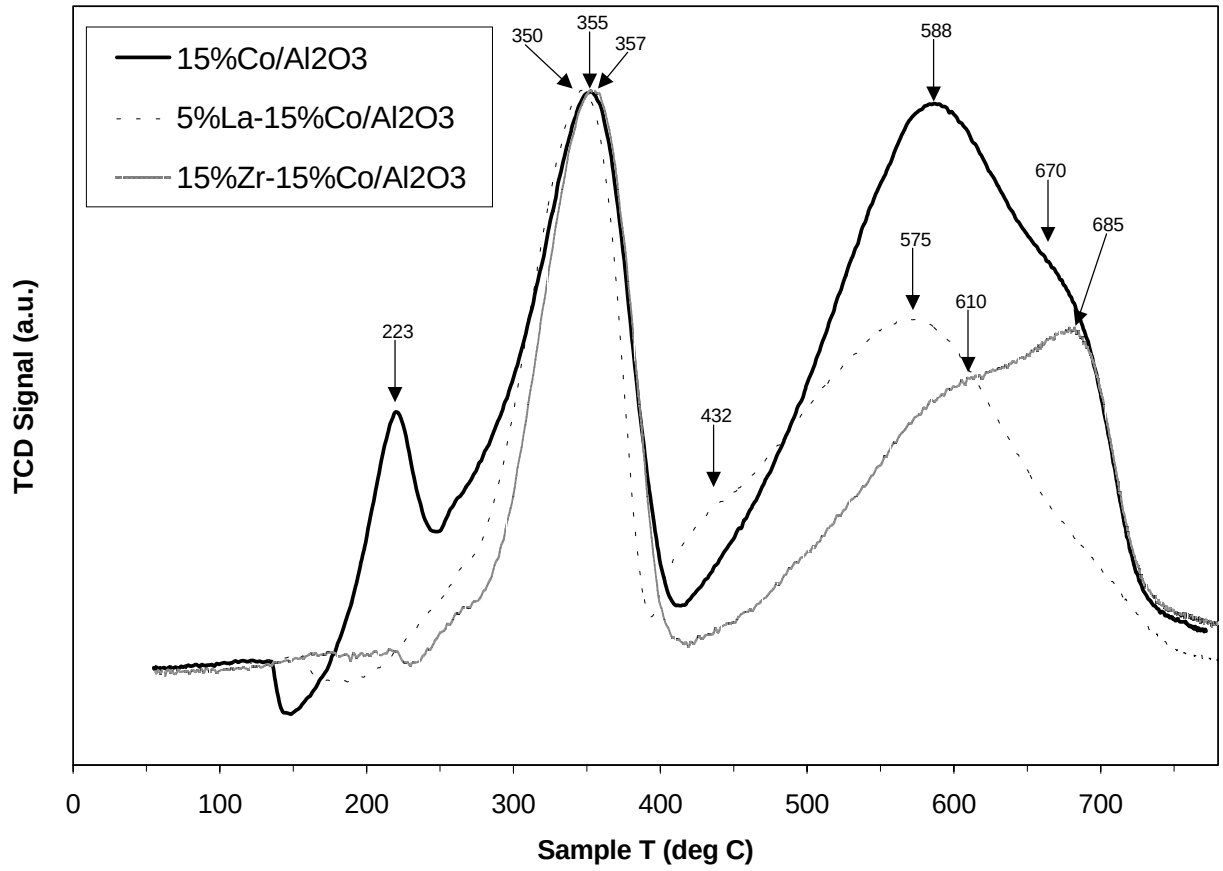

Figure 12. Effect of La or Zr additive on the reduction temperature of 15%Co/Al_2O_3.

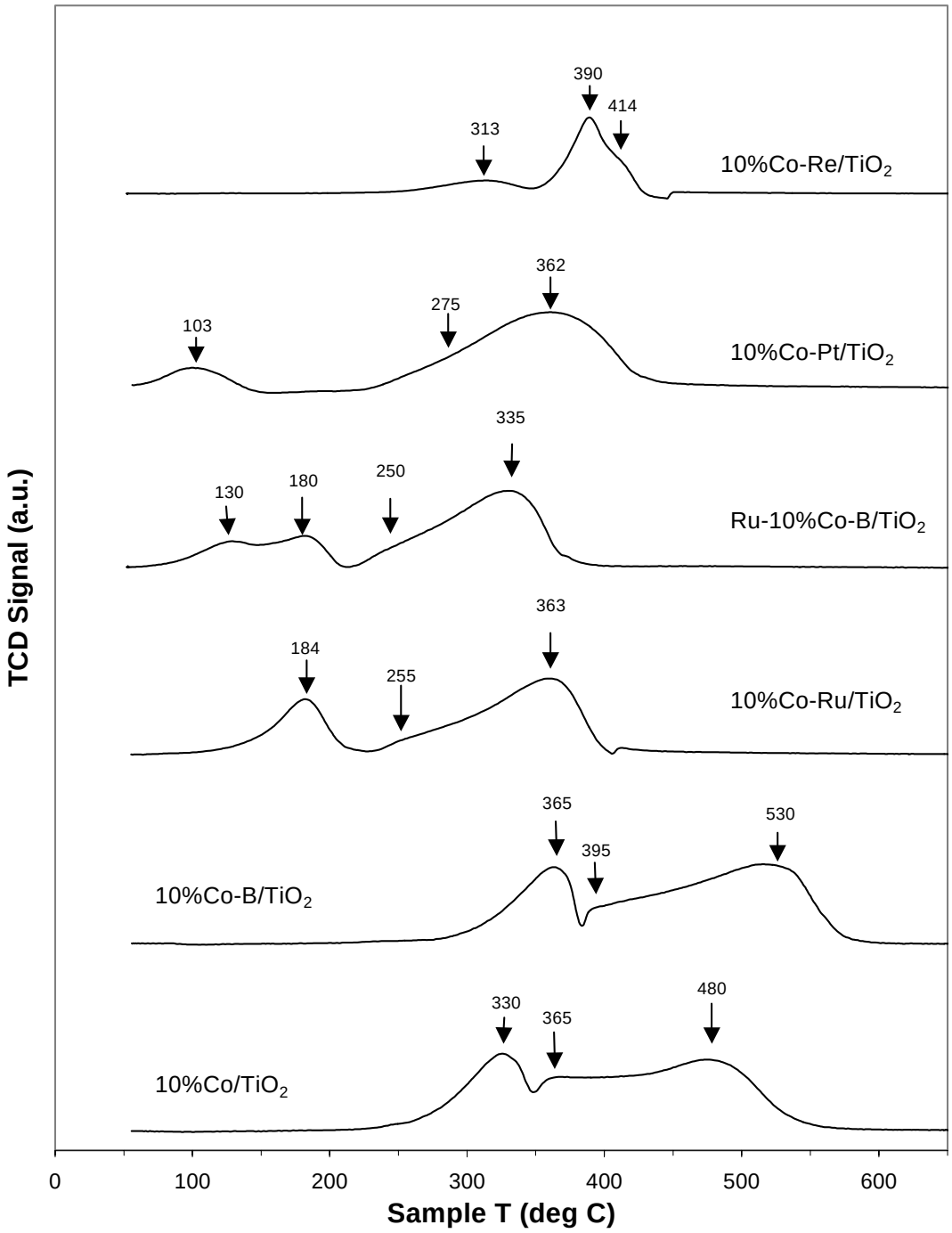

Figure 13. Effect of promoter addition on the reduction temperature of 10%Co/TiO_2.

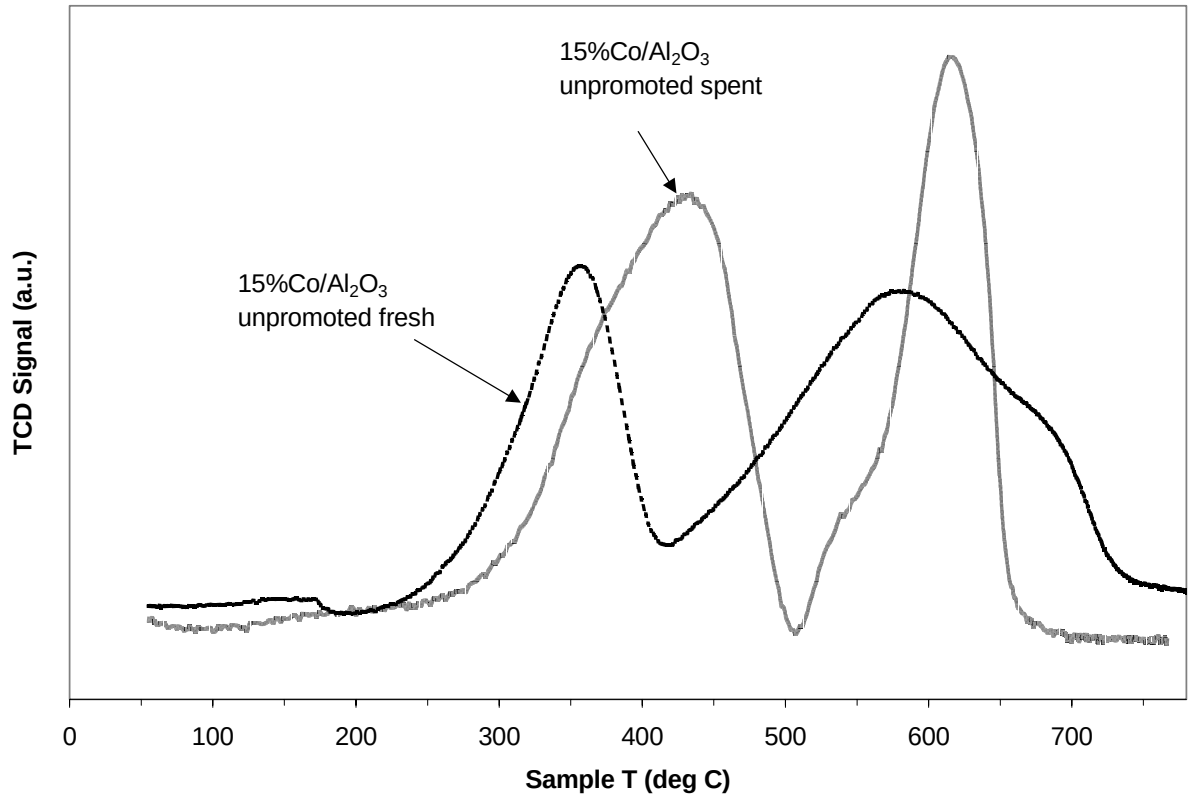

Figure 14. TPR profiles of fresh and spent unpromoted 15%Co/Al_2O_3 catalysts.

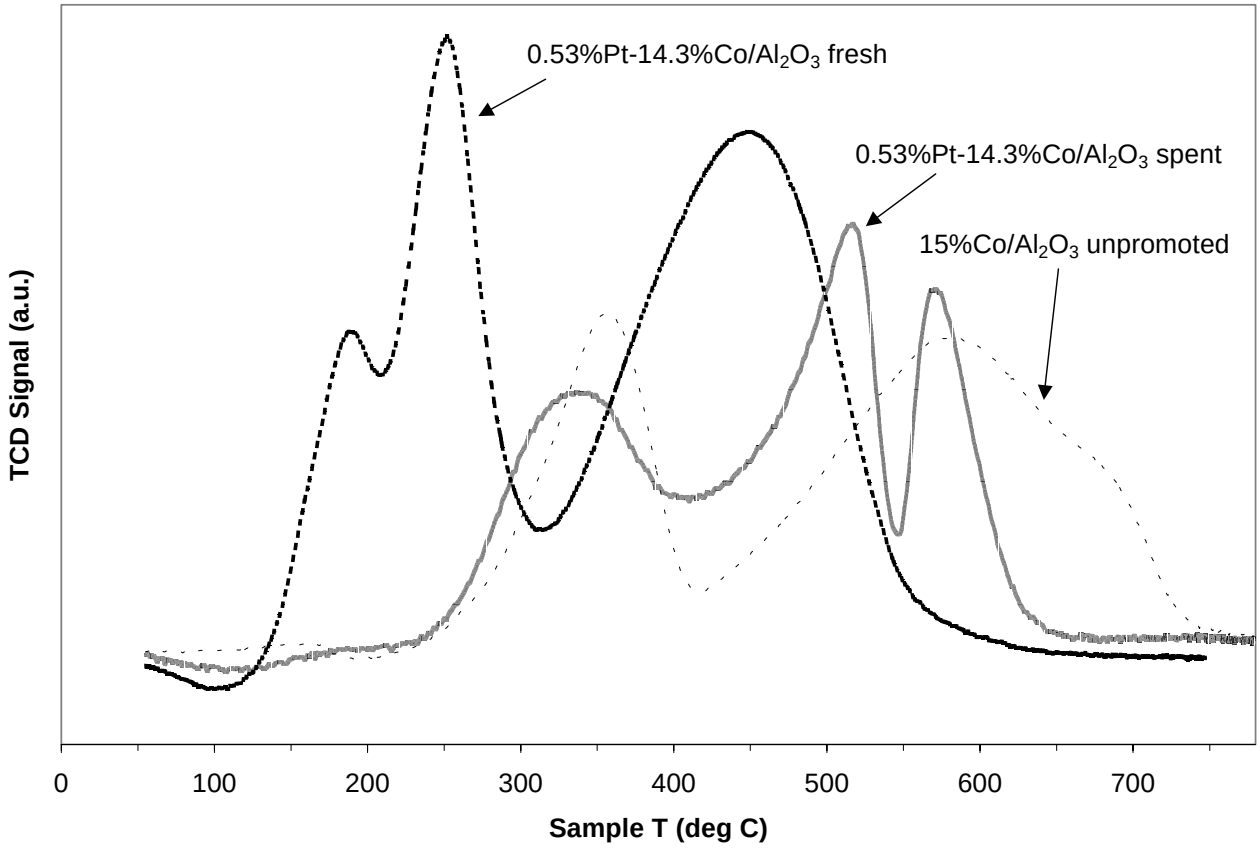

Figure 15. TPR profiles of fresh and spent 14.3%Co/Al_2O_3 catalysts promoted by 0.53% Pt referenced to the unpromoted fresh 15%Co/Al_2O_3 catalyst.

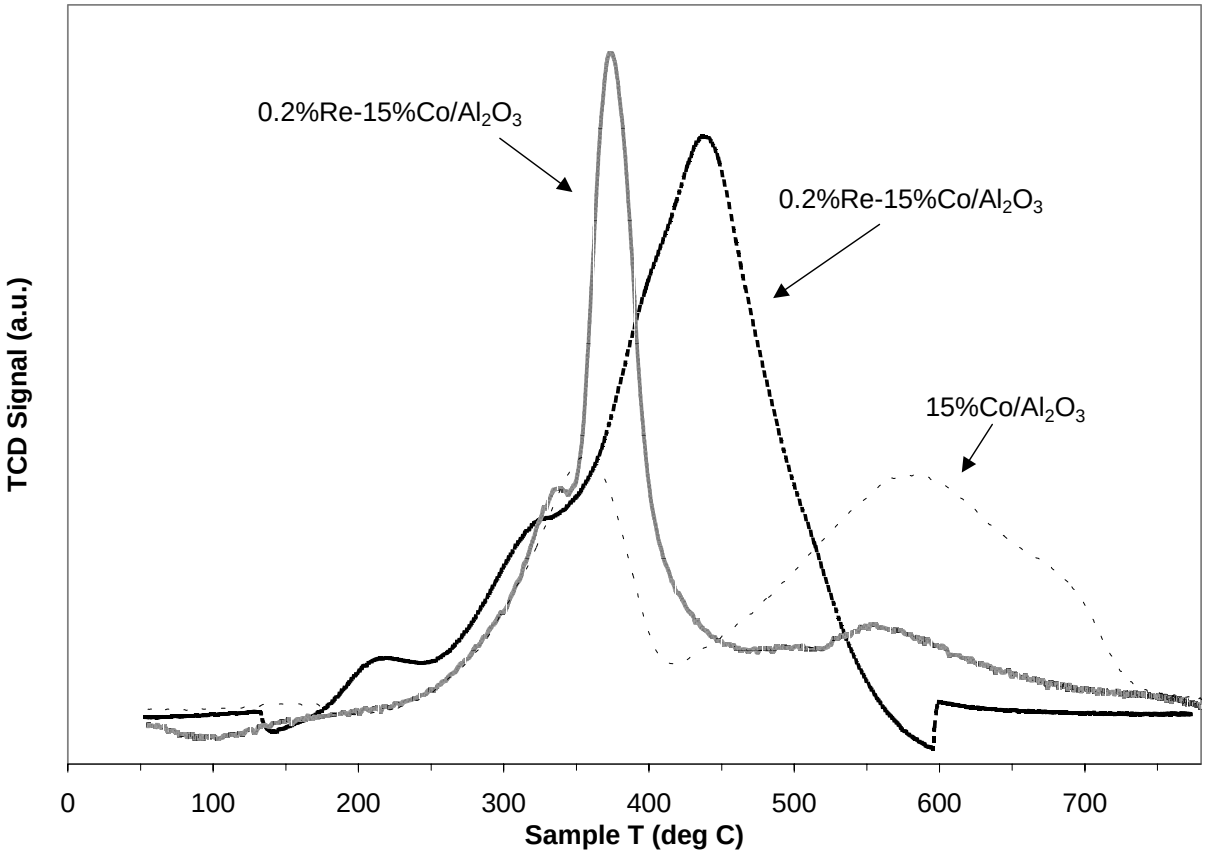

Figure 16. TPR profiles of fresh and spent $15\%Co/Al_2O_3$ catalysts promoted by 0.2% Re referenced to the unpromoted fresh $15\%Co/Al_2O_3$ catalyst.

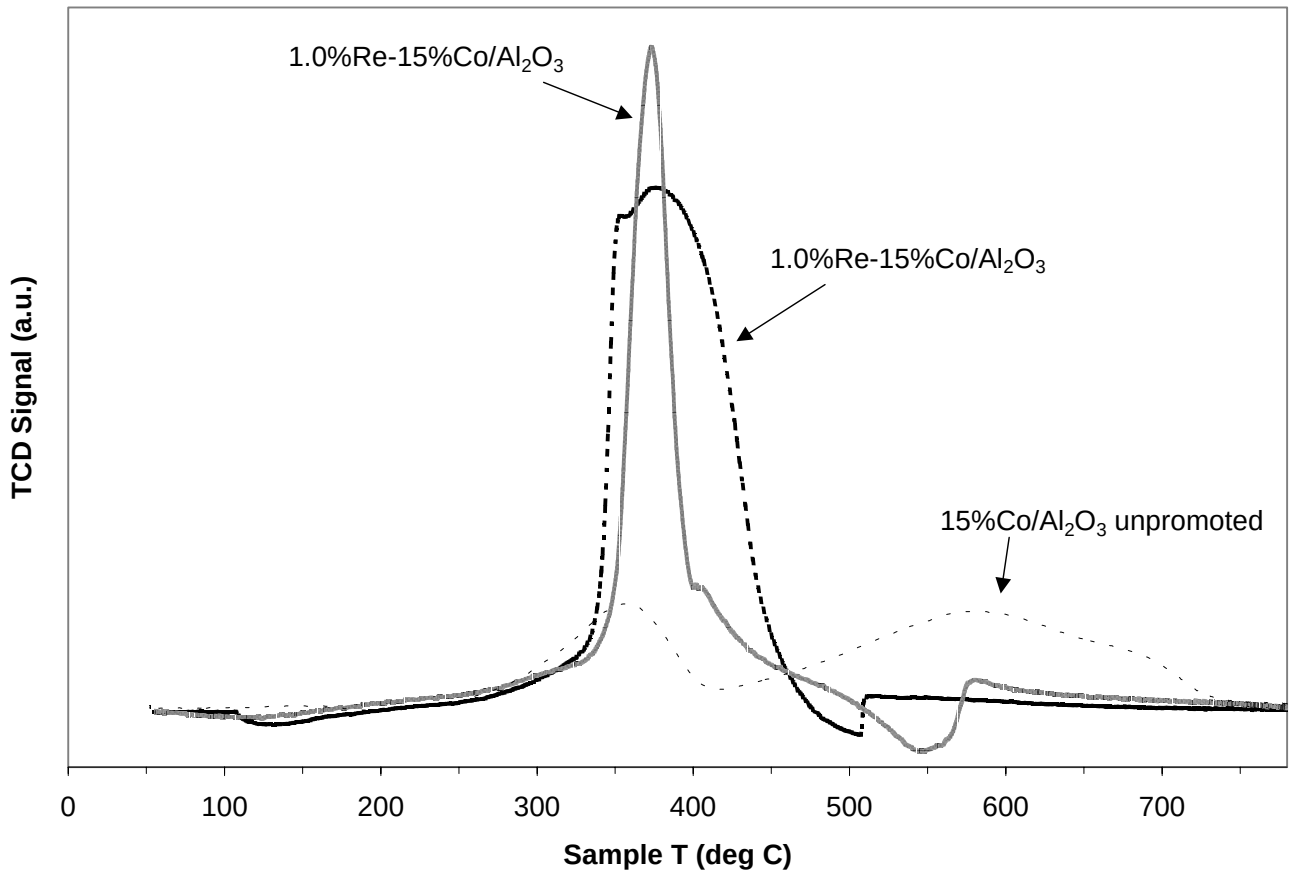

Figure 17. TPR profiles of fresh and spent $15\%Co/Al_2O_3$ catalysts promoted by 0.2% Re referenced to the unpromoted fresh $15\%Co/al_2O_3$ catalyst.

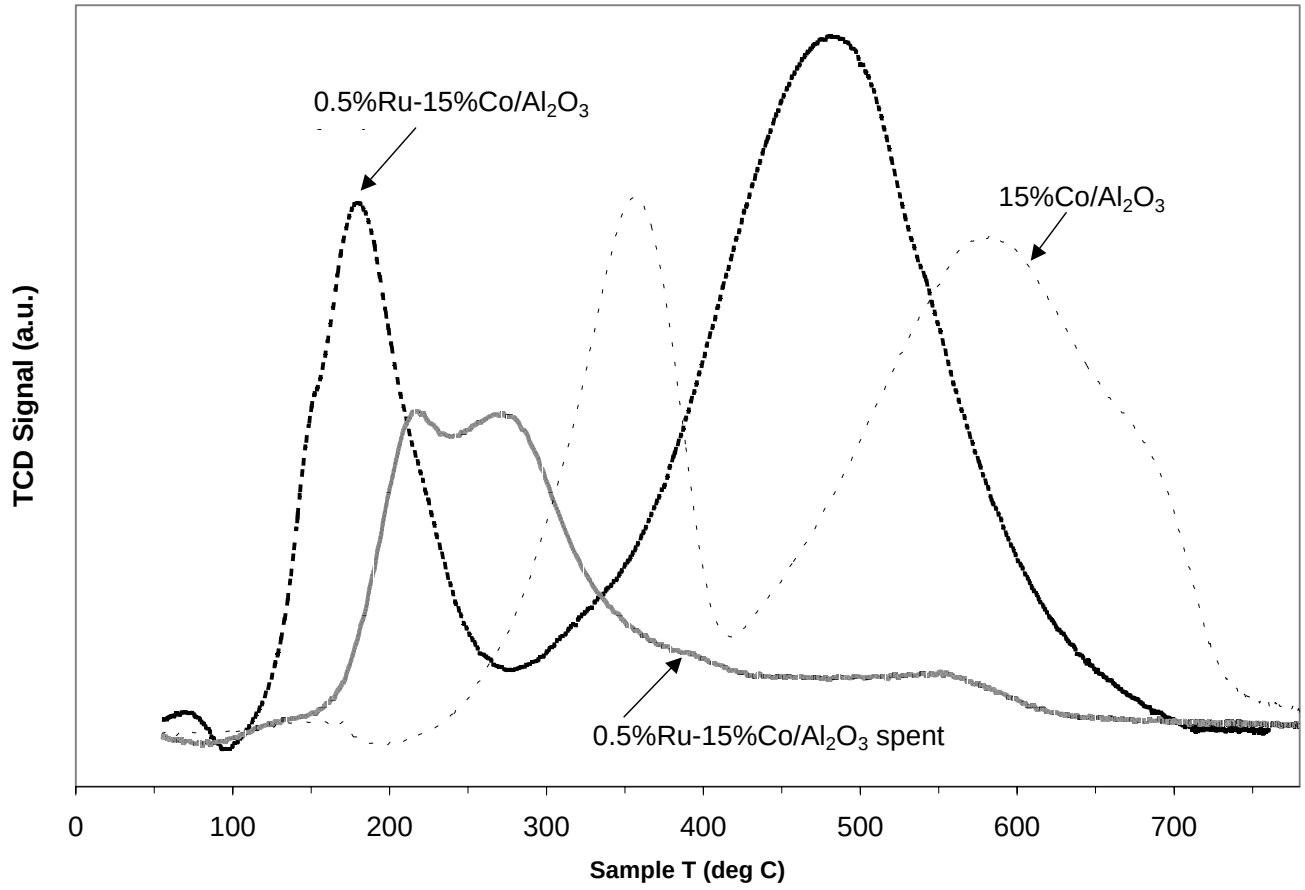

Figure 18. TPR profiles of fresh and spent $15\%Co/Al_2O_3$ catalysts promoted by 0.5% Ru referenced to the unpromoted fresh $15\%Co/Al_2O_3$ catalyst.

F. Fischer Tropsch Synthesis: Support, Loading, and Promoter Effects on the Reducibility of Cobalt Catalysts

Abstract

Temperature programmed reduction (TPR) and hydrogen chemisorption combined with reoxidation measurements were used to define the reducibility of supported cobalt catalysts. Different supports (e.g., Al_2O_3, TiO_2, SiO_2, and ZrO_2 modified SiO_2 or Al_2O_3) and a variety of promoters, including noble metals and metal cations, were examined. Significant support interactions on the reduction of cobalt oxide species were observed in the order $Al_2O_3 > TiO_2 > SiO_2$. Addition of Ru and Pt exhibited a similar catalytic effect by decreasing the reduction temperature of cobalt oxide species, and for Co species where a significant surface interaction with the support was present, while Re impacted mainly the reduction of Co species interacting with the support. For catalysts reduced at the same temperature, a slight decrease in cluster size was observed in H_2 chemisorption/pulse reoxidation with noble metal promotion, indicating that the promoter aided in reducing smaller Co species that interacted with the support. On the other hand, addition of non-reducible metal oxides such as B, La, Zr, and K was found to cause the reduction temperature of Co species to shift to higher temperatures, resulting in a decrease in the percentage reduction. For both Al_2O_3 and SiO_2, modifying the support with Zr was found to enhance the dispersion. Increasing the cobalt loading, and therefore the average Co cluster size, resulted in improvements to the percentage reduction. Finally, a slurry phase impregnation method led to improvements in the reduction profile of Co/Al_2O_3.

Keywords: alumina, cobalt, Fischer-Tropsch synthesis, metal-support effects, TPR, TPD, promoters

Introduction

Supported cobalt catalysts are important for the Fischer-Tropsch synthesis of high molecular weight, paraffinic waxes, which can be hydrocracked to produce lubricants and diesel fuels. One important focus in the development of this process is the improvement of the catalyst activity by increasing the number of active Co metal sites that are stable under reaction conditions. Therefore, it is important to understand how the structural parameters of the catalyst influence the activity and stability of catalysts. For example, to improve the number of active sites, the Co is most often present as dispersed clusters on a high surface area support such as SiO_2, TiO_2, or Al_2O_3. In this particular study, it is observed that not only does choice of support largely determine the number of active sites stabilized after reduction, but it also strongly influences the percentage of the cobalt oxide species that can be reduced. Therefore, for a reduction temperature of 623 K, which is a typical standard reduction temperature for Co FTS catalysts, a tradeoff exists between the cobalt dispersion and the percentage of cobalt oxide species reduced. Supports such as SiO_2, which yield a large cluster size, offer the highest percentage reduction at 623 K, while supports like Al_2O_3, which stabilize a smaller cluster size, have significant support interactions which impede the reduction. That is, after reduction at 623 K for 10 h, a significant fraction of the Co oxide species interacting with the support remains in a non-reduced state.

In order to gain access to the active sites, noble metal promoters are often employed. These noble metal promoters, such as Pt or Ru, reduce at a lower temperature than the cobalt oxides, and catalyze cobalt reduction, presumably by hydrogen spillover from the promoter surface [1-12]. Thus, addition of small amounts of noble metal shifts the reduction temperature of cobalt oxides and cobalt species interacting with the support to lower temperatures. Due to the added expense of the promoter, it is important to determine the appropriate loading of

promoter to maximize the availability of active cobalt surface sites for participation in the reaction, after catalyst activation. In this work, we have studied the addition of Pt, Ru, and Re to a number of different supported Co catalysts.

Textural promoters, such as catalyst supports and support modifiers, are used typically to increase the dispersion of the clusters, improve attrition resistance, enhance sulfur tolerance, or electronically modify the active metal site. In this work, a number of different metal oxide promoters are incorporated to increase dispersion and/or improve attrition resistance. These modifiers, added by impregnation and calcination, included Zr, La, B, and K. The aim of this part of the study is to determine if addition of textural promoters influence significantly the reducibility of the Co oxide clusters.

Due to its high resistance to attrition in the continuously stirred tank reactor (CSTR) or slurry bubble column reactor (SBCR) and its ability to stabilize a small cluster size, Al_2O_3 is a particularly appealing support for Co based FTS catalysts [13]. However, due to the strong interactions of Co species with the support, more insight is needed in understanding the effect of the loading and size distribution on both the reducibility and the stability of these clusters during FTS. In this work, TPR and H_2 TPD/reoxidation are used to examine a series of Co/Al_2O_3 catalysts prepared with different loadings by an incipient wetness impregnation (IWI) method. Finally, a catalyst prepared by IWI with a nominal loading of 25% Co was compared with a catalyst prepared by a slurry impregnation method following a Sasol patent. As is evident from this work, each parameter plays an important role in the accessing of Co metal sites for reaction.

H_2 TPD followed by pulse reoxidation is a useful technique [11], because it quantifies the actual dispersion (cluster size) by taking into account the percentage reduction of cobalt. The desorption of chemisorbed hydrogen yields an active site count, while the uptake of oxygen for

the reduced catalyst at high temperature provides an estimate of the percentage of cobalt metal that was reduced. Combined, the dispersion is determined as follows:

%Dispersion

= (#Co^0 atoms on surface × 100)/(total # Co^0 atoms)

= (#Co^0 atoms on surface × 100)/(total # Co atoms in sample)(fraction reduced)

Defining the dispersion in this way, an estimate of the actual cluster size can be determined. Without including the percentage of reduction in the calculation, the percentage dispersion is underestimated and, therefore, the resulting cluster size will be overestimated. This correction to the dispersion becomes particularly important in the study of promoted catalysts.

Experimental

Catalyst Preparation

Davisil silica gel 644 (100-200 mesh, surface area 300 m^2/g, pore volume 1.15 cm^3/g), Degussa P25 titania (120-200 mesh, surface area 45 m^2/g, 0.50 cm^3/g), Condea Vista Catalox B γ-alumina (100-200 mesh, 200 m^2/g, pore volume 0.4 cm^3/g) and zirconia modified Davisil 952 silica (60-80 mesh, 309 m^2/g, pore volume 1.61 cm^3/g) were used as support materials for the preparation of cobalt FTS catalysts. The support was calcined at 673 K. Cobalt loadings of 10, 15, 20 and 25% were used. For example, a three-step incipient wetness impregnation method was used to add a total of 15 wt % cobalt to the supports, with a drying procedure at 353K in a rotary evaporator following each impregnation. Noble metal promoted catalysts were prepared with different loadings of ruthenium, platinum, or rhenium by adding the noble metal solution after cobalt addition and prior to calcination. Additional metal cation promoted catalysts were prepared by incorporating boron, potassium, zirconium, or lanthanum to the support after adding

cobalt and prior to calcination. Following cobalt addition, the promoter was added by incipient wetness impregnation. The precursors utilized for noble metal addition were ruthenium nitrosylnitrate, tetraammineplatinum (II) nitrate, and rhenium oxide. For the metal cation precursors, boric acid, potassium carbonate, zirconium nitrate, and lanthanum nitrate were employed. After promoter addition, the catalysts were again dried in a rotary evaporator at 353 K. Catalysts were calcined only one time in air at 673 K for 4 hrs following the final impregnation step. One exception was the boron promoted TiO_2 catalyst, where the boric acid precursor was added to the support and calcined prior to cobalt addition.

To understand the influence of loading of Co on the reducibility of clusters, a series of Co/Al_2O_3 catalysts was prepared by IWI following the procedure outlined above. The catalysts were prepared on 100 m^2/g, 150 m^2/g, and 200 m^2/g Condea Vista Catalox (or Puralox) B γ-Al_2O_3 supports and the Co loading was approximately 15%, 25%, and 33%, respectively. Multiple impregnations of 5% Co were performed with drying steps in a rotary evaporator. Finally one calcination step was employed after the final impregnation.

One Co/Al_2O_3 catalyst with a loading of 25% was also prepared by a slurry impregnation method. In this method, which follows a Sasol patent [13], the ratio of the volume of loading solution used to the weight of alumina was 1:1, such that approximately 2.5 times the pore volume of solution was used to prepare the catalyst. Two impregnation steps were used to load 12.5% of Co by weight. Between each step the catalyst was dried under vacuum in a rotary evaporator at 333 K and the temperature was slowly increased to 373 K. After the second impregnation/drying step, the catalyst was calcined in the usual manner.

To study the effect of calcination procedure on noble metal promoted catalysts, a series of catalysts with different loadings of Re was prepared where the catalyst was calcined after each sequential impregnation of 5% Co (total of 3 times) after drying and one more time after loading

of the Re promoter. This series of catalysts is labeled “with interval calcination”. The Re promoted catalysts prepared by the standard procedure, where there was only one calcination after loading both Co and promoter, are labeled “without interval calcination procedure.”

Inductively Coupled Plasma

Inductively coupled plasma (ICP) was used to obtain weight percentages of Co metal in the sample. First, the catalyst powder was dissolved in a mixture of aqua regia and HF. A nebulizer was used to introduce the sample to the plasma torch at a diameter of less than 10 microns in Ar carrier. The torch is located in an induction coil, carrying high frequency AC. The electrically conducting ionized gas was thus heated by Joule’s effect to temperatures in the vicinity of 10,000 K. Under these conditions, the particles were atomized and partially ionized. When reverting to lower energy states, photons were emitted and detected for element analysis. A Spectrametrics ICP unit was utilized to verify the Co loadings and for the Zr loadings in the case of the supports modified by ZrO_2.

BET Surface Area Measurements/BJH Pore Size Distributions

The surface area, pore volume, and average pore radius of the supports and catalysts were measured by BET using a Micromeritics Tri-Star system. Prior to the measurement, the sample was slowly ramped to 433K and evacuated for 4hrs to approximately 6.7 Pa. Results of physisorption measurements are shown in Tables 1 and 2. Pore size distributions (PSD) of a number of supports and catalysts were also quantified by the Barrett, Joyner, Halenda (BJH) desorption model, which provides a relationship where the amount of adsorbate lost during a desorption step gives the average size of the pore emptied during that desorption step. Experimentally, the adsorption branches were employed, and PSDs are shown in Figure 1. Cumulative pore volumes from BJH adsorption/desorption are also given in Tables 1 and 2.

Temperature Programmed Reduction

Temperature programmed reduction (TPR) profiles of catalysts were recorded using a Zeton Altamira AMI-200 unit. Calcined fresh samples were first purged in flowing inert gas to remove traces of water. TPR was performed using a 10% H_2/Ar mixture referenced to Ar at a flowrate of 30 ccm. The sample was heated from 323 K to 1073 K using a heating ramp of 10 K/min.

H_2 Chemisorption by TPD and % Reduction by Reoxidation

The amount of chemisorbed hydrogen was measured using the Zeton Altamira AMI-200 unit, which incorporates a thermal conductivity detector (TCD). The sample weight was always 0.220 g. A typical catalyst was activated using hydrogen at the desired reduction temperature (573 K for TiO_2 and 623 K for other catalysts) for 10 hrs and cooled under flowing hydrogen to 373 K. The sample was held at 373 K under flowing argon to remove physisorbed and/or weakly bound species, prior to increasing the temperature slowly to the reduction temperature. At that temperature, the catalyst was held under flowing argon to desorb the remaining chemisorbed hydrogen until the TCD signal returned to the baseline. The TPD spectrum was integrated and the number of moles of desorbed hydrogen determined by comparing to the areas of calibration pulses of hydrogen in argon. Prior to experiments, the sample loop was calibrated with pulses of N_2 in a helium flow and compared against a calibration line produced from using gas tight syringe injections of N_2 into a helium flow.

After TPD of H_2, the sample was reoxidized [11] at the activation temperature by pulses of pure O_2 in helium carrier referenced to helium gas. After oxidation of the cobalt metal clusters (when the entire O_2 pulse was observed by the TCD), the number of moles of O_2 consumed was determined, and the percentage reduction was calculated assuming that Co^0 reoxidized to Co_3O_4.

The calculations are summarized below:

Calibration Value (L gas/Area Units) = (Loop Volume × % Analytical Gas)/(Mean Calibration Area × 100)

H_2 Uptake (moles/g cat) = (Analytical Area from TPD × Calibration Value)/(Sample Weight × 24.5)

% Dispersion= (H_2 uptake × Atomic Weight × Stoichiometry)/(% Metal)

= (Number Co^0 Atoms on Surface × 100)/(Total Number Co^0 Atoms)

= (Number Co^0 Atoms on Surface × 100)/(Total Number Co Atoms in Sample × Fraction Reduced)

O_2 Uptake (moles/g cat) = (Sum of Consumed Pulse Areas × Calib Value)/(Sample Weight × 24.5)

Assuming $Co^0 + 2/3O_2 = 1/3Co_3O_4$,

Fraction Reduced = (O_2 uptake × 2/3 × atomic weight)/(% metal)

Diameter of Spherical Crystallite = 6000/(density × maximum area × Dispersion)

Results and Discussion

Surface Area Measurements

Results of surface area measurements by adsorption of nitrogen at 77 K (Tables 1 and 2) show that the BET surface areas for the 15% loaded Co catalysts on 200 m^2/g γ-Al_2O_3 were all close to 160 m^2/g. A weight % loading of 15% metal is equivalent to 20% by weight Co_3O_4. If the Al_2O_3 is the only contributor to the area, then the area of the Co/Al_2O_3 catalysts should be 0.80 ×200 m^2/g = 160 m^2/g, which matches the measured value. Similarly, with the 15% loaded Co catalysts on 311 m^2/g 644 Davisil SiO_2 and the 20% Co loaded catalysts on 295 m^2/g 952 Davisil SiO_2, the BET areas should be approximately 0.80 ×311 m^2/g = 249 m^2/g and 0.73 ×295

m^2/g = 215 m^2/g, respectively. However, the values are somewhat lower (approximately 210 m^2/g and 200 m^2/g, respectively), which indicates some pore blockage by cobalt oxide clusters. Finally, for the 10% loaded Co catalysts on 45 m^2/g Degussa P25 TiO_2, the BET areas should be approximately 0.87 ×45 m^2/g = 39 m^2/g, very close to the measured values. In Table 2, which displays the Co/Al_2O_3 catalysts with different loadings on three different surface area supports, the increase in average pore size for the highest loading of approximately 33% indicates that some pore blockage of the smaller pores occurred.

Support Effects

Figure 2(a) shows the TPR profiles for the unpromoted cobalt catalysts. For the two SiO_2 supported catalysts, two peaks are apparent and these are attributed to the reduction of Co_3O_4 to CoO, which then reduces at higher temperatures to metallic Co^0, as observed for reduction of bulk cobalt oxide Co_3O_4. As shown in the figure, the addition of surface ZrO_2 to silica did not significantly affect the reducibility, although there may have been a slight shift to higher temperatures. The TiO_2 and Al_2O_3 supported cobalt catalysts displayed broad peaks at temperatures that are higher than observed for silica, due to the interaction of the Co surface species with the support.

Figure 2(b) shows the TPR of the 15% Co/Al_2O_3 catalyst directly after calcination, and another after it was reduced at 623 K for 10 hrs. By taking the difference of the two TPR spectra, it is observed that only a small fraction of the Co surface species responsible for the broad peak is reduced during the standard reduction procedure at 623 K for 10 hours.

In the TPR, the temperature was not ramped high enough to observe the reduction of bulk cobalt aluminate species, which has been shown to occur above 1073 K with up to 30% loading of cobalt [14]. Therefore, the broad peak on the unpromoted catalyst (ca. 700 to 1000 K) is attributed to the reduction of Co surface species that interact with the support, and the different

shoulders are likely due to varying degrees of interaction with the support as a function of cluster size. The smallest Co surface species, with the greatest interaction with the support, are therefore likely represented by the shoulder at 950 K. The precise identity of these species is not clear, although it is surmised that the species are either the result of a strong interaction between very small cobalt oxide clusters and the support (deviating from bulklike cobalt oxides and reducing at higher temperatures than the bulk oxides) or small surface Co species which include support atoms in the structure (reducing at temperatures below that of bulk Co-aluminate). Hereafter, the species responsible for this peak will be referred to loosely as "Co surface support species".

Al_2O_3 supported Co Catalysts

Influence of Co Loading

As the cobalt loading is increased, important changes in the degree of interaction of the cobalt species with the support are observed. Figure 2(c) shows a reduction profile for the 25% Co/Al_2O_3 catalyst prepared by IWI. In contrast with the 15% loaded catalyst, there is a remarkable decrease in the intensity of the reduction shoulder at 950 K, while there is the appearance of a sharp peak at 600 K. These differences are attributed to the increase in the average cluster size and the resulting loss of interaction with the support. The 25% Co catalyst starts to resemble the two step reduction of bulklike Co_3O_4. Again, a TPR was conducted following the 10 h standard reduction at 623 K, and the catalyst showed a higher percentage reduction, indicated by the smaller peaks remaining after difference in comparison with the 15% loaded Co catalyst (Figure 2(b)).

These changes in reducibility become more apparent when considering several catalysts prepared with different loadings by IWI on three different surface area γ-Al_2O_3 supports, as shown in Figure 3. Moving upward from the 15% loaded catalyst prepared on 200 m^2/g to the

150 m^2/g support, the low temperature peak of the profile is shifted by 60 K. At a loading of approximately 25% and higher, there is the appearance and sharp growth in a peak at 600 K, which is attributed to the reduction of bulklike CoO species. Also, the maximum in the broad peak shifts stepwise to lower temperature with loss in interaction due to (1) increased loading resulting in increased cluster size or (2) lower support surface area. As expected, the highest loaded catalyst (34.3%) on the lowest surface area support (100 m^2/g) showed the greatest resemblance to reduction of bulk Co_3O_4.

In agreement with the results of TPR, H_2 chemisorption/pulse reoxidation results in Table 3 indicate that improvements in the percentage reduction are obtained by increasing the average cluster size by either increasing loading or switching to lower surface area supports with the same loading. The results also stress the importance of including the percentage of reduction measurement in the dispersion calculation, so that the actual number of total Co metal atoms in the sample are used in the denominator, instead of the total Co atoms, as shown below.

$$\%D = \frac{Number\ Co^o\ atoms\ on\ surface\ x\ 100}{total\ number\ Co^o\ atoms} = \frac{Number\ Co^o\ atoms\ on\ surface\ x\ 100}{(total\ number\ Co\ atoms)(\ fraction\ reduced)}$$

This correction is important in the study of promoters to follow.

Slurry Phase Impregnation

The reduction profile of the 15% Co catalyst prepared by the standard IWI method indicates heterogeneity of oxide cluster size, with each cluster size yielding a different interaction with the support, resulting in a broad reduction peak with a high temperature shoulder. The average cluster size was significantly less than 10 nm, within the size range reported to undergo deactivation by oxidation under FTS conditions in the reactor [15,16].

However, increasing the loading by IWI indicates an even wider range of cluster size, as a sharp shoulder occurs at 600 K corresponding to reduction of bulklike CoO.

Using a slurry phase impregnation method following a recipe in a Sasol patent, an attempt was made to decrease the heterogeneity in cluster size distribution, while maintaining the cluster size above the 10 nm threshold by keeping the loading at 25%. As shown in Figure 4, the sharp peak at 600 K generated by the IWI catalyst is not present in the catalyst prepared by the slurry method. Results of H_2-chemisorption/pulse reoxidation in Tables 3 and 4 indicate that while the average cluster size on the IWI was 13.7 nm, the slurry method catalyst was only slightly lower, at 11.8 nm.

Cluster Resistance to Reduction Treatment

Table 5 shows the results of an experiment where the 15% Co/Al_2O_3 catalyst was ramped by 1 K/min to a desired reduction temperature and then held for 10 h for reduction in hydrogen. The catalyst was then cooled to 373 K and ramped by 10 K/min to the treatment temperature in Ar to desorb the chemisorbed H_2. Each TPD of H_2 was followed by pulse reoxidation. This proceeded in a stepwise manner for reduction temperatures of 473 K, 573 K, 673 K, 773 K and 873 K. Afterwards, a fresh sample was analyzed by ramping directly to 773 K by 1 K/min and reduced for 10 h at 773 K. TPD and pulse reoxidation were conducted in the same manner. Without considering the fraction of cobalt that is reduced, there is a gradual decrease in the average cluster size as the reduction temperature is increased (Table 5). However, the results in Table 5 demonstrate that the corrected average cluster size does not change significantly after reduction at each temperature. Rather, pulse reoxidation reveals that the percentage reduction changes at each step, increasing greatly the number of sites available for reaction. Changing the heating rate (direct heating versus slow ramp and hold) may cause some growth of the cluster, 6.2 nm for direct versus 5.6 nm for ramp and hold. It appears that the smaller particles are being

reduced using the ramp and hold procedure as the temperature is increased since there is a progressive decrease in average particle size: 5.9 nm, 673 K; 5.6 nm, 773 K; and 5.2 nm, 873 K. The only exception is the first value reported after reduction at 573 K. However, comparing this reduction temperature with the TPR spectra indicates that the entire cluster may not be reduced. Therefore, a lower value of the average cluster size at this temperature may be indicative of partial reduction of the cluster.

Promotion by Pt

Figure 5 shows a TPR comparison of Pt promoted Co/Al_2O_3 with the unpromoted catalysts at two different loadings of cobalt – 15% prepared by IWI and 25% prepared by the slurry impregnation method. The addition of Pt caused the peaks to shift markedly to lower temperatures, presumably due to spillover of H_2 from the metallic promoter to reduce the Co oxide and Co surface support species. Of particular importance, peaks attributed to the reduction of Co surface support species [17] are reduced at lower temperatures (ca. 100 K shift), freeing up the availability of metal atoms for catalytic reaction.

Results of H_2 chemisorption by TPD (Table 4) indicate that the number of surface sites increases with addition of the Pt promoter. By performing pulse reoxidation, it is clear that the gain in Co^0 site density is mainly due to an enhancement in the reducibility of the clusters, and not to improvements in the actual dispersion (cluster size) of the reduced cobalt. However, for both the 15% and 25% cobalt catalysts, addition of Pt appears to cause a slight decrease in the cluster size. This is reasonable, because the comparison was conducted at the same reduction temperature of 623 K, and addition of Pt should cause a fraction of the smaller Co surface species that interact with the support to be reduced in this temperature range, resulting in a slightly smaller average cluster size.

Increasing the Co loading alone caused a lowering of the reduction temperature of both the unpromoted and especially so for the promoted catalysts, as observed previously [14]. With the promoted catalyst, for example, the maximum for the peak attributed to the reduction of Co surface species interacting with the support decreased by 35 K (from 760 K to 725 K), while the lower temperature peak attributed to reduction of cobalt oxides shifted by 70 K (from 500 K to 430 K). Results of H_2 chemisorption by TPD and pulse reoxidation (Table 4) revealed that, for both unpromoted and promoted catalysts, there were significant increases (from 30% to 42% for unpromoted and from 60% to 71% for promoted) in the percentage reduction of the catalyst, with a doubling of the average cluster size. These findings are in agreement with a previous investigation [18].

Promoter Addition and Calcination Pretreatment Effects

The addition of Ru to the catalyst had a similar effect on the TPR as Pt did. Figure 6 shows that addition of 0.2 wt % Ru results in an improvement in the reducibility of the catalyst, but that increasing the promoter loading above 0.5 wt % only resulted in marginal enhancement. As with the case of Pt, H_2 chemisorption (Table 4) indicates that addition of 1% Ru has a greater impact on the cobalt reducibility than the dispersion, resulting in an almost twofold improvement in the number of active sites available for reaction after reduction at 623 K, while maintaining essentially the same average particle size.

The reduction of Re oxide occurs at a higher temperature than Pt oxide or Ru oxide. Figure 6 shows that although there appears to be no improvement in the reduction of the low temperature peak assigned to the reduction of cobalt oxides, Re still plays a role by decreasing the reduction temperature of Co species for which there is a significant surface interaction with the support. The reduction of Co oxides appears as the low temperature shoulder to the sharp peak for reduction of the Co surface support species with the addition of Re. Figure 6 shows that

Re oxide reduces at 620 K, which explains the lack of effect on the low temperature peak responsible for reduction of cobalt oxides. A previous study of promotion of cobalt catalysts by Re [12] found that rhenium oxide on alumina reduced at approximately 698 K, a value that falls between our two TPR peaks for the unpromoted Co/Al_2O_3 catalyst. TPR profiles in Figure 6 show that cobalt oxide crystallites have essentially been reduced before the Re oxide is reduced, so no spillover effect can operate to aid in reducing those species. However, H_2 spillover from the reduced Re metal occurs to facilitate reduction of Co species interacting with the support only after the reduction peak of Re oxide to Re metal is achieved. Again, Table 4 shows by H_2 chemisorption that addition of Re improves the degree of reduction of the catalyst more than the dispersion (cluster size).

Figure 7 shows profiles for two different series of Re promoted 15% Co/Al_2O_3 catalysts. The difference between the two series of catalysts is in the preparation. The dark line spectra correspond to catalysts prepared by loading the Co by three successive incipient wetness impregnation steps followed by loading of the promoter, where the catalyst was dried between each impregnation step. Only one calcination was used after the last step (loading of the promoter). The other series of catalysts was prepared in a similar manner, except that the catalyst was calcined after each sequential impregnation and drying step, for a total of four times (3 times for Co and 1 time for promoter). Clearly, there is a strong advantage with respect to reducibility by decreasing the number of calcination steps used to prepare the catalyst. This suggests that excessive calcination increases the formation of Co surface support species, which are more difficult to reduce.

Figure 8 provides a comparison of different Al_2O_3 supported cobalt catalysts with and without the addition of metal and metal cation promoters. Addition of noble metals aids in promoting the reduction rate, and consequently increases the amount of available Co metal

surface area (see H_2 chemisorption data, Table 4), but their effect on percentage dispersion is minimal. In contrast, as shown in Figure 8 and Table 4, addition of the irreducible ZrO_2 depresses the reduction rate (and hence the H_2 chemisorption) but increases the corrected dispersion. Addition of La_2O_3 had a small negative effect on reduction rate without influencing the dispersion relative to the unpromoted catalyst. As shown in Table 4, increasing the reduction temperature increased the percentage reduction without significantly altering the cluster size. With the ZrO_2-containing catalyst, the average cobalt clusters were much smaller (Table 4). Therefore, it was expected that the interaction with the support (and perhaps the promoter cation) would be noticeably different in the TPR. Recall that the second peak corresponds to reduction of Co-support interaction species to Co^0, and that the high temperature shoulder at 950 K in the unpromoted catalyst is attributed to the interaction of smaller clusters with the support. For the ZrO_2 promoted catalyst, the relative intensity of the high temperature shoulder at 950 K is greater than for the unpromoted. Addition of the noble metal promoters (Pt, Ru, or Re), in the amount of 0.5% by weight, to the Co/ZrO_2-Al_2O_3, was found to improve the percentage reduction more than the dispersion.

Also, for the ZrO_2 and La_2O_3 promoted samples, there was a noticeable attenuation in the intensity of the peaks corresponding to reduction of Co surface species interacting with the support in comparison to the other samples. In considering the results in Table 4 for percentage reducibility, it is presumed that the rest of the cobalt is present as aluminates, or perhaps some other mixed oxide form including the metal oxide promoter that reduces above 1073 K. In a previous study [14], decreasing the cobalt loading (and presumably, cluster size) changed the ratio of peaks corresponding to oxide and aluminates in favor of aluminates. Another investigation [19], where different atomic contents of Co and Pt were used, yielded results similar to the present study.

SiO_2, ZrO_2 modified SiO_2, and TiO_2 supported Catalysts

TPR shows that, in contrast with the Al_2O_3 supported catalysts, there appeared to be little interaction of the cobalt species with the SiO_2 support (see Figure 2). This is reasonable, since for the SiO_2 supported catalysts, a much larger cobalt cluster size was determined by H_2 chemisorption and pulse reoxidation (Table 6). This suggests that during preparation, cobalt species interact more strongly with Al_2O_3 than SiO_2, resulting in the stabilization of a smaller cluster size for a comparable loading and support surface area. Addition of either Ru or Pt to the support had a similar effect by decreasing the reduction temperature of the cobalt, as shown in the TPR spectra of Figure 9. Both promoters had a more important role in increasing the rate of reduction of the first peak that corresponds to reduction of Co_3O_4 to CoO with a remarkable shift from 570 K to 400 K. On an atom of promoter per atom of Co basis, Figure 9 indicates that Pt was more effective than Ru in enhancing the reduction of Co. In both cases, approximately 4% atomic (with respect to Co) loading of promoter was optimal for a catalyst with a loading of 15% Co. Adding a larger amount of noble metal promoter showed little further improvement in reducibility. H_2 chemisorption and pulse reoxidation results shown in Table 6 for an atomic loading of 8% (corresponding to 3.8 wt % Pt and 2.0 wt % Ru) indicate that the cluster size decreased with percent reducibility with the addition of noble metal promoters. Because the reduction profiles of noble metal promoted SiO_2 catalysts occur over a wider range of temperature than for the unpromoted catalyst, they appear to be less susceptible to sintering. Unlike the Co/Al_2O_3 catalysts, which displayed only a little change in the cluster size with increased percentage reducibility, a notable decrease was found in the series of Co/SiO_2 catalysts. Addition of the cation, K^+, shifts both reduction peaks to higher temperatures, with a noticeable broadening of the peaks (Figure 10).

Figure 11 in conjunction with Table 6 shows that similar promoter effects were observed between the ZrO_2-SiO_2 and SiO_2 supported Co catalysts, which displayed a larger average cluster size and less support effects, while the TiO_2 supported Co catalysts showed similar promoter effects as the Al_2O_3 supported catalysts. Data in Tables 4 and 6 indicate that both Al_2O_3 and TiO_2 stabilized a smaller average cluster size than the SiO_2 based catalysts and exhibited greater interactions with the support. Ru and Pt particularly enhanced the rate of reduction of bulk-like cobalt oxides (first peak) for all supports, and for the reduction of Co species where a significant interaction with the support was present (the broad high temperature reduction peak for the Al_2O_3 and TiO_2 catalysts). A moderate enhancement was achieved for Pt and Ru promotion for the ZrO_2-SiO_2 catalyst for reduction of CoO to Co^0 (second sharp peak), while only a slight shift was observed for the promoted SiO_2 catalysts.

In all cases, Re had a different effect from Pt and Ru. Re played a more important role in catalyzing the reduction of the second peak, attributed to reduction of Co support species to Co^0, particularly when a strong interaction of the support was present (Al_2O_3 and TiO_2 supported catalysts). The first peak, corresponding to reduction of bulk cobalt oxides, changed very little or not at all for all supported catalysts studied, with Re as the promoter.

Role of Promoters and Cluster Size in Improving Reducibility

If the dispersion is based on the total cobalt that is present, the results indicate that the catalysts prepared in this study are in the range reported by others [20]. However, if the dispersion is considered on the basis of the fraction of cobalt reduced, a different conclusion is reached. As shown in Figure 12 for the silica and titania-based catalysts and Figure13 for the alumina supported catalysts, the dispersions within a group of similar catalysts are essentially the same. For example, for the 15% Co/Al_2O_3 catalyst, the corrected dispersions of all catalysts, noble metal (i.e., Pt, Ru, Re) promoted and unpromoted, are in the 16-20% range; this is true

even though the percentage of cobalt that is reduced varies from 25% to 70%. The incorporation of 5 wt. % La does little to alter the dispersion from that of the unpromoted catalyst. Interestingly, 10% zirconia promotes the dispersion by about a factor of 2 in comparison with the unpromoted Al_2O_3 catalyst. However, the percentage reducibility drops to a third of the value for the unpromoted catalyst, leading to an overall loss in the availability of surface cobalt atoms.

Increasing the Co loading to 25 wt % causes an increase in the fraction reduced by about 40%, but a decrease in the dispersion of nearly 50%. Thus, the number of surface cobalt atoms is essentially the same for the 15% and 25% catalysts. Figure 14 shows the relationship between percentage reducibility and average cluster size, as determined by H_2 TPD/pulse reoxidation measurements. The sharp decrease in reducibility occurs below approximately 10 nm, the same cluster size below which catalyst deactivation by reoxidation processes has been reported to occur [15,16].

Conclusions

TPR and H_2 chemisorption with pulse reoxidation were carried out on cobalt Fischer Tropsch catalysts prepared using different supports (e.g., Al_2O_3, TiO_2, SiO_2, ZrO_2 modified SiO_2,ZrO_2 modified Al_2O_3) employing a variety of promoters, including noble metals and metal cations. The different supports did not stabilize a similar cluster size, and TPR screening indicated that the interaction between cobalt surface species and the support increased greatly for supports that stabilized smaller clusters (i.e., Al_2O_3 and TiO_2). Addition of Ru and Pt exhibited a similar catalytic effect on decreasing both the reduction temperatures of cobalt oxides (first peak in TPR) and Co species where a significant interaction with the support was present (broad second peak). Re mainly catalyzed the reduction of the second peak in TPR attributed to reduction of Co species interacting with the support. H_2 chemisorption/pulse reoxidation suggested that, for catalysts prepared with a noble metal promoter and reduced at the same

temperature, the increase in the number of active sites was due mainly to improvements in the percentage reduction rather than the actual dispersion (cluster size). Increasing the cobalt loading, and therefore the average Co cluster size, was found to exhibit improved reducibility by decreasing interactions with the support. Addition of metal oxides (B, La, K, and Zr) was found to decrease the reducibility of the catalyst, thereby lowering the availability of surface Co atoms. In the case of Zr, the cobalt cluster size decreased markedly, and the resulting decrease in reducibility may be caused by greater surface interactions between the smaller Co species and the support.

From an initial catalytic activity standpoint, the number of surface Co metal sites available is directly proportional to the number of micromoles of H_2 desorbed per g of catalyst. Therefore, although Al_2O_3 catalysts are more difficult to reduce, the net result is that the availability of surface sites after reduction at 623 K is still much higher than for the SiO_2 and TiO_2 supported catalysts prepared in this work, due to the stabilization of a smaller cluster size. The trend for initial number of surface Co sites (623 K reduction) available follows Al_2O_3 > TiO_2 > SiO_2 in the order 135 >85 >35 micromoles per g of catalyst. Further gains in initial number of surface sites can be achieved by noble metal promotion, but the resulting effect on catalyst stability requires further study, as does the stability of the catalyst with Co cluster size. The effect of noble metal promoter addition on initial activity was confirmed by reaction testing in the CSTR, as shown in Table 7. Where a weak interaction of cobalt clusters with the support was present, as in the case of Co/SiO_2, only small gains in active sites were achieved with noble metal promoter addition, resulting in marginal gains in activity. However, noble metal promoter addition with cobalt on supports like Al_2O_3 and TiO_2, where significant interactions are present, increased the number of active sites by increasing the percentage reduction, and significant gains

in initial activity were realized. Finally, the slurry phase impregnation method appears to result in a more homogeneous distribution of clusters in comparison to the standard IWI method.

Acknowledgment

This work was supported by U.S. DOE contract #DE-FC26-98FT40308 and the Commonwealth of Kentucky. The authors are especially thankful to Professor Mark Dry for helpful discussions in the preparation of this manuscript.

REFERENCES

1. Knifton, J.F., Lin, J-J, U.S. Patent 4,366,259 (Dec, 1982).
2. Beuther, H., Kibby, C.L., Kobylinski, T.P., Pannell, R.B., U.S. Patent 4,413,064 (1983).
3. Beuther, H., Kibby, C.L., Kobylinski, T.P., Pannell, R.B., U.S. Patent 4,493,905 (1985).
4. Kobylinski, T.P., Kibby, C.L., Pannell, R.B., Eddy, E.L., U.S. Patent 4,605,676 (1986).
5. Beuther, H., Kobylinski, T.P., Kibby, C.L., Pannell, R.B., U.S. Patent 4,585,798 (1986).
6. Iglesia, E., Soled, S.L., Fiato, R.A., U.S. Patent 4,738,948 (1988).
7. Iglesia, E., Soled, S.L., Fiato, R.A., U.S. Patent 4,822,824 (1989).
8. Iglesia, E., Soled, S.L., Fiato, R.A., and Via, G.H., *J. Catal.* **143** (1993) 345.
9. Bruce, L.A., Hoang, M. Hughes, A.E., and Turney, T.W., *Appl. Catal. A*, **100** (1993) 51.
10. Iglesia, E., Soled, S.L., Baumgartner, J.E., and Reyes, S.C., *J. Catal.* **153** (1995) 108.
11. Vada, S., Hoff, A., Adnanes, E., Schanke, D., and Holmen, A., Topics in Catal. **2** (1995) 155.
12. Hilmen, A.M., Schanke, D., and Holmen, A., *Catal. Lett.* **38** (1996) 143.
13. Espinoza, R. L., Visagie, J. L., van Berge, P. J., Bolder, F. H., U.S. Patent 5,733,839 (1998).
14. Wang, W-J, and Chen, Y-W, *Appl. Catal.* **77** (1991) 223.
15. Schanke, D., Hilmen, A. M., Bergene, E., Kinnari, K., Rytter, E., Adnanes, E., and Holmen, A., *Catal. Lett.*, **34** (1995) 269.
16. Hilmen, A. M., Schanke, D., Hanssen, K. F., and Holmen, A., *Appl. Catal. A*, **186** (1999) 169.
17. Ji, L., Lin, J., and H.C. Zeng, J. Phys. Chem. B **104** (2000) 1783.
18. Reuel, R.C. and Bartholomew, H., *J. Catal.* **85** (1984) 63.

19. Moraweck, B., Frety, R., Pecchi, G., Morales, M. and Reyes, P., *Catal. Lett.* **43** (1997) 85.

20. Iglesia, E., *Appl. Catal. A*, **161** (1997) 59.

Table 1
BET Surface Areas

Support/Catalyst	*BET SA* (m^2/g)*	*Pore Volume (Single Point) (cm^3/g)*	*Ave Pore Radius (nm)***	*Pore Volume (BJH Adsorp)*	*Pore Volume (BJH Desorp)*	*Calcination T (K)*
Condea Vista Catalox B γ-Al_2O_3	211	0.500	4.7	0.508	0.507	673
Davisil SiO_2 gel 644	311	1.135	7.3	1.142	1.141	673
Davisil 952 SiO_2	295	1.700	11.5	1.710	1.709	673
Degussa P25 TiO_2	47	0.369	15.5	0.374	0.374	673
15%Co/Al_2O_3	158	0.328	4.2	0.335	0.334	673, flow
15%Co-0.5%Pt/Al_2O_3	162	0.328	4.1	0.335	0.334	673, flow
15%Co-1%Ru/Al_2O_3	159	0.293	3.7	0.300	0.299	673, flow
15%Co-1%Re/Al_2O_3	154	0.288	3.8	0.295	0.294	673, flow
15%Co-5%La/Al_2O_3	155	0.299	3.9	0.306	0.305	673, flow
15%Co-10%Zr/Al_2O_3	161	0.332	4.1	0.339	0.338	673, flow
15%Co/SiO_2 (Davisil 644)	217	0.840	7.7	0.843	0.846	673, no flow
15%Co-3.8%Pt/SiO_2	217	0.787	7.3	0.790	0.789	673, no flow
15%Co-2%Ru/SiO_2	209	0.795	7.6	0.799	0.795	673, no flow
15%Co-0.5%K/SiO_2	211	0.836	7.9	0.839	0.835	673, no flow
20%Co/ZrO_2-SiO_2 (Davisil 952,10 wt % Zr)	200	0.883	8.8	0.888	0.887	673, flow
20%Co-0.5%Pt/ZrO_2-SiO_2	206	0.944	9.2	0.948	0.948	673, flow
20%Co-0.5%Ru/ZrO_2-SiO_2	197	0.880	8.9	0.889	0.887	673, flow
20%Co-0.5%Re/ZrO_2-SiO_2	192	0.857	8.9	0.861	0.861	673, flow
10%Co/TiO_2	38.1 (43.9)	---	n/a (10.9)	0.240	0.244	673, flow
10%Co-0.05%B/TiO_2	40.8 (48.3)	0.282	13.8 (11.9)	0.288	0.288	673, flow
10%Co-0.20%Ru/TiO_2	41.0 (47.5)	---	n/a (11.3)	0.269	0.269	673, flow
10%Co-0.20%Ru-0.05%B/TiO_2	43.4 (49.9)	0.273	12.6 (11.2)	0.279	0.279	673, flow
10%Co-0.34%Re/TiO_2	44.4 (51.0)	0.266	11.9 (10.7)	0.273	0.272	673, flow
10%Co-0.5%Pt/TiO_2	40.7 (46.9)	0.264	13.0 (11.5)	0.270	0.269	673, flow

* For TiO_2 supported catalysts, estimates of cumulative surface areas are shown in parenthesis from BJH adsorption.
** For TiO_2 supported catalysts, where pore size was not available from single point adsorption, an estimate is provided from BJH adsorption.

Table 2

BET Surface Areas of Co/Al_2O_3 Series Prepared by IWI with Different Loadings, Confirmed by ICP Analysis

Support/Catalyst	*BET SA (m^2/g)*	*Pore Volume (Single Point) (cm^3/g)*	*Ave Pore Radius (nm)*	*Pore Volume (BJH Adsorp)*	*Pore Volume (BJH Desorp)*	*Calcination T (K)*
15%Co/Al_2O_3 (200 m^2/g)	161.5	0.335	4.1	0.342	0.341	673K, flow
26%Co/Al_2O_3 (200 m^2/g)	130.1	0.264	4.1	0.272	0.271	673K, flow
33.3%Co/Al_2O_3 (200 m^2/g)	107.3	0.249	4.6	0.260	0.259	673K, flow
15%Co/Al_2O_3 (150 m^2/g)	121.5	0.333	5.5	0.338	0.337	673K, flow
24.4%Co/Al_2O_3 (150 m^2/g)	107.7	0.295	5.5	0.304	0.303	673K, flow
28%Co/Al_2O_3 (150 m^2/g)	87.5	0.243	5.6	0.250	0.250	673K, flow
11%Co/Al_2O_3 (100 m^2/g)	99.7	0.317	6.4	0.322	0.321	673K, flow
27%Co/Al_2O_3 (100 m^2/g)	81.4	0.276	6.8	0.283	0.282	673K, flow
34.3%Co/Al_2O_3 (100 m^2/g)	71.8	0.262	7.3	0.278	0.277	673K, flow
Slurry Phase Impregnation Catalyst						
25% Co/Al_2O_3 (150 m^2/g)	89.0	0.228	4.8	0.233	0.233	673K, flow

Table 3

H_2 Chemisorption (TPD) and Pulse Reoxidation Results for Al_2O_3 Supported Catalysts Prepared by the IWI Method, with Changes in Loading and Support Surface Area

Sample Name	*Red. T (K)*	*μmoles H_2 desorbed per g cat*	*Uncorr. %D*	*Uncorr. Avg. diam. (nm)*	*μmoles O_2 pulsed per g*	*% Red.*	*Corr. %D*	*Corr. Avg. diam. (nm)*
15%Co (200 m^2/g)	623	70.5	5.5	18.6	495	29	19.1	5.4
26%Co (200 m^2/g)	623	94.4	4.5	23.2	1476	52	8.6	12.1
33.3%Co (200 m^2/g)	623	72.4	2.6	39.9	2376	64	4.0	25.5
15%Co (150 m^2/g)	623	79.3	6.2	16.6	823	49	13.9	7.4
24.4%Co (150 m^2/g)	623	102.5	4.8	21.4	1814	64	7.6	13.7
11%Co (100 m^2/g)	623	71.5	7.7	13.5	645	52	14.7	7.0
27%Co (100 m^2/g)	623	59.6	2.6	39.7	1947	63	4.1	25.2
33.4%Co (100 m^2/g)	623	45.8	1.6	63.9	2886	67	2.4	42.8

Table 4

H_2 Chemisorption (TPD) and Pulse Reoxidation Results
For Al_2O_3 (200 m^2/g) Supported Catalysts, With and Without Promoter

Sample Name	*Red. T (K)*	*μmoles H_2 desorbed per g cat*	*Uncorr. %D*	*Uncorr. Avg. diam. (nm)*	*μmoles O_2 pulsed per g*	*% Red.*	*Corr. %D*	*Corr. Avg. diam. (nm)*
15%Co/Al_2O_3	623	66.9	5.3	19.6	509	30	17.5	5.9
15%Co-0.5%Pt/Al_2O_3	623	140.6	11.0	9.3	1024	60	18.4	5.6
15%Co-1%Ru/Al_2O_3	623	115.5	9.7	11.4	823	50	18.2	5.7
15%Co-1%Re/Al_2O_3	623	168.2	13.2	7.8	1187	70	19.4	5.5
15%Co-5%La/Al_2O_3	623	59.8	4.7	22.0	450	27	19.1	5.4
15%Co-10%Zr/Al_2O_3	623	45.5	3.6	28.9	195	11	32.4	3.2
15%Co-10%Zr/Al_2O_3	773	139.7	11.0	9.4	499	29	37.9	2.7
15%Co-10%Zr/Al_2O_3	873	154.6	12.2	8.5	637	38	31.9	3.2
15%Co-10%Zr-0.5%Pt/Al_2O_3	623	142.4	11.2	9.2	549	32	35.0	3.0
15%Co-10%Zr-0.5%Ru/Al_2O_3	623	111.6	8.8	11.8	511	30	29.2	3.5
15%Co-10%Zr-0.5%Re/Al_2O_3	623	122.7	9.6	10.7	549	32	30.1	3.4
25%Co/Al_2O_3 (Sasol method)	623	77.7	3.7	28.2	1174	42	8.7	11.8
25%Co-0.5%Pt/Al_2O_3 (Sasol method)	623	149.0	7.0	14.7	1994	71	9.4	11.0
25%Co0.5%Ru/Al_2O_3 (IWI method)	623	136.2	6.4	16.1	2016	71	9.0	11.4
25%Co-0.5%Re/Al_2O_3 (IWI method)	623	170.5	8.0	12.8	2053	73	11.0	9.4

Table 5

Resistance of Cluster to Reduction Temperature and Heating Rate.
Results of H_2 Chemisorption by TPD

Sample Name	*Red. T (K)*	*μmoles H_2 desorbed per g cat*	*Uncorr. %D*	*Uncorr. Avg. diam. (nm)*	*μmoles O_2 pulsed per g*	*% Red.*	*Corr. %D*	*Corr. Avg. diam. (nm)*
$15\%Co/Al_2O_3$	473	26.3	2.1	49.9	-	-	-	-
	573	38.6	3.0	34.0	232	14	22.3	4.6
	673	77.6	6.1	16.9	462	27	22.3	5.9
	773	131.8	10.4	10.0	953	56	19.4	5.6
	873	152.8	12.0	8.6	1021	60	19.9	5.2
$15\%Co/Al_2O_3$*	773	122.1	9.6	10.8	971	57	16.8	6.2

* Direct temperature ramp.

Table 6

H_2 Chemisorption (TPD) and Pulse Reoxidation Results for SiO_2 and TiO_2 Supported Catalysts, With and Without Promoter

Sample Name	*Red. T (K)*	*μmoles H_2 desorbed per g cat*	*Uncorr. %D*	*Uncorr. Avg. diam. (nm)*	*μmoles O_2 pulsed per g*	*% Red.*	*Corr. %D*	*Corr. Avg. diam. (nm)*
15%Co/SiO_2	623	16.9	1.3	77.6	1078	64	2.1	49.7
15%Co-3.8%Pt/SiO_2	623	25.0	2.0	52.5	1222	72	2.7	37.8
15%Co-2%Ru/SiO_2	623	37.8	3.0	34.8	1249	74	4.0	25.7
15%Co-0.5%K/SiO_2	623	17.9	1.4	73.2	994	59	2.0	51.1
20%Co/SiO_2	623	13.2	1.6	66.3	1652	73	2.1	48.4
20%Co/ZrO_2-SiO_2	623	47.6	2.8	36.8	1149	51	5.5	18.8
20%Co-0.5%Pt/ZrO_2-SiO_2	623	59.0	3.5	29.7	1207	53	6.6	15.7
20%Co-0.5%Ru/ZrO_2-SiO_2	623	61.4	3.6	28.5	1247	55	6.6	15.7
20%Co-0.5%Re/ZrO_2-SiO_2	623	59.0	3.5	29.7	1308	58	6.0	17.2
10%Co/TiO_2	573	42.8	5.1	20.0	593	52	9.7	10.6
10%Co-0.2%Ru/TiO_2	573	66.6	7.8	13.3	722	64	12.2	8.5
10%Co-0.34%Re/TiO_2	573	65.6	7.7	13.4	685	61	12.8	8.1
10%Co-0.05%B/TiO_2	573	37.4	4.4	23.5	429	38	11.6	8.9
10%Co-0.2%Ru-0.05%B/TiO_2	573	63.1	7.4	13.9	692	61	12.2	8.5

Table 7

Trends in Initial Catalytic Activity (H_2:CO = 2:1)

Catalyst	Space Velocity (SL syngas/g_{cat}/h)	P (psig)	T (psig)	Conversion (X_{CO})
15%Co/Al_2O_3	5	275	493	22.7
0.5%Pt-15%Co/Al_2O_3	5	275	493	40.2
10%Co/TiO_2	2	350	503	58.4
0.2%Ru-10%Co/TiO_2	2	350	503	77.9
15%Co/SiO_2	1	350	493	64.3
1.9%Pt-15%Co/SiO_2	1	350	493	76.0

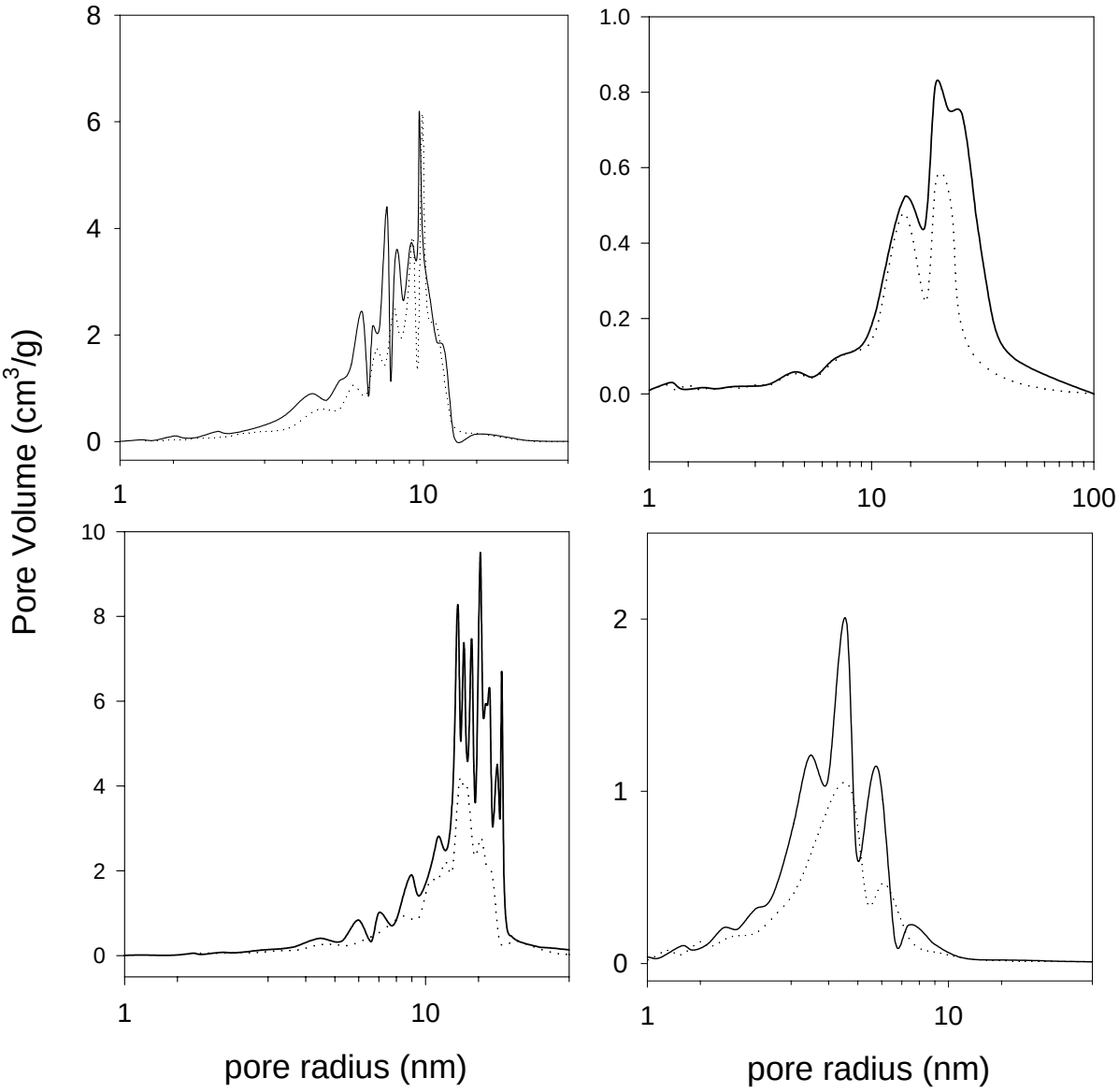

Figure 1. Pore size distributions for supports (solid lines) and catalysts (dotted lines) from BJH adsorption measurements of adsorbed N_2. Top left: Davisil 644 SiO_2 and 15%Co/SiO_2; Bottom left: Davisil 952 SiO_2 and 20%Co/ZrO_2-SiO_2; Top right: Degussa P25 TiO_2 and 10%Co/TiO_2; and Bottom right: Condea Vista Catalox B g-Al_2O_3 and 15%Co/Al_2O_3.

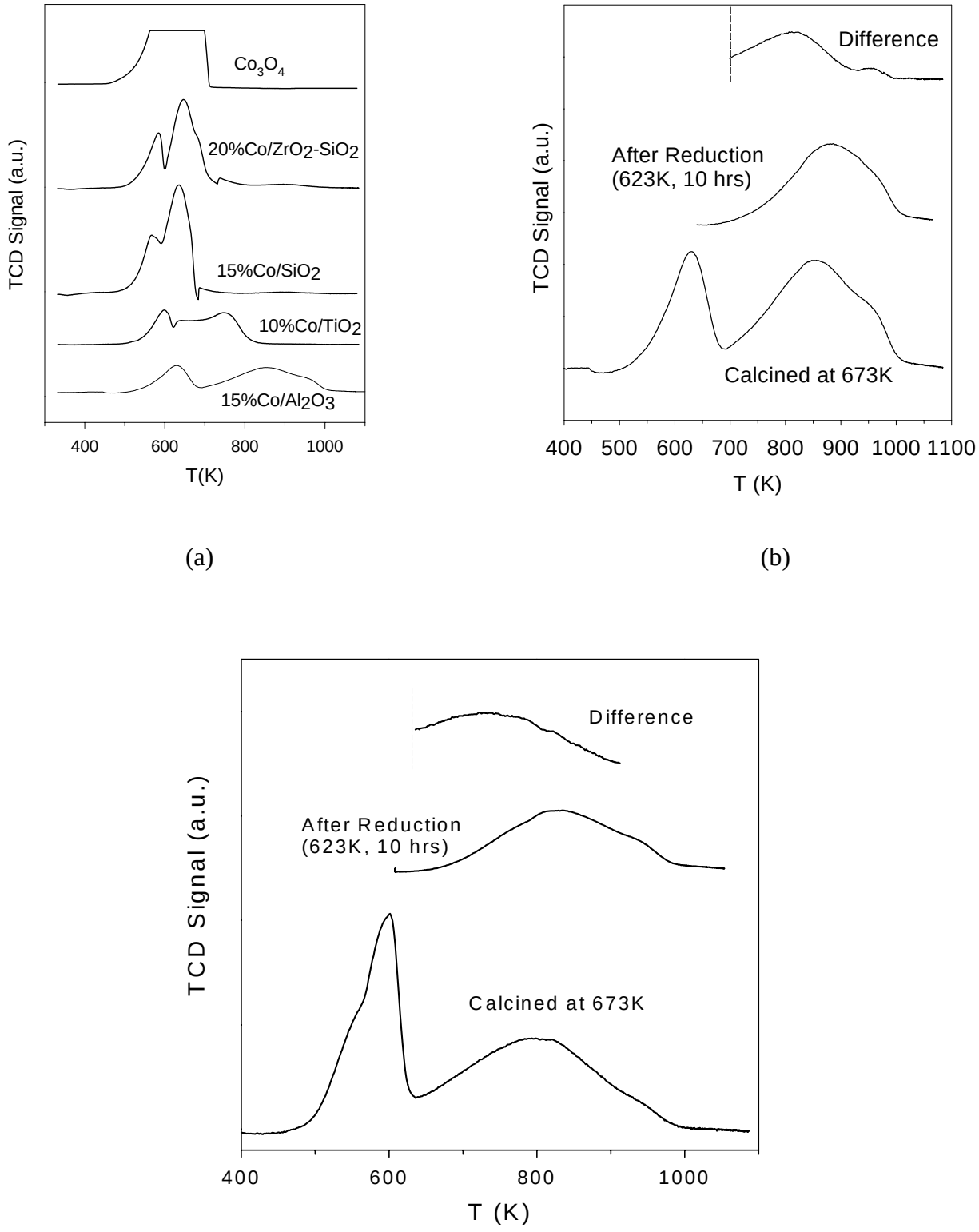

Figure 2. (a) TPR of unpromoted Co catalysts. (b) TPR of 15%Co/Al_2O_3 after calcination (bottom); after reduction at 623K for 10 hrs (middle); and the difference showing the degree of reduction of the second peak (top). (c) Same comparison for 25%Co/Al_2O_3 catalyst prepared by IWI.

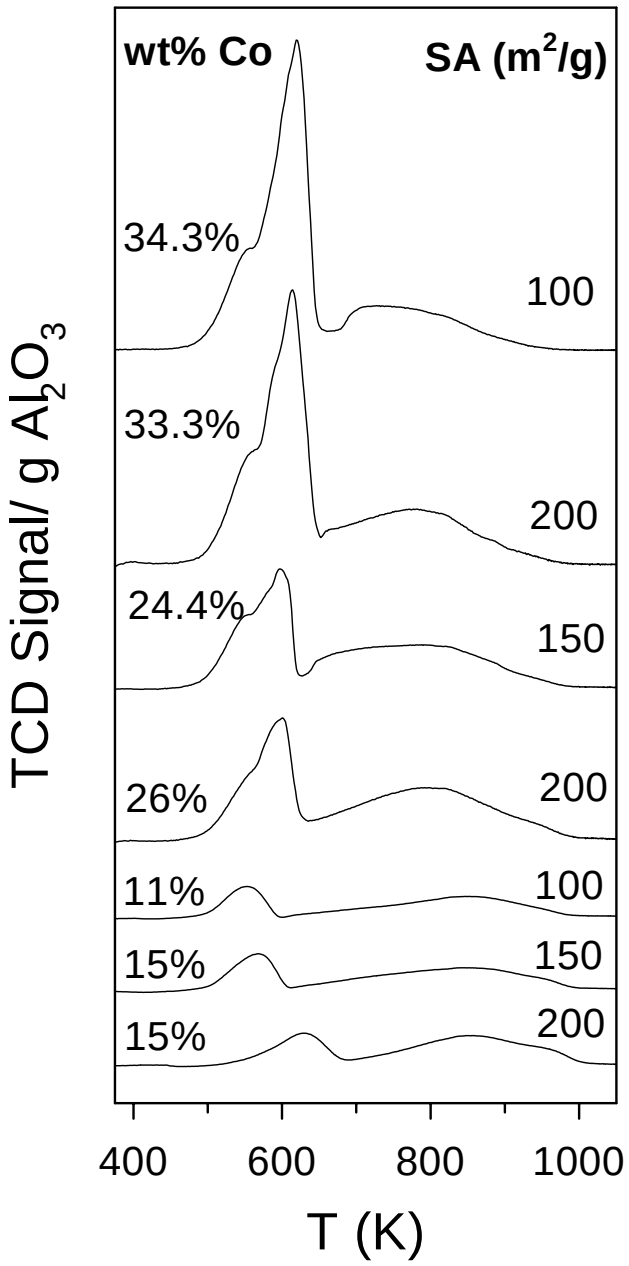

Figure 3. Influence of loading and support surface area on the Co/Al_2O_3 catalyst reduction profile.

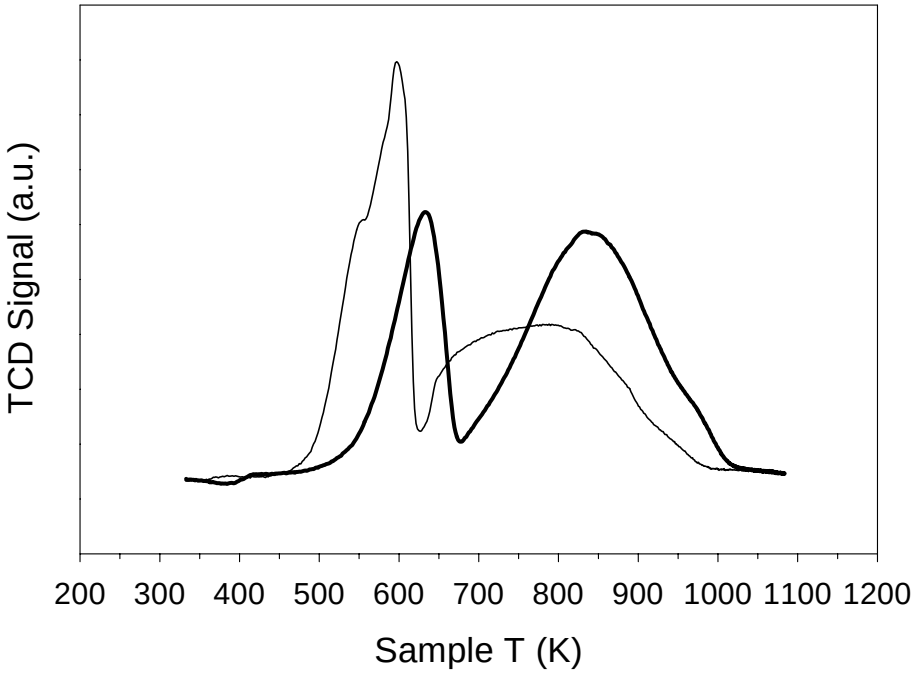

Figure 4. Reduction profiles of 25% catalysts prepared by the standard IWI method (light curve) and by the slurry phase impregnation method (dark curve).

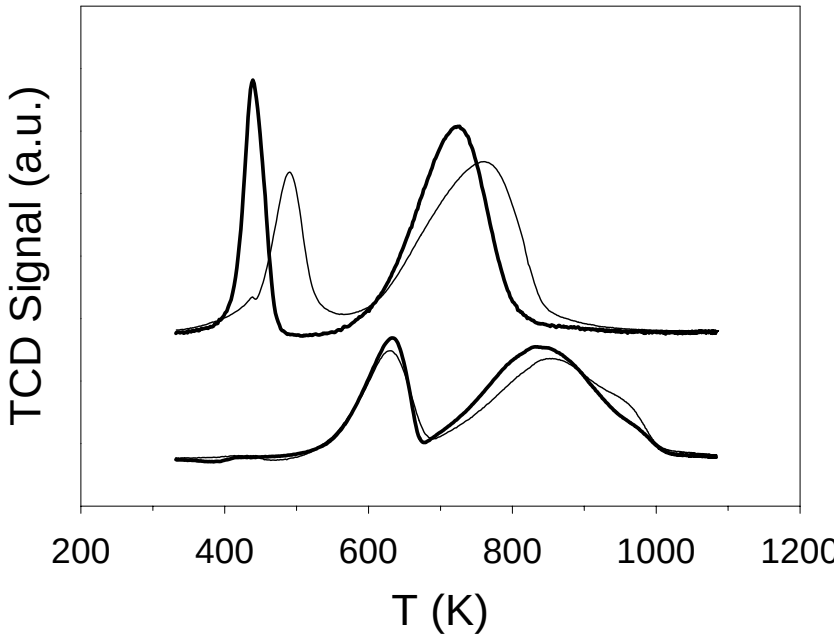

Figure 5. Comparisons of unpromoted (bottom) and 0.5% Pt promoted (top) Co/Al_2O_3 FTS catalysts with 15% (light) and 25% (bold) loadings of Co. Note that the intensity of the 15% catalyst was increased by 1.7 to account for differences in loading in order to more easily compare shifts in the peak positions.

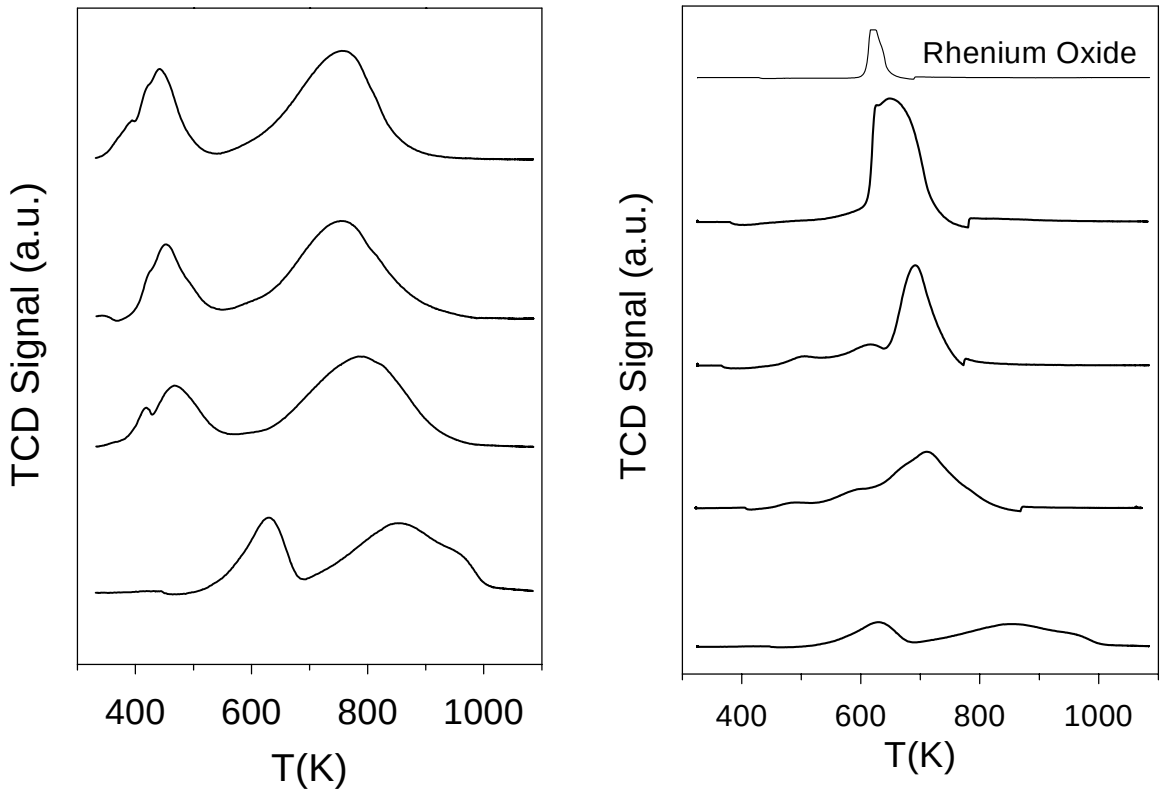

Figure 6. (Left) Comparative TPR spectra of unpromoted (bottom) 15%Co/Al_2O_3 catalyst with those promoted with (moving up) 0.2%, 0.5%, and 1.0% Ru. (Right) Comparative TPR spectra of unpromoted (bottom) 15%Co/Al_2O_3 catalyst with those promoted with (moving up) 0.2%, 0.5%, and 1.0% Re. Top spectra is the reduction of Re_2O_7 precursor (unsupported).

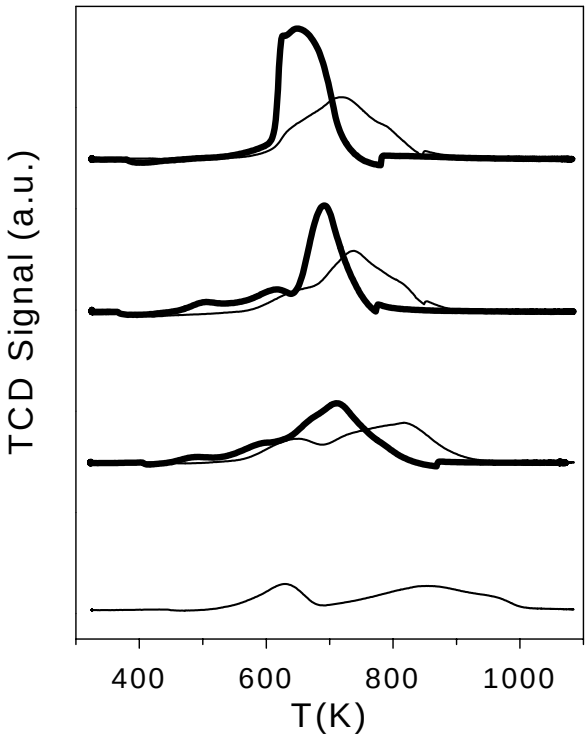

Figure 7. Comparative TPR spectra of unpromoted (bottom) 15%Co/Al_2O_3 catalyst with those promoted with (moving up) 0.2%, 0.5%, and 1.0% Re with (light) and without (dark) interval calcination.

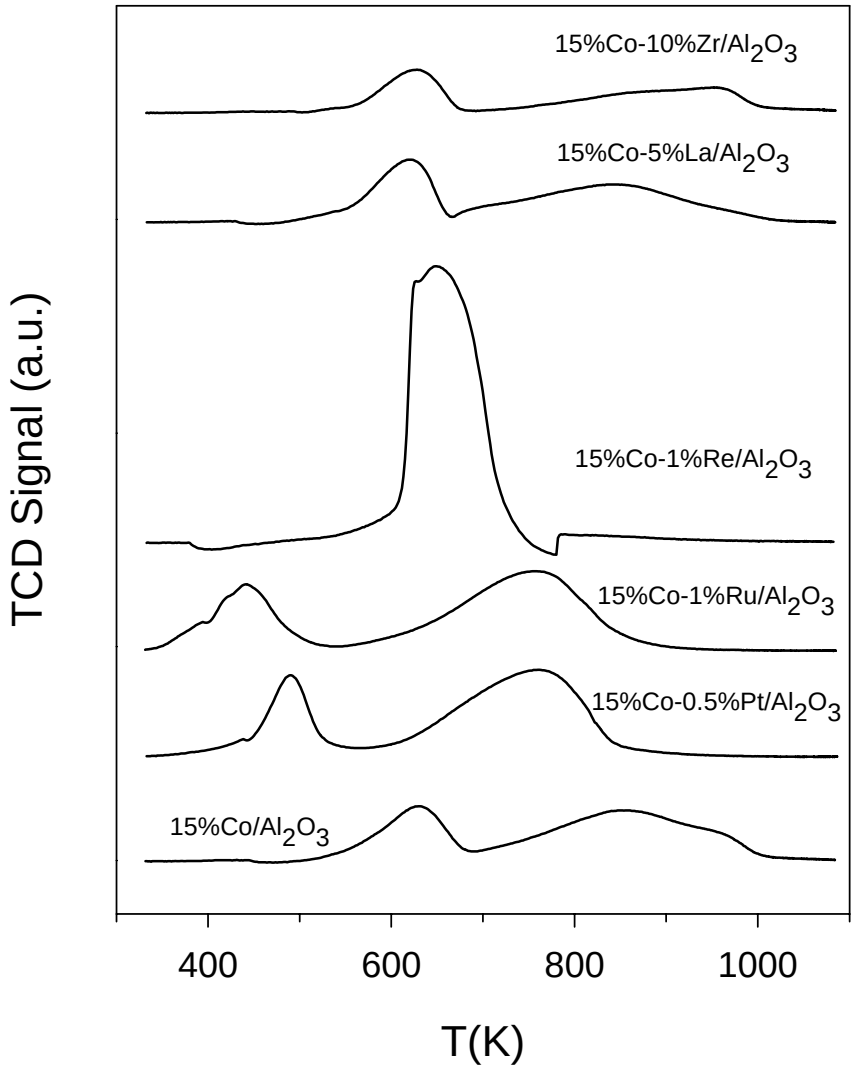

Figure 8. TPR comparison of Al_2O_3 supported Co catalysts with and without metal and metal cation promoters.

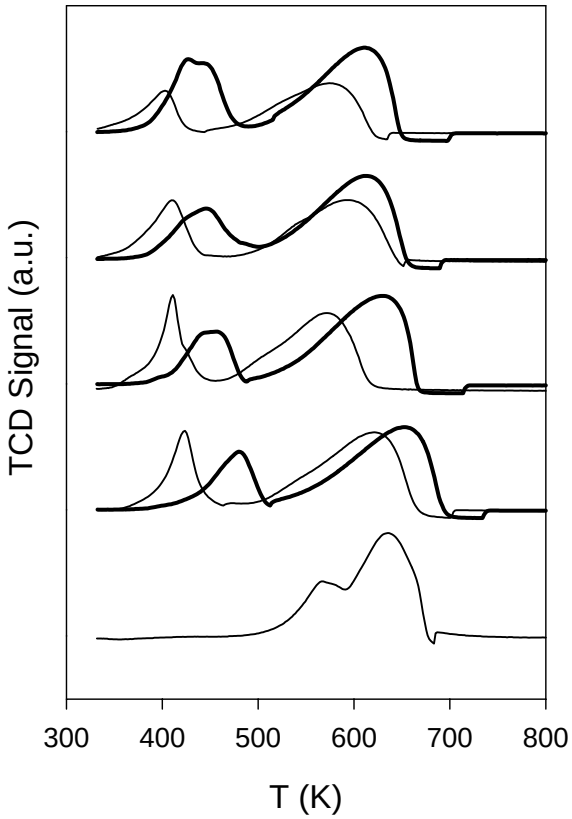

Figure 9. TPR comparison of unpromoted (bottom) and promoted 15% Co/SiO_2 catalysts with increasing atomic percentages (with respect to Co) of Ru (bold) and Pt (light) in the order (moving up) 0.8%, 2%, 4%, and 8% (corresponding to 3.8 wt % Pt and 2.0 wt % Ru).

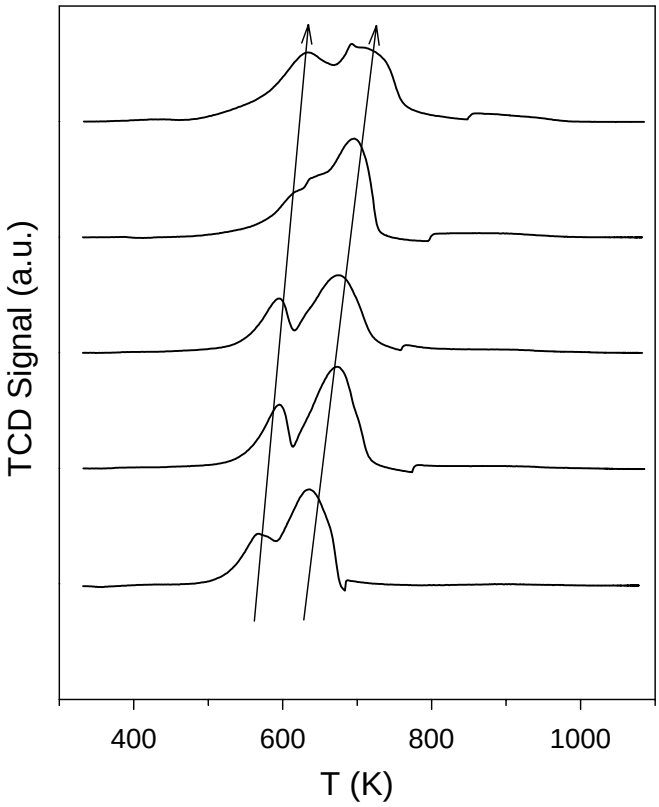

Figure 10. TPR comparison of unpromoted (bottom) and K^+ promoted SiO_2 supported Co catalysts with (moving up) increasing wt. % loading of K^+ in theorder 0.5%, 1.5%, 3.0%, and 5.0%.

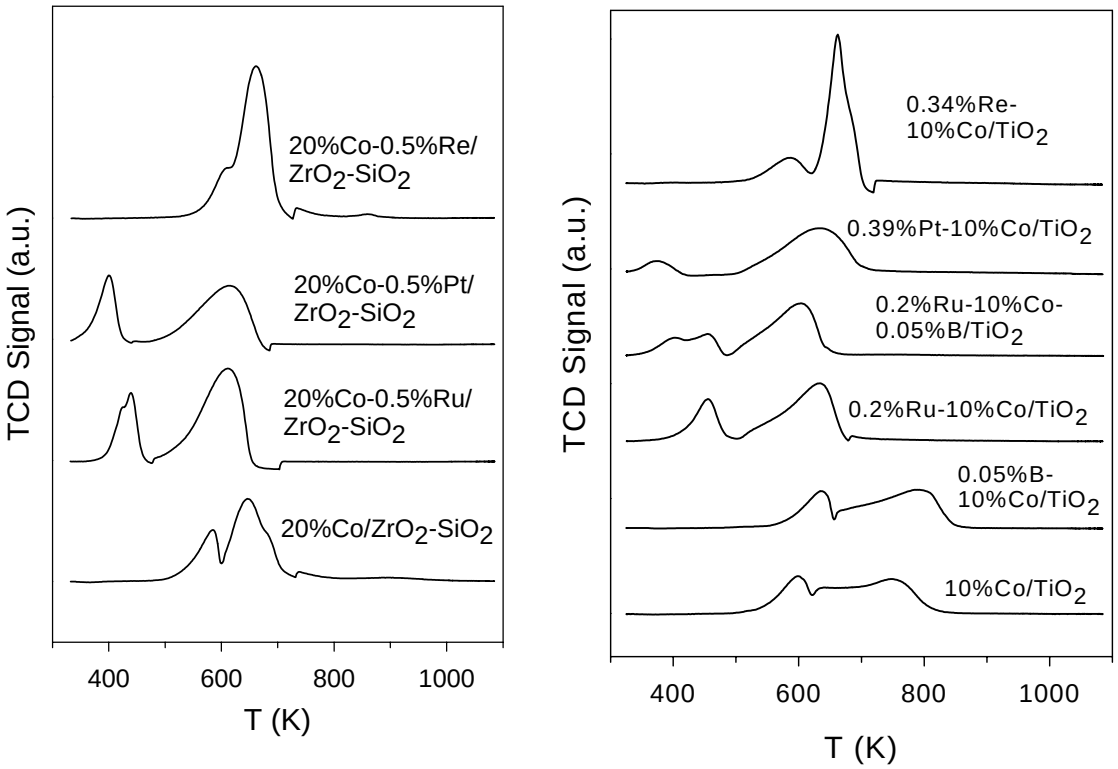

Figure 11. TPR comparison of promoted (left) ZrO_2-SiO_2 and (right) TiO_2 catalysts.

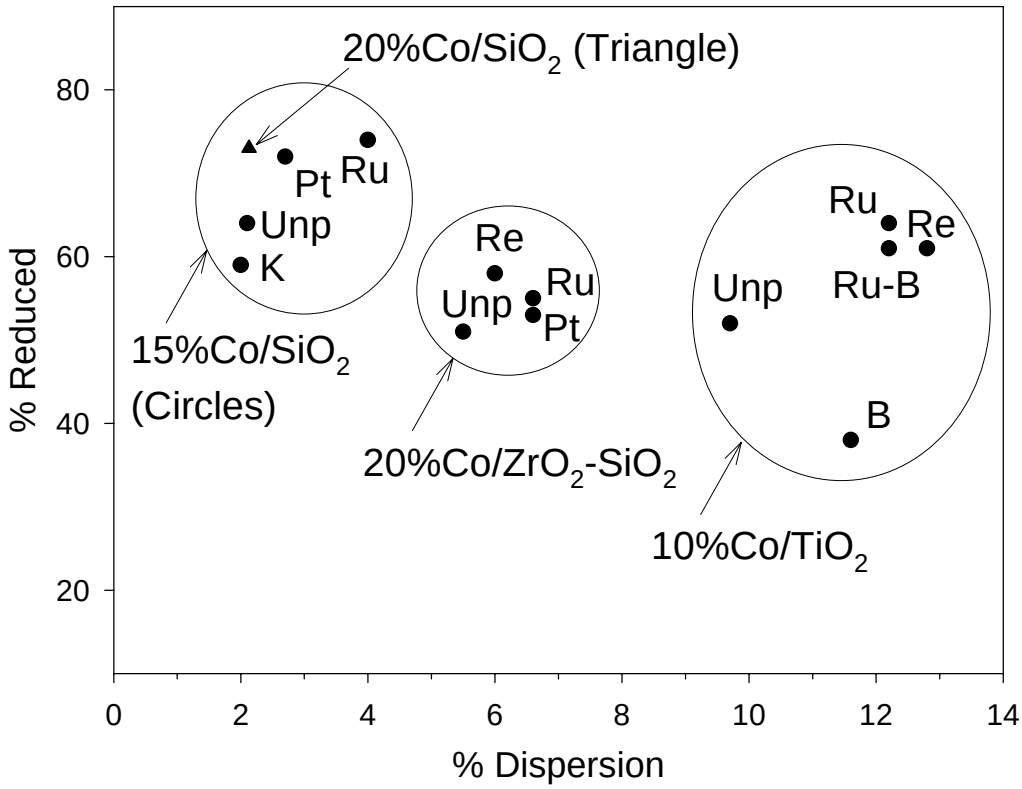

Figure 12. Percentage reducibility versus the dispersion for unpromoted (unp) and promoted SiO_2, ZrO_2, and TiO_2 supported cobalt catalysts after reduction at 623 K.

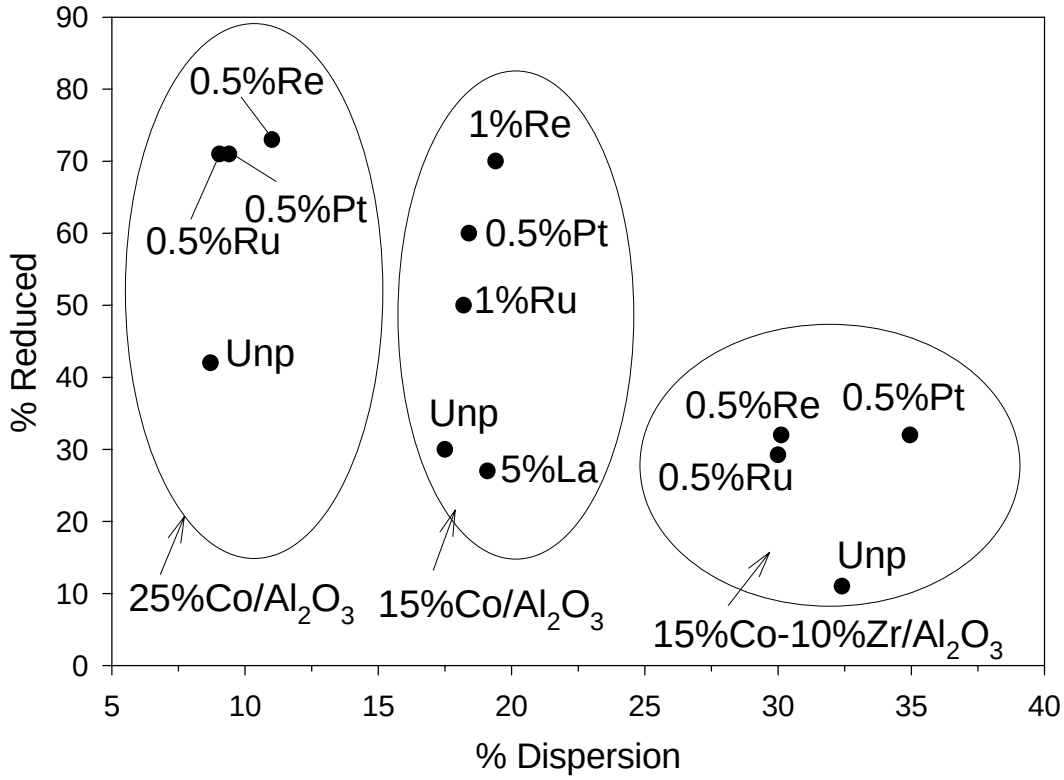

Figure 13. Percentage reducibility versus the dispersion for unpromoted (unp) and promoted Al_2O_3 and ZrO_2-Al_2O_3 catalysts after reduction at 623 K.

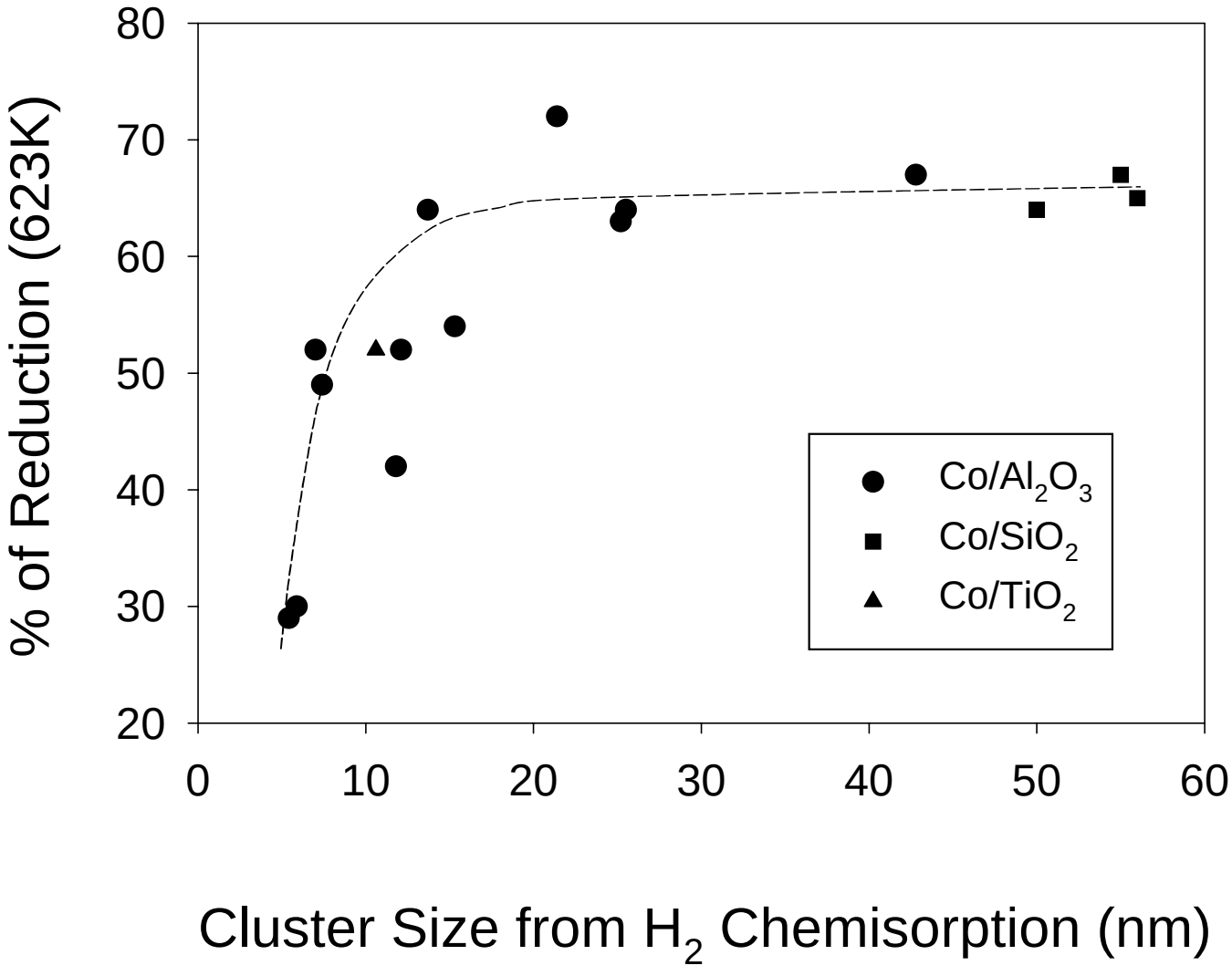

Figure 14. Percentage of reduction versus cluster size for unpromoted supported Co catalysts after reduction at 623 K.

G. Characterization of Pt-Re Promoted Co/Al_2O_3 Catalysts

Introduction

We are continuing to study the impact on reducibility of cobalt oxides by the use of different supports and by the incorporation of different promoters and additives to supported cobalt catalysts. The reduction of Co_3O_4, which is present on the catalyst after calcination, is a two step process which passes through an intermediate CoO phase before reduction to the metal. In our prevoius investigations, we found by temperature programmed reduction that a $15\%Co/Al_2O_3$ displayed a broad second peak attributed to the reduction of cobalt species interacting with the support. In agreement, hydrogen chemisorption with pulse reoxidation revealed that the unpromoted catalyst displayed poor percentage reduction of only 30% after reduction at 623K, the standard activation temperature of Co FTS catalysts. While promotion of supported Co catalysts with the noble metal promoters Pt and Ru had a similar effect on catalyzing both reduction steps of Co_3O_4 to Co metal, Re only aided in catalyzing the second step when a significant interaction of the Co species with the support was present, such as found on Al_2O_3 supported catalysts. After reduction at 623K, therefore, the number of Co active sites increases remarkably with the addition of noble metal promoter, thereby increasing the initial activity under reaction testing.

We have investigated the possibility of a synergism between Pt and Re on the reducibility of supported Co oxides, and are testing the catalysts in the CSTR to draw conclusions as to the effect of Pt-Re promotion and synergism on the catalyst stability.

Catalyst Preparation

Condea Vista Catalox B γ-alumina (100-200 mesh, 200 m^2/g, pore volume 0.4 cm^3/g) was used as support material for the preparation of 15% loaded cobalt FTS catalysts. A three-step

incipient wetness impregnation method was used to add 15 wt % cobalt to the supports with a drying procedure at 353K in a rotary evaporator following each impregnation. Noble metal promoted catalysts were prepared with different loadings of platinum and/or rhenium after cobalt addition and prior to calcination. Where both promoters were added, the Pt was loaded first. Catalysts were calcined only one time in air at 673K for 4hrs following the final impregnation step.

Catalyst Characterization

BET Surface Area

BET measurements were conducted using a Micromeritics Tri-Star system for all catalysts to determine the loss of surface area, if any, following loading of the metal. Prior to testing, samples were slowly ramped to 433K and evacuated for 4hrs to approximately 50mTorr.

Temperature Programmed Reduction

Temperature programmed reduction (TPR) profiles of catalysts were recorded using a Zeton Altamira AMI-200 unit. Calcined fresh samples were first purged in flowing inert gas at 623K to remove traces of water. TPR was performed using a 10%H_2/Ar mixture referenced to Ar at a flowrate of 30 ccm. The sample was heated from 323K to 1073K using a heating ramp of 10K/min and the H_2 consumption measured using a thermal conductivity detector (TCD)..

H_2 Chemisorption by TPD and % Reducibility by Pulse Reoxidation

The amount of chemisorbed hydrogen was measured using the Zeton Altamira AMI-200 unit. The sample weight was always 0.220 g. The catalyst was activated using hydrogen at 623K for 10hrs and cooled under flowing hydrogen to 373K. The sample was held at 373K under flowing argon to prevent adsorption of physisorbed and weakly bound species, prior to increasing the temperature slowly to the activation temperature. At that temperature, the catalyst was held under flowing argon to desorb the remaining chemisorbed hydrogen until the TCD

signal returned to the baseline. The TPD spectrum was integrated and the number of moles of desorbed hydrogen determined by comparing to the areas of calibration pulses of hydrogen in argon. Prior to experiments, the sample loop was calibrated with pulses of N_2 in a helium flow and compared against a calibration line produced from using gas tight syringe injections of N_2 into a helium flow. The volume of the loop was found to be 52 μL.

After TPD of H_2, the sample was reoxidized at 623K by pulses of pure O_2 in helium carrier referenced to helium gas. After oxidation of the cobalt metal clusters (where the entire O_2 pulse was observed by the TCD), the number of moles of O_2 consumed was determined, and the percent reducibility was calculated assuming that Co^0 reoxidized to Co_3O_4.

Diffuse Reflectance Infrared Fourier Transform Spectroscopy (DRIFTS) of adsorbed CO

Infrared spectroscopy of adsorbed CO was performed on a Nicolet Nexus 870 FT-IR which is equipped with a DTGS detector. The catalyst was mixed with KBr and placed into a Spectra-Tech High Temperature/High Pressure DRIFTS cell with ZnSe windows that allowed us to perform in situ thermal pretreatments. For each IR spectrum, taken at a resolution of 8 cm^{-1}, 128 scans were added. Samples were pre-reduced ex-situ under H_2:He (2:1) flow of 100 ccm/g catalyst at 623 K and passivated with 1%O_2 in helium at room temperature for 24 hours. Prior to each spectrum, the catalyst was re-reduced in situ in a flow of 33%H_2 in helium for one hour, held in helium for 30 minuted and cooled under helium flow (note: oxygen scrubbers were employed) to room temperature. The background was recorded at this time. Then, the catalyst was exposed to 1%CO in helium for 30 minutes at room temperature, scanned, purged in helium for 30 minutes, and scanned again. The latter step was employed to remove the contributions of gas phase and weakly adsorbed CO.

Results and Discussion

Results of surface area measurements by physisorption of nitrogen are reported in Table 1. Results show that the BET surface area for the 15% loaded Co catalysts on 200 m^2/g γ-Al_2O_3 were all close to 160 m^2/g. A weight % loading of 15% metal is equivalent to 20% by weight Co_3O_4. If the Al_2O_3 is the main contributor to the area, then the area of the Co/Al_2O_3 catalysts should be $0.80 \times 200\ m^2/g = 160\ m^2/g$, which matches the measured value. As shown in Table 1, addition of small quantities of noble metal promoters did not measurably impact the BET area.

Figure 1 shows the results of TPR. The unpromoted catalyst exhibits two peaks, and remarkably, the second peak is much broader than observed for similarly loaded TiO_2 and SiO_2 supported Co catalysts. Note that in the TPR, we did not ramp the temperature high enough to observe the reduction of bulk cobalt aluminate species, which has been shown to occur above 1073 K with up to 30% loading of cobalt. Therefore, the broad peak on the unpromoted catalyst (ca. 700 to 1000 K) is attributed to the reduction of Co surface species interacting with the support, and the different shoulders are likely due to varying degrees of interaction with the support as a function of cluster size. The smallest Co surface species, with the greatest interaction with the support, are therefore likely represented by the 950 K shoulder. The precise identity of these species is not clear, although it is surmised that the species are either the result of a strong interaction between very small cobalt oxide clusters and the support (deviating from bulklike cobalt oxides and reducing at higher temperatures than the bulk oxides) or small surface Co species which include support atoms in the structure (reducing at temperatures below that of bulk Co-aluminate). Hereafter, the species responsible for this peak will be referred to loosely as "Co surface support species". The addition of 0.5%Pt caused the peaks to shift markedly to lower temperatures, presumably due to spillover of H_2 from the metallic promoter to reduce the Co oxide and Co surface support species.

The reduction of Re oxide occurs at higher temperatures than Pt oxide. Figure 1 shows that although there appears to be no improvement in the reduction of the low temperature peak assigned to the reduction of cobalt oxides, Re still plays a valuable role in decreasing the reduction temperature of Co species for which there is a significant surface interaction with the support. Our previous work shows that Re oxide reduces at 620K, which may explain the lack of effect on the low temperature peak responsible for reduction of cobalt oxides. TPR profiles in Figure 1 show that bulk cobalt oxide has essentially been reduced before the Re oxide is reduced, so no spillover effect can operate to aid in reducing those species. However, H_2 spillover from the reduced Re metal occurs to facilitate reduction of Co species interacting with the support only after the reduction peak of Re oxide to Re metal is achieved.

By keeping the same number of moles of noble metal promoter but by varying the ratio of Pt and Re, interesting effects on reduction are observed in TPR. The best molar ratio appears to be 50%Pt and 50%Re. Relative to Pt promoted catalyst, the addition of Re appears to sharpen the peaks somewhat, while relative to Re, both peaks are shifted to lower temperatures. Since our preliminary findings show that Re promotion results in a more stable catalyst than Pt promotion of Co/Al_2O_3, addition of Pt to a Re-promoted catalyst may aid in catalyzing Re reduction.

Results of H_2 chemisorption by TPD (Table 2) after reduction at 623K indicate that the number of surface sites increases with addition of either Pt or Re promoter. By performing pulse reoxidation, it is clear that the remarkable gain in Co^0 site density is mainly due to an enhancement in the reducibility of the clusters, and not to improvements in the actual dispersion (cluster size) of the reduced cobalt. Addition of Pt or Re causes a fraction of the smaller Co surface species that interact with the support to be reduced in this temperature range. Results of H_2 chemisorption by TPD and pulse reoxidation (Table 2) revealed that, for both unpromoted

and promoted catalysts, there were significant increases (from 30% to approximately 60% with addition of 0.5% noble metal promoter). Maintaining the 50%Pt/50%Re molar ratio but doubling the loading increased the percentage further to 72%. This is in line with the further observed shifts of both peaks in the TPR.

DRIFTS of adsorbed CO is useful for probing the electronic and geometric effects of promoters on supported metal catalysts. Figure 2 shows the resulting spectra after purging the gas phase and weakly bound species with helium at room temperature. The linear stretch vibration of CO adsorbed on Co occurs at approximately 1980 cm^{-1}, while the bridged species are observed at lower wavenumbers. An interesting trend emerges where increasing Re concentration results in a decrease in the linear to bridge-bonded CO ratio (Table 3). Typically, an increase in bridge bonded CO is the result of larger clusters present on the catalyst. The possibility also exists that the increase in linear bonded CO for the Pt promoted catalyst may be the result of a geometric alloying effect, whereby Pt might break up the geometry to Co sites. Clearly, adsorption of CO also occurs on the promoter. For CO on Pt, the band occurs at approximately 2080 cm^{-1}. However, one cannot rule out the possibility of an electronic effect.

To test for the possibility of alloy formation, we are continuing to study these catalysts by High Resolution Transmission Electron Microscopy. With this technique, we may be able to determine if there are changes in the lattice spacing due to alloy formation. At this time, important differences were observed for Pt and Re promoted catalysts in terms of reducibility and catalyst stability. Future catalytic testing results combined with characterization should provide insight into the nature of these differences.

Table 1

BET surface areas

Support/Catalyst	BET SA (m^2/g)	Ave Pore Size (nm)	Calcination T (K)
Condea Vista Catalox B γ-Al_2O_3	200	-	-
Unpromoted 15%Co/ γ-Al_2O_3	161.5	4.14	623, flow
0.5%Pt/15%Co/Al_2O_3	156.1	3.97	623, flow
0.477%Re/15%Co/Al_2O_3	160.2	3.94	623, flow
0.239%Re/0.25%Pt/15%Co/Al_2O_3	157.7	4.01	623, flow
0.477%Re/0.5%Pt/15%Co/Al_2O_3	160.5	3.92	623, flow
0.358%Re/0.125%Pt/15%Co/Al_2O_3	166.5	3.92	623, flow
0.120%Re/0.375%Pt/15%Co/Al_2O_3	161.5	3.96	623, flow

Table 2

H_2 Chemisorption by TPD and Percentage Reduction by Pulse Reoxidation

Sample Description	Red T(K)	Micromoles H_2-Desorbed/g	Uncorr. Disp.	Uncorr. Diam. (nm)	% Reduced	Corr. Diam. (nm)	Corr. Dispersion
Unpromoted 15% Co/Al_2O_3	623	70.5	5.5%	18.6	29%	5.4	19.1%
with 0.5% Pt	623	151	11.9%	8.7	64%	5.6	18.6%
with 0.120% Re/0.375% Pt	623	148.6	11.7%	7.7	61%	5.4	19.2%
with 0.239% Re/0.25% Pt	623	157.7	12.4%	7.3	63%	5.2	19.7%
with 0.358% Re/0.125% Pt	623	139.7	11.0%	9.5	61%	5.7	18.0%
with 0.477% Re	623	136.7	10.7%	9.6	65%	6.2	16.5%
with 0.477% Re/0.5% Pt	623	175.5	13.8%	7.5	72%	5.4	19.2%

Table 3

Linear to Bridged Ratio for Adsorbed CO as Measured by DRIFTS

Catalyst	L/B
15% Co/AL_2O_3	0.296
0.5% Pt-15% Co/Al_2O_3	0.258
0.375% Pt-0.20% Re-15% Co/Al_2O_3	0.308
0.235% Re-0.25% Pt-15% Co/Al_2O_3	0.269
0.477% Re-0.5% Pt-15% Co/Al_2O_3	0.242
0.36% Re-0.125% Pt-15% Co/Al_2O_3	0.207
0.477% Re-15% Co/Al_2O_3	0.195

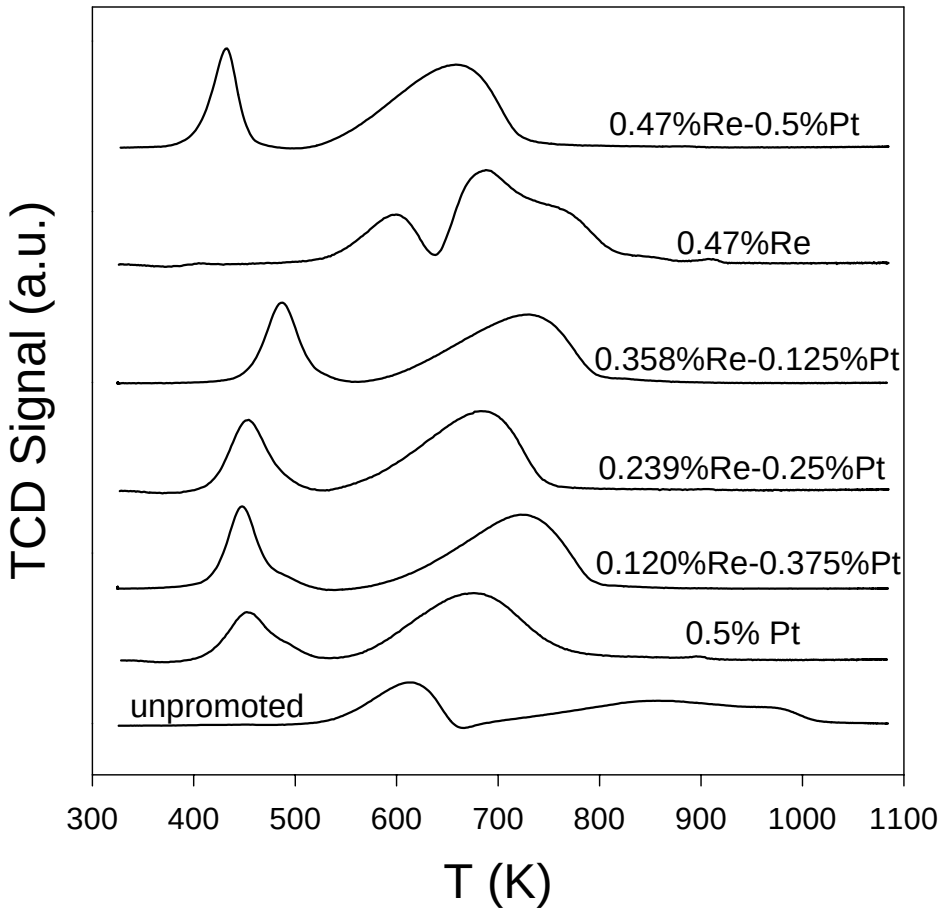

Figure 1. TPR profiles of Pt and/or Re promoted 15% Co/Al_2O_3 catalysts.

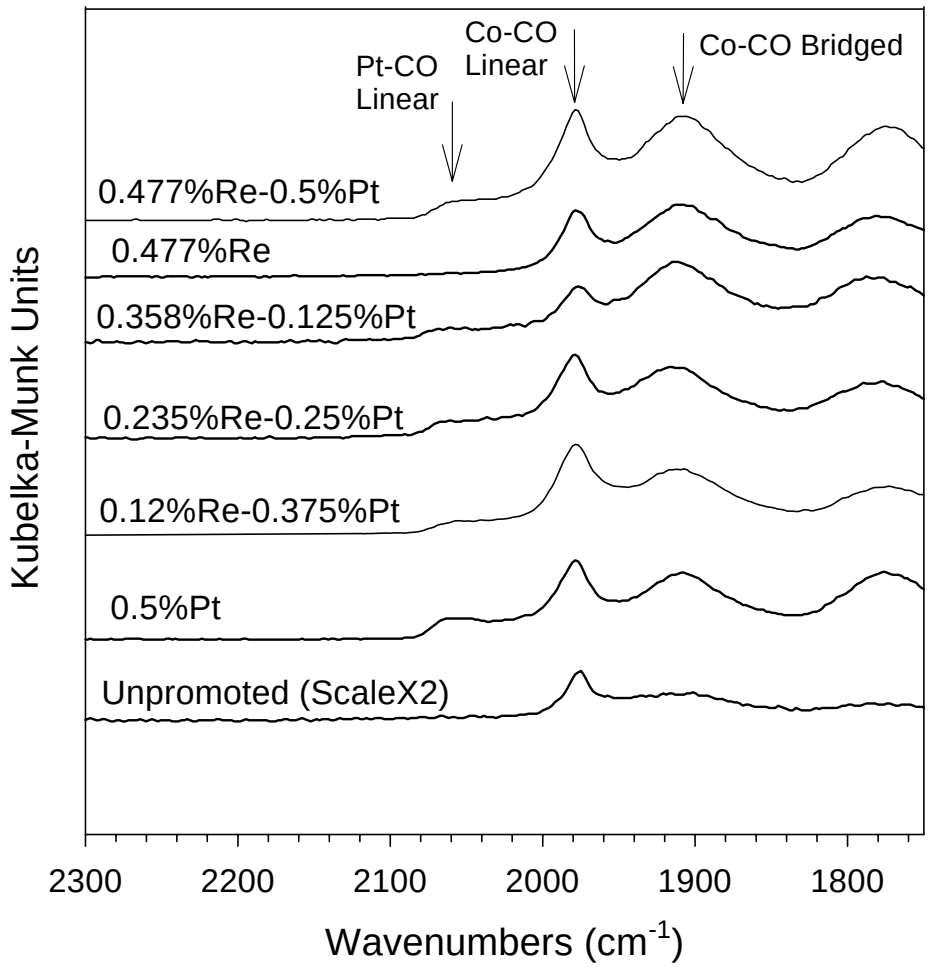

Figure 2. DRIFTS of adsorbed CO profiles of Pt and/or Re promoted 15% Co/Al_2O_3 catalysts.

H. EXAFS Characterization of Used 0.2% Re - 15% Co/Al_2O_3 Catalysts

ABSTRACT

The deactivation of a promoted 0.2%Re-15%Co/Al_2O_3 catalyst during Fischer-Tropsch synthesis in a CSTR was investigated. A novel method was utilized to isolate samples of catalyst from the reactor during the course of the reactor run, so that the catalyst was cooled in the solid wax for XAFS investigation. Results showed, as suggested in an earlier study of spent noble metal promoted catalysts, that the deactivation involves two processes. EXAFS strongly indicates significant cluster growth with time on-stream by a sintering process as a major component to the deactivation. However, in line with our previous investigation, XANES of the most heavily deactivated samples indicates that a fraction of Co species underwent a phase transformation to a phase resembling that of $CoAl_2O_4$. Addition of metal promoters to achieve reduction of Co species in interaction with the support results in higher initial activity by the formation of additional active sites. However, these additional Co metal clusters are unstable and are likely the cause of the higher initial deactivation rates of these catalysts during Fischer-Tropsch synthesis.

INTRODUCTION

Extended X-ray absorption fine structure (EXAFS) spectroscopy is a powerful tool in that it provides information on the local structure surrounding the type of atom under investigation. For example, the average coordination information can be obtained [1,2], which is very useful for obtaining information regarding the dispersion of fresh catalysts, as well as the changes in the cluster size of supported metal catalysts during the course of a reaction. In some cases, information regarding cluster morphology can also be predicted [1,2]. It is important to note that, although EXAFS provides information regarding the local structure surrounding an atom, including atom type, degree of coordination, radial distances, and disorder parameters, the

method represents an average over all the clusters present on the catalyst. XANES, on the other hand, can provide qualitative information on the oxidation states of species present on supported metal catalysts [3].

Re addition was found to catalyze the reduction of the very well dispersed Co species in interaction with the support, thereby increasing the number of Co active metal sites for reaction. The reduction of these additional species showed a slight lowering of the average cluster size in H_2 chemisorption/pulse reoxidation measurements in reference to the unpromoted catalyst, demonstrating that they were more highly dispersed. However, while the initial catalytic activity by addition of Re promoter was increased relative to the unpromoted catalyst, the deactivation rate was higher. Therefore, one focus of this paper was to use XAFS techniques to provide information on the nature of the deactivation of these small cobalt metal clusters, which were reduced in the presence of the Re, during the course of Fischer Tropsch synthesis. In order to carry out these experiments, we developed a method of isolating catalyst samples in the solid wax directly from the CSTR during the course of reaction testing.

EXPERIMENTAL

Catalyst Preparation

Condea Vista Catalox (high purity γ-alumina, 100-200 mesh, 200 m^2/g) was the support for the cobalt FTS catalysts. To obtain a cobalt loading of 15%, a three step incipient wetness impregnation (IWI) was used with intermediate drying steps at 353 K in a rotary evaporator following each impregnation. The promoter was added after the third drying step by IWI of an aqueous solution of rhenium oxide salt. The catalyst was dried and then calcined under air flow at 673 K for 4 hrs following promoter addition. The cobalt loading was verified by ICP analysis.

Temperature Programmed Reduction

Temperature programmed reduction (TPR) profiles of catalysts were recorded using a Zeton Altamira AMI-200 unit. Calcined fresh samples were first purged in flowing inert gas to remove traces of water. TPR was performed using a 10% H_2/Ar mixture referenced to Ar at a flowrate of 30 ccm. The sample was heated from 323 K to 1073 K using a heating ramp of 10 K/min. Results are shown in Figure 1.

H_2 Chemisorption by TPD and % Reducibility by Reoxidation

The amount of chemisorbed hydrogen was measured using the Zeton Altamira AMI-200 unit, which incorporates a thermal conductivity detector (TCD). The sample weight was always 0.220 g. The catalyst was activated using hydrogen at 623K for 10 hrs and cooled under flowing hydrogen to 373 K. The sample was held at 373 K under flowing argon to prevent adsorption of physisorbed and weakly bound species, prior to increasing the temperature slowly to the reduction temperature. At that temperature, the catalyst was held under flowing argon to desorb the remaining chemisorbed hydrogen until the TCD signal returned to the baseline. The TPD spectrum was integrated and the number of moles of desorbed hydrogen determined by comparing to the areas of calibration pulses of hydrogen in argon. Prior to experiments, the sample loop was calibrated with pulses of N_2 in a helium flow and compared against a calibration line produced from using gas tight syringe injections of N_2 into a helium flow.

After TPD of H_2, the sample was reoxidized [4] at the activation temperature by pulses of pure O_2 in helium carrier referenced to helium gas. After oxidation of the cobalt metal clusters (where the entire O_2 pulse was observed by the TCD), the number of moles of O_2 consumed was determined, and the percentage reduction was calculated assuming that Co^0 reoxidized to Co_3O_4.

In order to estimate the average cluster size, the percentage reduction was included in the dispersion calculation as follows, assuming a H:Co stoichiometric ratio of 1:1, as reported previously [5].

$$\%D = (\text{number of surface } Co^0 \text{ atoms})/(\text{number of total } Co^0 \text{ atoms})$$

$$\%D = (\text{number of surface } Co^0 \text{ atoms})/[(\text{number of total Co atoms})(\text{percentage reduction})]$$

In Table 1, the dispersions and cluster sizes are first reported as uncorrected, which assumes that all of the cobalt is reduced. Then, the percentage reduction is included in the calculation and the corrected dispersion and cobalt cluster size is reported. This demonstrates the importance of considering the fraction of cobalt species reduced in any estimate of dispersion based on chemisorption measurements.

XAFS

Used catalyst samples were obtained from the continuously stirred tank reactor (CSTR) at different points of catalyst deactivation with time onstream. The catalyst particles, well-mixed with the reactor wax, were removed by a pressure letdown valve to a collection trap under inert gas. The wax was allowed to cool, sealing the catalyst in the solid wax matrix for EXAFS analysis.

XAFS spectra at the Co *K* edge were obtained at the National Synchrotron Light Source (NSLS) at Brookhaven National Laboratory (BNL) in Upton, New York at beamline X18b. The X-rays were tuned by a Si(111) double crystal monochromator, which was detuned slightly to prevent glitches from harmonics. The used catalyst in the wax was pressed into a disk and loaded into a XAFS cell, which was cooled to liquid nitrogen temperatures prior to scanning under flowing helium. XAFS spectra of the Co foil, Co_3O_4, CoO, and $CoAl_2O_4$ were also measured. Several scans of the catalyst samples were obtained and the spectra averaged to improve the signal to noise ratio.

XANES and EXAFS spectra were first background corrected and normalized by dividing by the height of the edge jump to account for the concentration of Co atoms in the sample. For EXAFS spectra, appropriate splines were used to remove the background based on the Nyquist criteria [6]. The Chi function in energy space was extracted and converted to *k* space and weighted with either k^0 or k^3 weighting for examination of the changes in coordination number of the different *Z* scatterers. To obtain information on Co-Co coordination and therefore, changes in the cluster size, the k^3-weighted spectrum was transformed from *k* space to *r* space to obtain the radial distribution function. The EXAFS spectrum for the first Co-Co coordination shell was isolated and the inverse Fourier Transform was conducted. Fitting of the spectra in k space was carried out using FEFFIT [4]. Theoretical EXAFS were generated using FEFF [7] using model Co metal crystal parameters generated by Atoms [8]. In order to use coordination number as a fitting parameter, S_0^2 was first obtained from analysis of the Co foil assuming a fixed coordination number N_1 of 12 for the first shell. The other fitting parameters utilized by FEFFIT included the overall E_0 shift e_0 applied to each path, *delr* to account for lattice expansion, and $sigma^2$, which is based on a correlated Debye model used to approximate the mean square disorder in the path length of each path [8].

RESULTS AND DISCUSSION

Figure 2 shows the points during the initial deactivation period of the catalyst where the catalyst was removed. Figure 3 shows the k^0 and k^3-weighted radial distribution functions for the used catalyst withdrawn from the reactor at 1800 hours onstream and a comparison against those of the standards. The aim of this part of the investigation was to determine whether the small Co metal clusters showed signs of reoxidation, as had been suggested in earlier reports [9,10], or whether the main cause of the deactivation was by growth of the Co metal cluster by a sintering mechanism, leading to a loss of surface sites.

Figure 3 displays the normalized XANES spectra of the catalyst samples removed at 1800 and 2135 hours onstream with a comparison against those of the reference compounds, including the Co metal foil and CoO, Co_3O_4, and $CoAl_2O_4$ standards. Interestingly, as noted previously in other spent catalysts [11], the XANES reveals two contributions, a strong contribution of the reduced Co metal and three small peaks which match very well the positions of the $CoAl_2O_4$ standard. The positions are more pronounced when one considers the derivative spectra. These suggest the possibility that a small fraction of the clusters may have undergone a phase transformation to an oxidized state. In comparison with our earlier study [11], the extent of formation of this oxidized phase is less pronounced than the unpromoted catalyst, indicating that Re promoter may play a role in suppressing its formation.

Both the k^0 and k^3-weighted radial distribution functions displayed in Figure 4 for the used catalyst withdrawn from the reactor at 1800 hours onstream strongly resemble the corresponding spectra of the Co foil. Surprisingly, even in the k^0-weighted spectra, there is not a peak present at low R between 1 and 2 Angstroms that suggests an increase in the Co-O coordination, in comparison with the references where the Co is in an oxidized state. Also, a comparison in k^3 of the CoO, Co_3O_4, and $CoAl_2O_4$ standards show the Co-Co distances are shifted to higher R, as expected, in comparison with the Co foil. However, there is no indication of a contribution from Co-Co distance at these higher R in the used catalyst sample, rather only the Co-Co distance which matched closely that found in the Co metal foil. Therefore, this suggests that if there is deactivation due to reoxidation, it is either likely limited to the surface of the catalyst or a surface phase, unable to be viewed by EXAFS, or the reoxidation is part of a dynamic oxidation/reduction cycle. That is, the EXAFS results suggest that the small Co metal clusters do not sustain a bulk reoxidized CoO or Co_3O_4 phase under the normal partial pressures of H_2O encountered in the Fischer Tropsch reactor in the presence of the reducing syngas.

Figure 5 shows the EXAFS data $Chi(k)*k^3$ v. k, the Fourier transform magnitude in r-space, and the first shell inverse transforms for Co metal and catalysts. The inverse transform is the solid line, while the plotted points indicate the fitting obtained from FEFFIT. It is clear by the augmentation of the intensity of the envelope in k-space and by the growth in the Fourier transform peak for Co-Co coordination, that the average metal cluster size has experienced an increase in size with time onstream in the CSTR. Table 2 shows the direct parameters obtained from FEFFIT analysis with their corresponding uncertainties.

Clearly, a substantial increase in Co-Co coordination as cobalt metallic phase is evident during the initial stages of the deactivation period, with a leveling off achieved at approximately 1800 hours of time onstream. This time also correlates very well with the greatest degree of deactivation in the CO conversion, as shown in Figure 2. Therefore, one cannot rule out a sintering mechanism as the main reason for the catalyst deactivation. Certainly, there is an additional fraction of Co metal reduced by addition of Re promoter as shown by the shift in reduction peaks to lower temperature, as demonstrated in Figure 1. This leads to a higher fraction of very small Co metal clusters at the onset of reaction testing. These may be the result of the reduction of a surface phase of Co containing atoms of the support in their structure, or the reduction of very tiny Co oxide clusters which interact with the support and deviate from bulklike Co metal behavior. In either case, their resulting reduction results in a fraction of very small cobalt metal clusters, which causes a lowering of the average cluster size, as demonstrated by H_2 chemisorption/pulse reoxidation measurements in Table 1, in reference to the unpromoted catalyst.

These clusters, therefore, will have a higher surface free energy than the clusters reduced at the same temperature on the unpromoted catalyst. Such unstable clusters, with a greater number of dangling bonds, may therefore be more susceptible to cluster growth, although the

actual kinetics of the process is not yet well understood. On the basis of XPS evidence which indicated surface oxidation of small Co clusters under H_2O/syngas mixtures, it is possible that the sintering may be the result of a dynamic reoxidation/reduction cycle. Such cycles have been shown previously to result in metal cluster growth.

One should also consider the possibility that a fraction of the small metal clusters underwent a phase transformation to an oxidized state during reaction. XANES suggest the formation of a $CoAl_2O_4$-like phase, which may not be seen directly by EXAFS. Loss of small metal clusters to an oxidized phase would also result in an increase in the average Co metal cluster size, which would show increased Co-Co coordination in the metallic phase. However, if the oxidation was sustained, then one would also expect to see the appearance and growth of a Co-O peak as well as a contribution from a Co-Co coordination at higher R for an oxidized Co phase, especially after the extent of deactivation observed in Figure 2. The EXAFS results presented here as a function of time onstream suggest an increase in the Co cluster size only, most likely the result of a slow loss of surface sites by a sintering process. Finally, addition of Re promoter does aid in reducing the Co species, thereby generating a greater number of initial active sites, improving the initial activity. However, the resulting catalyst also showed a higher initial rate of deactivation than the unpromoted catalyst, indicating that promoter addition alone does not guarantee a better catalyst from the standpoint of long-term stability.

CONCLUSIONS

The deactivation of a promoted 0.2%Re-15%Co/Al_2O_3 catalyst in a CSTR was investigated. A novel method of isolating samples of catalyst directly from the reactor during the course of reaction testing in solid wax for XAFS investigation was demonstrated. Results showed, as suggested in an earlier study of spent noble metal promoted catalysts, that the deactivation likely involves two processes. First, EXAFS of samples with time onstream

strongly indicates significant cluster growth by a sintering process as a major component to the deactivation. However, in line with our previous investigation, XANES of the most heavily deactivated samples indicates that a fraction of Co species underwent a phase transformation to a phase resembling that of $CoAl_2O_4$. Addition of metal promoters to achieve reduction of Co species in interaction with the support results in unstable Co metal clusters, which are likely the cause of the higher initial deactivation rates of these catalysts during Fischer-Tropsch synthesis.

REFERENCES

1. Greegor, R.B., and Lytle, F.W., J. Catal. 63 (1980) 476.
2. Jentys, A., PCCP 1 (1999) 4059.
3. Bart, J.C.J., Adv. in Catal. 34 (1986) 203.
4. Vada, S., Hoff, A., Adnanes, E., Schanke, D., and Holmen, A., Topics in Catal. 2 (1995) 155.
5. Jacobs, G., Das, T.K., Zhang, Y.-Q., Li, J., Racoillet, G., and Davis, B.H., Appl. Catal. A: Gen., (2002) 233, 263.
6. Newville, M., Automated Background Removal for XAFS Data (1997).
7. Newville, M., Using FEFF to model XAFS data (1998).
8. Ravel, B., EXAFS Analysis Using FEFF and FEFFIT, Workshop (June 27, 2001).
9. Schanke, D., Hilmen, A.M., Bergene, E., Kinnari, K., Rytter, E., Adnanes, E., and Holmen, A., Catal. Lett. 34 (1995) 269.
10. Hilmen, A.M., Schanke, D., Hanssen, K.F., and Holmen, A., Appl. Catal A: General 186 (1999) 169.
11. Jacobs, G., Zhang, Y.-Q., Das, T.K., Li, J., Patterson, P.M., and Davis, B., Stud. Surf. Sci. Catal. 139 (2001) 415.

Table 1

H_2 chemisorption (TPD) and pulse reoxidation results for Al_2O_3 (200 m^2/g) Supported catalysts, with and without Re promoter

Catalyst	μ*mol* H_2 *desorbed per g cat*	*Uncorr %D*	*Uncorr diam. (nm)*	μ*mol* O_2 *pulsed per g cat*	*% Red*	*Corr %D*	*Corr diam. (nm)*
15%Co/Al_2O_3	67	5.3	19.6	509	30	17.6	5.9
0.2%Re-15%Co/Al_2O_3	142	11.2	9.2	939	55	20.4	5.1
0.5%Re-15%Co/Al_2O_3	143	11.3	9.2	993	59	19.1	5.4
1.0%Re-15%Co/Al_2O_3	168	13.2	7.8	1187	70	18.9	5.5

Table 2

Best-fit values for average coordination number ($N_{1)}$ for the first Co-Co shell, shift in E_0, Debye-Waller factor (σ^2), lattice expansion (*delr*), and fractional misfit (*r*). Relative uncertainties are also displayed.

Sample	N_1	ΔN_1	e_0	Δe_0	σ^2	$\Delta\ \sigma^2$	*delr*	Δ*delr*	*r*-factor
355 hours	2.68	0.43	2.56	1.94	0.00359	0.00133	-0.0258	0.0120	0.115
665 hours	3.47	0.37	3.10	1.27	0.00422	0.00093	-0.0216	0.00808	0.045
980 hours	5.61	0.28	5.49	0.59	0.00389	0.00043	-0.0166	0.00375	0.018
1340 hours	6.50	0.32	7.21	0.57	0.00399	0.00043	-0.00673	0.00368	0.017
1800 hours	7.56	0.27	7.74	0.41	0.00455	0.00032	-0.00407	0.00268	0.0088
2135 hours	7.65	0.34	7.70	0.50	0.00500	0.00041	-0.00303	0.00339	0.013

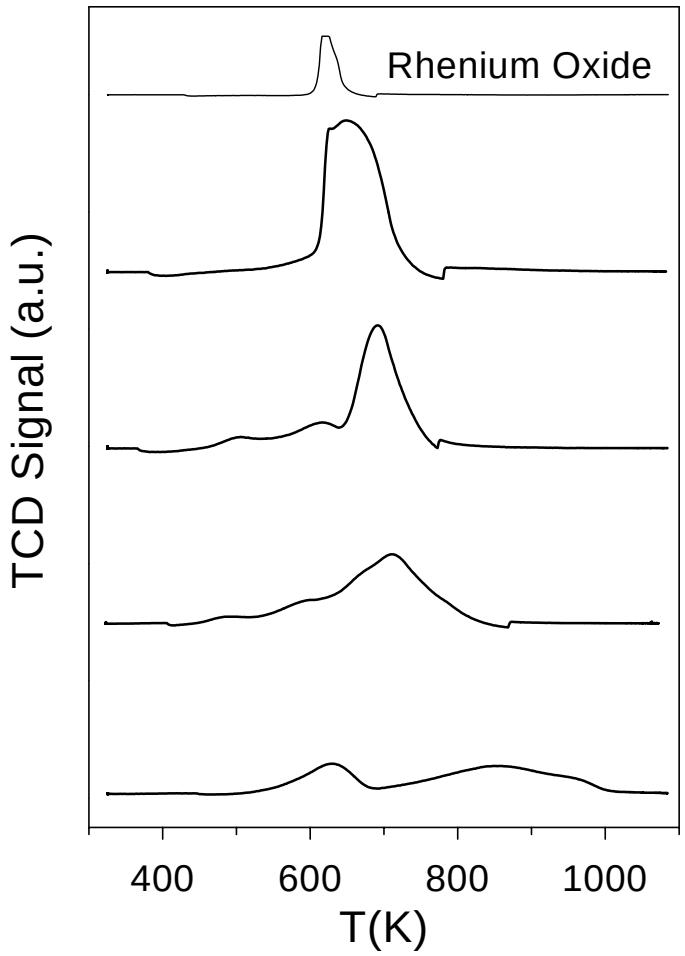

Figure 1. Comparative TPR spectra of unpromoted (bottom) 15%Co/Al_2O_3 catalyst with those promoted with (moving up) 0.2%, 0.5%, and 1.0% Re. Top spectra is the reduction of Re_2O_7 precursor (unsupported).

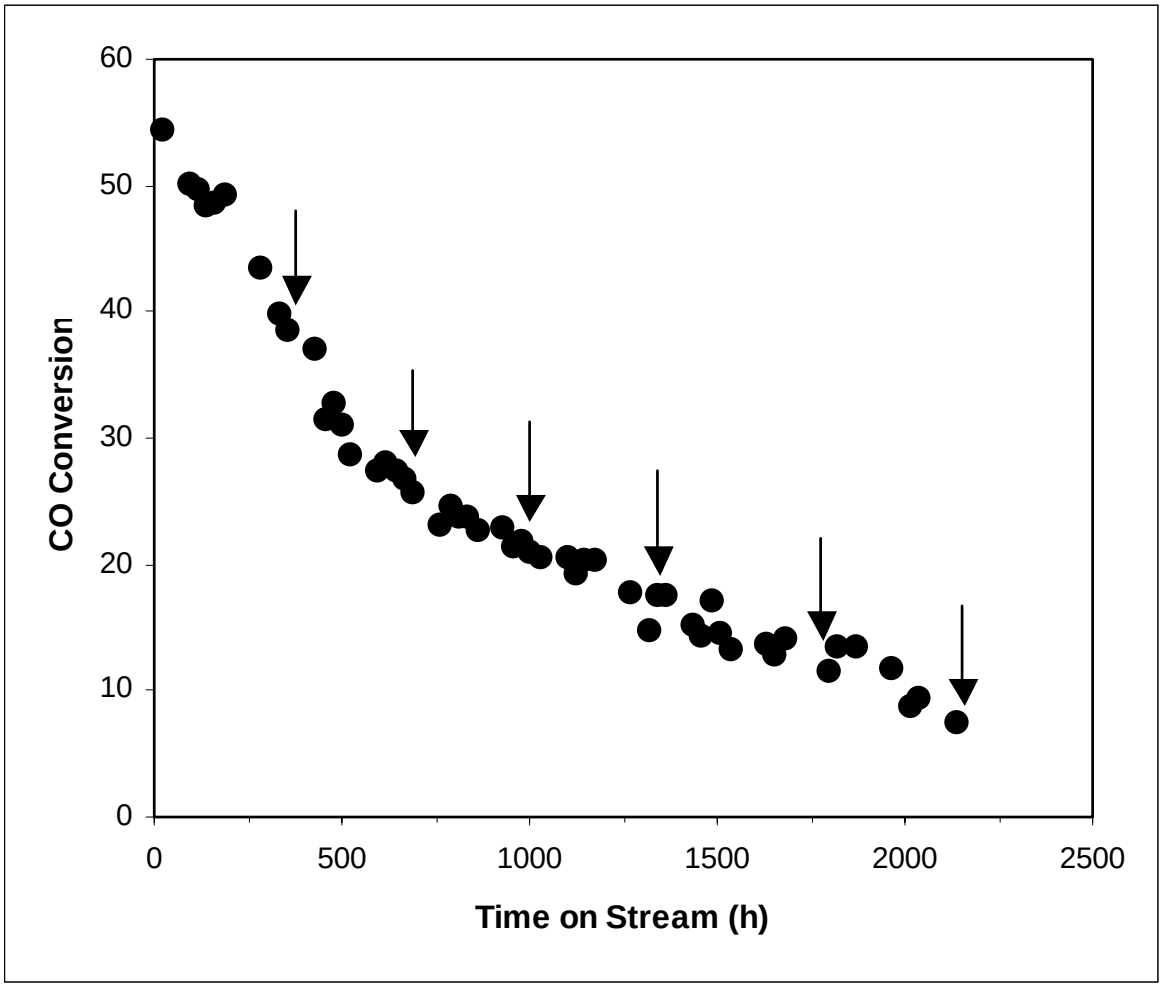

Figure 2. Deactivation profile of the 0.2%Re-15%Co/Al_2O_3 catalyst. Reaction testing conditions were as follows: 493K, 275 psig, 34 SL CO/g cat hr. Arrows indicate points where wax-containing catalyst samples were removed from the reactor for EXAFS analysis.

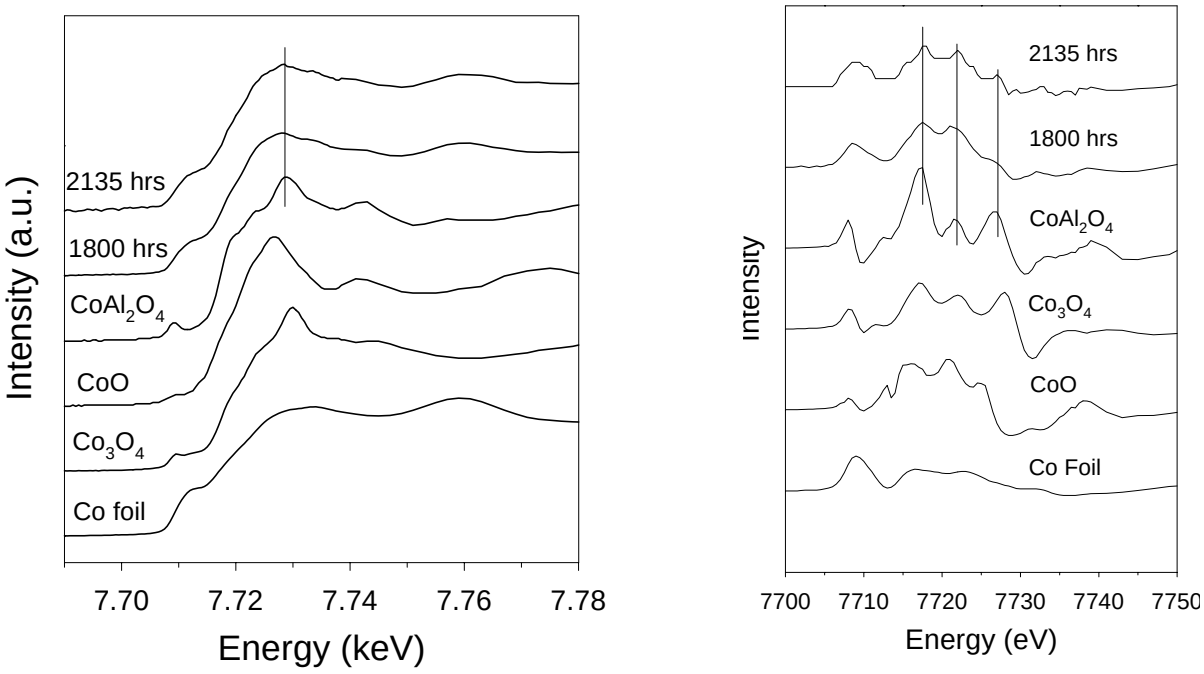

Figure 3. Normalized Co *K*-edge XANES spectra (left) and XANES derivative spectra (right) of the used catalyst after deactivation time of 1800 hours and 2135 hours in the Fischer-Tropsch Synthesis CSTR reactor versus those of comparative standards, including Co metal foil, Co_3O_4, CoO, and $CoAl_2O_4$.

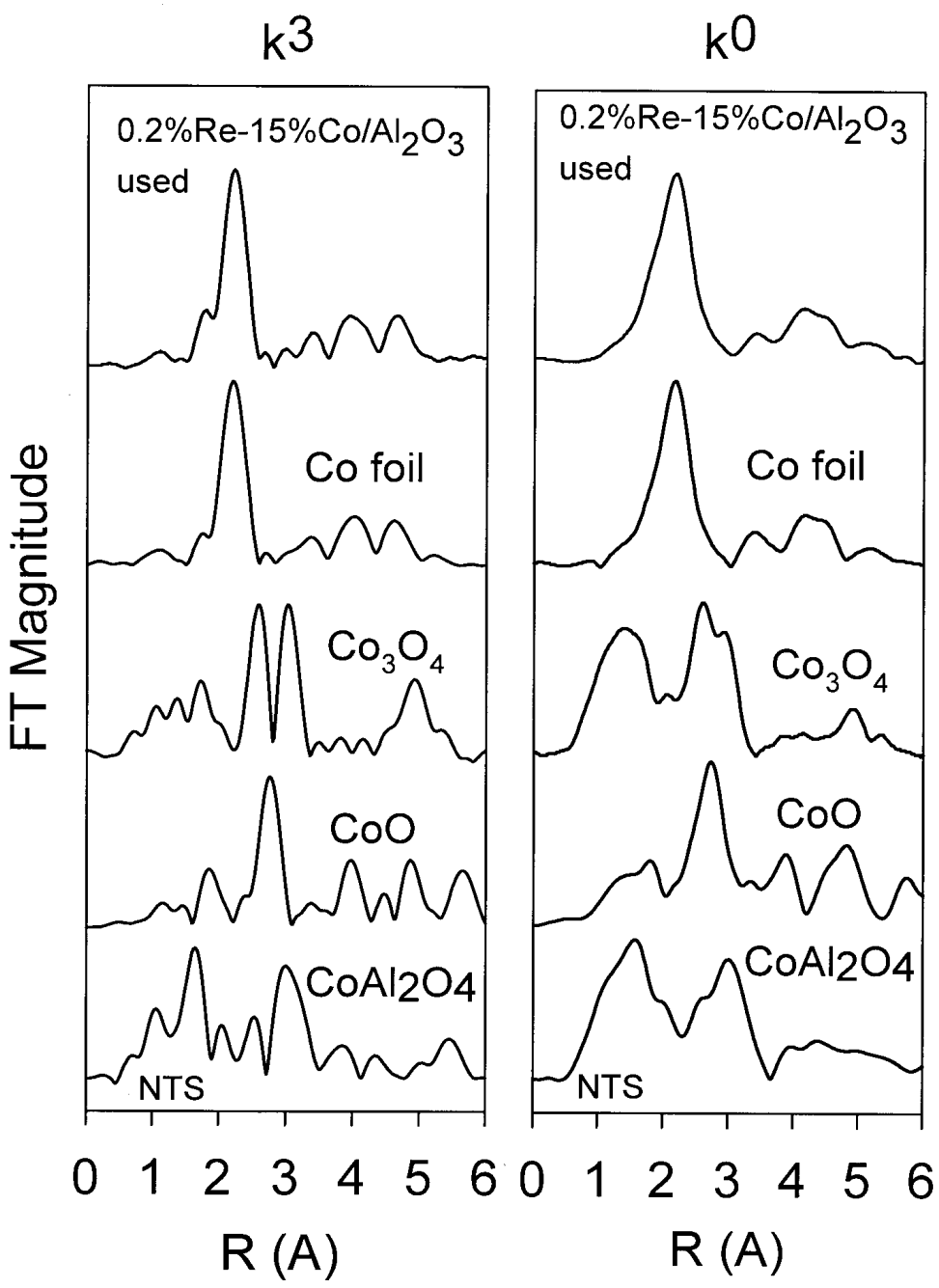

Figure 4. k^3 and k^0-weighted Fourier transform magnitudes of Co *K*-edge EXAFS spectra of the used catalyst after deactivation time of 1800 hours in the Fischer-Tropsch Synthesis CSTR reactor versus those of comparative standards, including Co metal foil, Co_3O_4, CoO, and $CoAl_2O_4$.

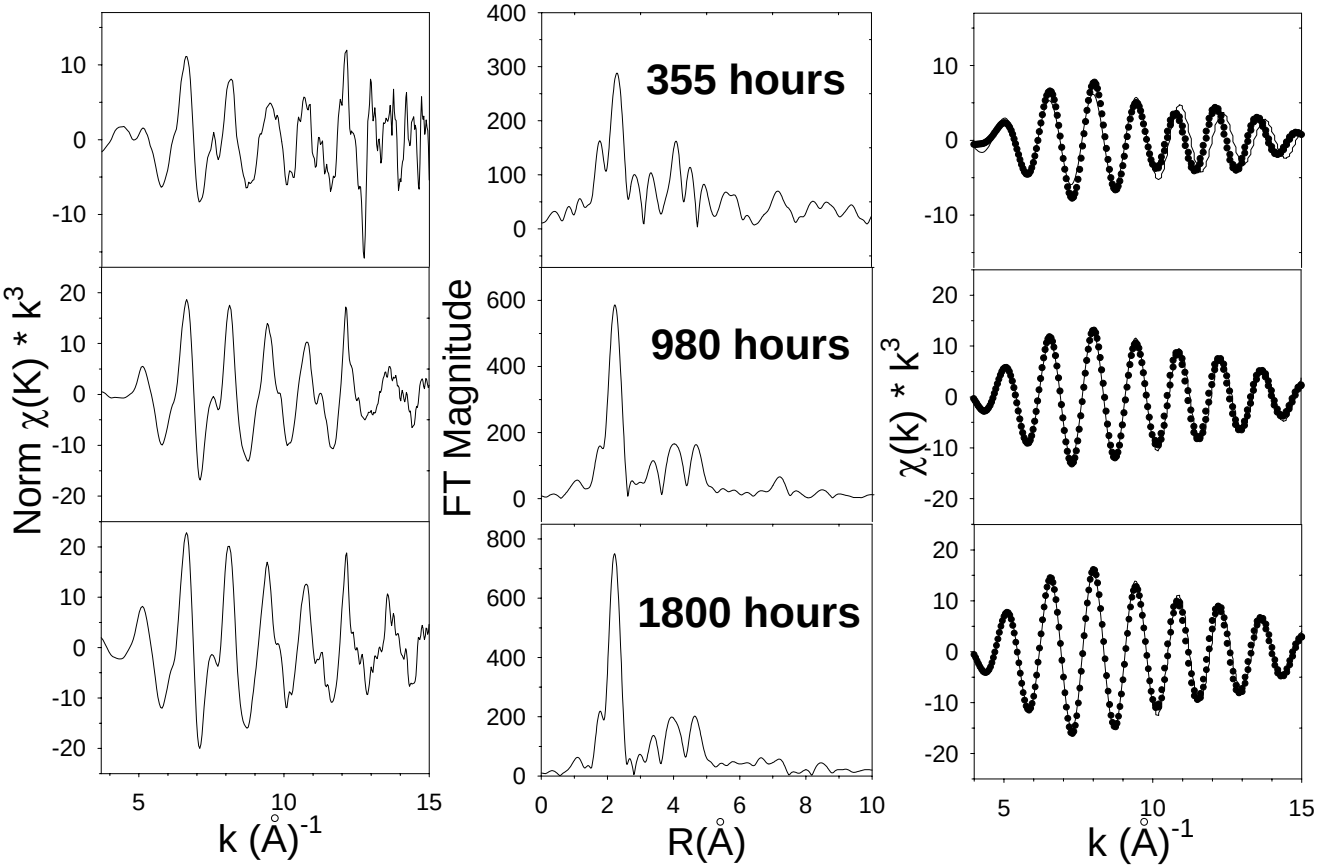

Figure 5. EXAFS results $\chi(k)\cdot k^3$ vs k, the Fourier transform magnitude, and first shell inverse transforms for used 0.2%Re-15%Co/γ-Al_2O_3 catalysts sampled during deactivation at 355, 980, and 1800 hours onstream, respectively. The solid lines represent the inverse transform, while the plotted points indicate the fit by FEFFIT.